

# Thermodynamic stability from Lorentzian path integrals and codimension-two singularities

---

**Hong Zhe (Vincent) Chen**

*Department of Physics, University of California,  
Santa Barbara, CA 93106, USA*

*E-mail:* [hzchen@ucsb.edu](mailto:hzchen@ucsb.edu)

ABSTRACT: It has previously been shown how the gravitational thermal partition function can be obtained from a Lorentzian path integral. Unlike the Euclidean case, the integration contour over Lorentzian metrics is not immediately ruled out by the conformal factor problem. One can then ask whether this contour can be deformed to pick up nontrivial contributions from various saddle points. In Einstein-Maxwell theory, we argue that the relevance of each black hole saddle to the thermal partition function depends on its thermodynamic stability against variations in energy, angular momentum, and charge. The argument involves consideration of constrained saddles where area and quantities associated with angular momentum and charge are fixed on a codimension-two surface. Consequently, this surface possesses not only a conical singularity, but two other types of singularities. The latter are characterized by shifts along the surface and along the Maxwell gauge group acquired as one winds around near the surface in a metric-orthogonal and connection-horizontal manner. We first study this enlarged class of codimension-two singularities in generality and propose an action for singular configurations. We then incorporate these configurations into the path integral calculation of the partition function, focusing on three-dimensional spacetimes to simplify the treatment of angular momentum.

---

## Contents

<b>1</b>	<b>Introduction</b>	<b>1</b>
1.1	Lorentzian path integral to thermal partition function: a review	2
1.2	Questions to be addressed and new ideas	5
1.3	Overview of this paper	9
<b>2</b>	<b>Codimension-two singularities</b>	<b>12</b>
2.1	Specifying codimension-two singularities	12
2.1.1	Conical and helical singularities	12
2.1.2	Holonomic singularity	14
2.1.3	Approximate stationarity	15
2.2	Regulating singularities using smooth configurations	16
2.2.1	Inequivalent resolutions of naively equivalent singularities	17
2.3	Curvatures for singular configurations	18
2.3.1	Geometric curvatures	19
2.3.2	Maxwell field strength	22
<b>3</b>	<b>Action for singular configurations</b>	<b>23</b>
3.1	Proposal for the action	23
3.1.1	(In)dependence on the cutoff shape	25
3.2	Variation of the action	28
3.3	Conditions for saddles and constrained saddles	29
3.3.1	Equations of motion near $\gamma$	30
3.3.2	Surface terms under unconstrained variations	31
3.3.3	Constrained saddles	32
<b>4</b>	<b>Thermal partition function</b>	<b>33</b>
4.1	Specifying the Euclidean path integral	34
4.2	Saddle-point evaluation	36
4.2.1	Empty thermal saddle	36
4.2.2	Black hole saddles	36
<b>5</b>	<b>Lorentzian formulation</b>	<b>41</b>
5.1	Codimension-two singularities	41
5.1.1	Spacelike $\gamma$ with no lightcones	42
5.1.2	Lightcones and resulting complications	46
5.2	Thermal partition function	53
5.2.1	Boundary conditions	54
5.2.2	Saddle-point evaluation	55

<b>6</b>	<b>Discussion</b>	<b>59</b>
6.1	Summary	59
6.2	Contributing saddles and the stability of black holes	60
6.3	Unstable saddles and the integral transform on Lorentzian time $T$	63
6.3.1	A simple Gaussian toy example	63
6.3.2	A more complete toy example: do unstable saddles contribute?	66
6.4	Equivalent boundary conditions, inequivalent singularities, and black hole sums	70
6.5	Other open problems and future directions	73
6.5.1	Subtleties of our new singularities and their action	73
6.5.2	Higher dimensions, angular momentum, and nonconstant modes on $\gamma$	76
6.5.3	Unstable variables	77

---

## 1 Introduction

Euclidean path integrals provide useful representations of various quantities in quantum field theories. With the inclusion of gravity, however, the Euclidean action becomes unbounded from below, due to the conformal mode of the metric. This conformal factor problem precludes the integration contour over Euclidean metrics as a possible choice for the gravitational path integral. One treatment of this problem is to simply rotate the contour of integration for the conformal mode [1], but this prescription seems rather ad hoc. An arguably more natural starting point is Lorentz signature [2–4]. In contrast to the Euclidean case, the integration contour over Lorentzian metrics is not immediately ruled out by the conformal factor problem. It then becomes a reasonable question to ask whether this integration contour can be deformed appropriately to pick up nontrivial contributions from various saddle points. A goal of this paper is to better understand the connection between this Lorentzian starting point and some established intuition about Euclidean gravitational saddles.

In particular, it has long been recognized that Euclidean gravitational solutions serve as important saddle points for path integrals in the semiclassical approximation. Consider, for example, the gravitational analogue of the grand canonical partition function

$$Z(\beta, \Omega, \Phi) = \text{tr} \left( e^{-\beta H_{\xi, \Phi}} \right), \quad (1.1)$$

where

$$H_{\xi, \Phi} = H - \Omega J - \Phi Q, \quad (1.2)$$

$H$  is the Hamiltonian generating evolution in a static (Lorentzian<sup>1</sup>) time direction  $\zeta$ ,  $J$  is the angular momentum generating rotation in a spatial direction  $\varphi$ , and  $Q$  is electric

---

<sup>1</sup>For the purposes of maintaining consistent notation, we will take the vector  $\zeta$  to be real in Lorentz signature and imaginary in Euclidean signature. The vector  $\varphi$  is real in both Euclidean and Lorentz signature. Equation (1.1) has the usual interpretation as a grand canonical partition function when  $\Omega$  and  $\Phi$  are real; to obtain real Euclidean boundary conditions for the path integral,  $\Omega$  and  $\Phi$  should instead be imaginary. See sections 4.1 and 5.2.1 for more details.

charge. More precisely, if the gravitational theory is holographically dual to a theory on its boundary, then eq. (1.1) would be the partition function of this boundary theory with operators  $H$ ,  $J$ , and  $Q$ . Notwithstanding the conformal factor problem, the gravitational partition function has been historically defined by a path integral over a set of bulk geometries with a given boundary manifold. In particular, the boundary has Killing vectors  $-i\zeta$  and  $\varphi$ , and contains a circle of length  $\beta$  generated by  $-i\xi = -i(\zeta + \Omega\varphi)$ . Other bulk fields are also integrated over and the boundary conditions for a Maxwell field in particular are parametrized by the electric potential  $\Phi$ . As Gibbons and Hawking [5] point out, such a path integral can then be semiclassically approximated by using Euclidean black holes as saddle points. Moreover, taking black hole thermodynamics seriously, one might expect only thermodynamically stable black holes to be relevant. However, it is difficult to verify this intuition from the Euclidean path integral without first specifying a viable choice of integration contour.

More recently, ref. [6] has made significant strides towards showing how these results can arise starting from a purely Lorentzian path integral. A key step in performing this path integral involves initially fixing the area of a codimension-two surface  $\gamma$ , giving rise to constrained saddles with conical singularities on  $\gamma$ . In this paper, we will study a larger class of codimension-two singularities and find that they appear in constrained saddles where area and quantities associated to angular momentum and charge are fixed on  $\gamma$ . To appreciate why this extended analysis is interesting and what it teaches us about the thermodynamic stability of relevant saddles, it is worthwhile to review some of the key points of ref. [6] below in section 1.1. Readers already familiar the analysis of ref. [6] may safely skip to section 1.2, where we sketch the new ideas to be explored in this paper.

### 1.1 Lorentzian path integral to thermal partition function: a review

While the goal is to recover the thermal partition function  $Z(\beta, \Omega, \Phi)$  of eq. (1.1), the starting point of ref. [6] is a purely Lorentzian path integral  $Z_L(T, \Omega, \Phi)$ . For simplicity and concreteness, let us focus on Einstein-Maxwell theory with a negative cosmological constant. The path integral  $Z_L(T, \Omega, \Phi)$  is then an integral over real Lorentzian geometries and Maxwell connections subject to certain boundary conditions parametrized by  $(T, \Omega, \Phi)$ . For example, the spacetime boundary is required to have a Lorentzian time circle  $S_{\text{time}}^1$  of parameter length  $T$  generated by the Killing vector  $\xi = \zeta + \Omega\varphi$ . The Maxwell field is also subject to boundary conditions that are again parametrized by an electric potential  $\Phi$ . Of course, the integrand of the path integral is  $e^{iI}$  where  $I$  is the Lorentzian action. At first glance, this integrand appears purely oscillatory, but, in contrast to the Euclidean conformal factor problem, such integrals can converge in an appropriate distributional sense as we will describe shortly.

A key point emphasized by ref. [6]<sup>2</sup> is that singular configurations must be included in the path integral  $Z_L(T, \Omega, \Phi)$ . In particular, to include configurations analogous to Euclidean black holes, the boundary cycle  $S_{\text{time}}^1$  must be allowed to contract in the bulk to a point on some codimension-two surface  $\gamma$ . The causal structure breaks down on  $\gamma$  and

---

<sup>2</sup>See also similar comments made by ref. [7] in the context of a Lorentzian simplicial path integral.

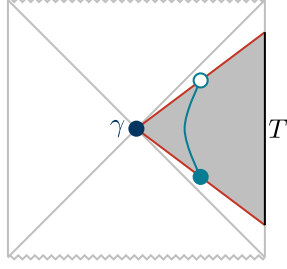


**Figure 1:** A conically singular constrained saddle constructed from a stationary black hole. The spacetime of the constrained saddle is the shaded region between the two red surfaces related by a boost around the bifurcation surface  $\gamma$ . The red surfaces are identified. The bifurcation surface  $\gamma$  is now conically singular, characterized by a hyperbolic opening angle. The teal curve shows a closed curve which is contractible to a point on  $\gamma$ .

this surface is conically singular, characterized by the opening angle around  $\gamma$ . Figure 1 illustrates one such configuration constructed as a quotient of the exterior of a Lorentzian stationary black hole with angular velocity  $\Omega$  and electric potential  $\Phi$ . This configuration is not a saddle for the full integral  $Z_L(T, \Omega, \Phi)$  because of the conical singularity on  $\gamma$ . Rather, it is a *constrained* saddle which extremizes the action  $I$  for a fixed value of the area of  $\gamma$  or, for later convenience, let us say fixed

$$\mathcal{S} = \frac{\text{Area}(\gamma)}{4G_N}, \quad (1.3)$$

where  $G_N$  is Newton's constant. Leaving the integral over  $\mathcal{S}$  for last, we can decompose

$$Z_L(T, \Omega, \Phi) = \int d\mathcal{S} Z_L(T, \Omega, \Phi; \mathcal{S}) \quad (1.4)$$

in terms of path integrals  $Z_L(T, \Omega, \Phi; \mathcal{S})$  over subcontours of fixed  $\mathcal{S}$ . The constrained saddle in fig. 1 is then a saddle for  $Z_L(T, \Omega, \Phi; \mathcal{S})$ . In fact, using Morse theory, ref. [6] argues that the contour of integration for  $Z_L(T, \Omega, \Phi; \mathcal{S})$  can always be deformed to pick up nontrivial contributions from constrained saddles constructed in this way.<sup>3</sup>

To leading order in the semiclassical approximation, the contribution  $Z_{\text{LBH}}(T, \Omega, \Phi; \mathcal{S})$  of such a constrained saddle is determined by the value of the action  $I$ ,

$$Z_{\text{LBH}}(T, \Omega, \Phi; \mathcal{S}) \sim e^{iI} = e^{\mathcal{S} - iT E_{\xi, \Phi}(\mathcal{S})}, \quad (1.5)$$

where

$$E_{\xi, \Phi}(\mathcal{S}) = E(\Omega, \Phi; \mathcal{S}) - \Omega J(\Omega, \Phi; \mathcal{S}) - \Phi Q(\Omega, \Phi; \mathcal{S}), \quad (1.6)$$

with  $E(\Omega, \Phi; \mathcal{S})$ ,  $J(\Omega, \Phi; \mathcal{S})$ , and  $Q(\Omega, \Phi; \mathcal{S})$  being the energy, angular momentum, and charge of the original black hole in fig. 1 with angular velocity  $\Omega$ , electric potential  $\Phi$ , and Bekenstein-Hawking entropy  $\mathcal{S}$ . Note, in particular, that the action has acquired an

<sup>3</sup>See section 6.2 for more details.

imaginary part  $\text{Im}(I_{\text{LBH}}) = -\mathcal{S}$ , as can be seen from applying a Lorentzian version of the Gauss-Bonnet theorem to the conical singularity [6, 8]. Substituting eq. (1.5) into eq. (1.4),

$$Z_{\text{LBH}}(T, \Omega, \Phi) \sim \int d\mathcal{S} e^{\mathcal{S} - iT E_{\xi, \Phi}(\mathcal{S})}, \quad (1.7)$$

one finds an integrand which grows exponentially with the integration variable  $\mathcal{S}$ . As written, the above integral does not converge, at least to a function of  $T$ .

However, unlike the conformal factor problem in Euclidean signature, this is both expected and manageable. It is expected because we are computing the gravitational analogue of the trace

$$Z_{\text{L}}(T, \Omega, \Phi) = \text{tr}(e^{-iT H_{\xi, \Phi}}). \quad (1.8)$$

If each energy window contains  $\sim e^{\mathcal{S}}$ -many states where  $\mathcal{S}$  grows polynomially with energy, then this trace, written as a sum over energy windows, behaves similarly to eq. (1.7).

Equation (1.8) also suggests that  $Z_{\text{L}}(T, \Omega, \Phi)$  has a good interpretation as a distribution in  $T$ , rather than as a function. For example, if we smear eq. (1.8) against a function  $f_{\beta}(T)$ , with the property that

$$\int_{-\infty}^{\infty} dT f_{\beta}(T) e^{-iT \omega} = e^{-\beta \omega} \quad (1.9)$$

for all  $\omega$  above the ground state eigenvalue of  $H_{\xi}$ , then we expect to recover the usual thermal partition function (1.1):

$$\int_{-\infty}^{\infty} dT f_{\beta}(T) Z_{\text{L}}(T, \Omega, \Phi) = Z(\beta, \Omega, \Phi). \quad (1.10)$$

Despite notational appearances, let us emphasize that the convention will always be to perform the  $T$  integral *before* the  $\mathcal{S}$  integral in  $Z_{\text{LBH}}(T, \Omega, \Phi)$  in order to realize its distributional meaning. Applying this integral transform to (1.7), one might then expect to find the corresponding contribution  $Z_{\text{BH}}(\beta, \Omega, \Phi)$  to the thermal partition function  $Z(\beta, \Omega, \Phi)$  to be given by

$$Z_{\text{BH}}(\beta, \Omega, \Phi) \stackrel{?}{\sim} \int d\mathcal{S} e^{\mathcal{S} - \beta E_{\xi, \Phi}(\mathcal{S})}. \quad (1.11)$$

Indeed, the above expression is what one would expect from the thermal trace (1.1) if we again identify  $e^{\mathcal{S}}$  as an approximate density of states. (However, the validity of eq. (1.11) will later be called into question.)

At last, we may approximate the final integral over  $\mathcal{S}$  by evaluating the integrand at its local maxima, *i.e.* at the local minima of the free energy

$$F(\beta, \Omega, \Phi; \mathcal{S}) = E_{\xi, \Phi}(\mathcal{S}) - \frac{1}{\beta} \mathcal{S} \quad (1.12)$$

$$= E(\Omega, \Phi; \mathcal{S}) - \Omega J(\Omega, \Phi; \mathcal{S}) - \Phi Q(\Omega, \Phi; \mathcal{S}) - \frac{1}{\beta} \mathcal{S} \quad (1.13)$$

with respect to  $\mathcal{S}$ . Extrema occur whenever the temperature of the original black hole in fig. 1,

$$\frac{1}{\beta_{\text{BH}}(\Omega, \Phi; \mathcal{S})} = \frac{dE_{\xi, \Phi}(\mathcal{S})}{d\mathcal{S}}, \quad (1.14)$$

coincides with the ensemble temperature  $1/\beta$ . In this sense, saddles for the path integral  $Z(\beta, \Omega, \Phi)$  correspond to black holes with temperature  $1/\beta$ , angular velocity  $\Omega$ , and electric potential  $\Phi$ . Indeed, the extremal values of the exponent in eq. (1.11) are simply minus the Euclidean action evaluated on these black holes.

Actually, eq. (1.11) suggests that not all black holes are relevant saddles for the final partition function  $Z(\beta)$ . In particular, the relevant saddles must not merely be extrema, but in fact are local *maxima* of the integrand in eq. (1.11) or, equivalently, local *minima* of the free energy  $F$  with respect to  $\mathcal{S}$ .<sup>4</sup> Changing variables from  $\mathcal{S}$  to  $E_{\xi, \Phi}$ , this can be understood physically as additionally requiring the positivity of specific heat  $C$ , given by

$$\frac{1}{C} = \frac{d}{dE_{\xi, \Phi}} \frac{1}{\beta_{\text{BH}}(\Omega, \Phi; E_{\xi, \Phi})}. \quad (1.15)$$

The conclusion of ref. [6] is therefore that relevant saddles for the thermal partition function  $Z(\beta)$  include only those black holes that are thermodynamically stable in the sense of having positive specific heat.

## 1.2 Questions to be addressed and new ideas

Although the results reviewed above seem satisfying, they leave some things to be desired. In particular, following thermodynamic intuition, shouldn't we have instead expected to find a more complete stability condition? For example, as ref. [6] remarks in its discussion, it would have been more natural to expect the free energy to be locally minimized with respect to *independent* variations of a complete set of thermodynamic variables, *e.g.* energy, angular momentum, and charge. Relatedly, the special treatment of  $\mathcal{S}$  seems rather undemocratic — what happens if we also fix other quantities in the path integral until after the integral transform on the Lorentzian time  $T$ ? These are the main questions which will motivate our extended analysis in this paper.

In particular, we will consider the consequences of fixing three independent quantities  $(\mathcal{S}, \mathcal{J}, \mathcal{Q})$  on a generically singular codimension-two surface  $\gamma$  in a subcontour path integral  $Z(T, \Omega, \Phi; \mathcal{S}, \mathcal{J}, \mathcal{Q})$ . Here,  $\mathcal{S}$  is again proportional to the area of  $\gamma$  as given in (1.3);  $\mathcal{J}$  is the integral of a local momentum density  $(p_{\text{BY}})_i$  on  $\gamma$  arising from a Brown-York-like construction; and

$$\mathcal{Q} = \frac{1}{g_{\text{M}}^2} \int_{\gamma} *F \quad (1.16)$$

---

<sup>4</sup>Let us refrain here from precisely defining the meaning of “relevant”. It should be evident that the local maxima of integrand in eq. (1.11) unambiguously contribute with nonzero weights to the integral on the RHS. Whether the integral receives contributions from extrema that are not local maxima of the integrand is a more subtle question. The answer depends on the precise definition of Lefschetz thimbles (*i.e.*, steepest descent contours flowing from extrema in the complexified space of the integration variables). We will postpone this discussion for section 6.3.2.

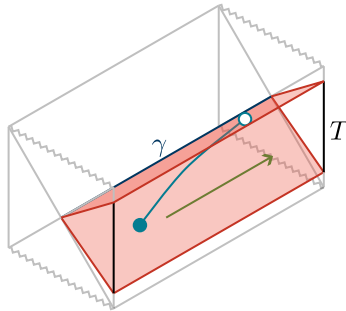


**Figure 2:** A conically and helically singular constrained saddle. An extra spatial symmetry direction is shown compared to fig. 1; *e.g.* this can be the (periodically identified) angular direction for a three-dimensional black hole. Whereas the red surfaces of constant time  $\hat{t}$  were presumably identified in fig. 1 in a way that trivializes near  $\gamma$ , they are shown here as identified after a relative shift, indicated by the green arrow. In particular, the teal closed curve does not become orthogonal to surfaces of constant  $\hat{t}$  even as the identified endpoints are pushed towards  $\gamma$ . The bifurcation surface  $\gamma$  now also has a helical singularity, characterized by the shift indicated in green.

is an electric charge as given by Gauss’s law from the electric flux  $*F$  across  $\gamma$ . If evaluated on the bifurcation surface  $\gamma$  of a stationary black hole solution, these quantities would coincide with the Bekenstein-Hawking entropy, angular momentum, and electric charge of the black hole (with the latter two ordinarily defined at the spacetime boundary). However, in generic spacetimes without preferred vector fields on  $\gamma$ , it is not immediately obvious how one should define  $\mathcal{J}$  from a momentum *dual-vector* density  $(p_{\text{BY}})_i$  on  $\gamma$ . We will therefore focus our analysis of angular momentum to  $D = 3$  spacetime dimensions, where the unit vector  $\chi^i$  on  $\gamma$  can be used to define  $\mathcal{J} \propto \int_{\gamma} \chi^i (p_{\text{BY}})_i$ . (Notwithstanding a few issues<sup>5</sup> such as this, most portions of this paper are written to allow immediate generalizations to higher dimensions.)

We will find that appropriate constrained saddles for  $Z(T, \Omega, \Phi; \mathcal{S}, \mathcal{J}, \mathcal{Q})$  can be constructed from the procedure illustrated in fig. 2. In particular, we start with a stationary black hole with the prescribed values of  $(\mathcal{S}, \mathcal{J}, \mathcal{Q})$  on its bifurcation surface  $\gamma$  — such a black hole might have an angular velocity  $\Omega_0$  and electric potential  $\Phi_0$  differing from  $\Omega$  and  $\Phi$ . The boundary Killing vectors  $\zeta$  and  $\varphi$  extend into the interior of this configuration, and it is useful to introduce a time coordinate  $\hat{t}$  coinciding with the Killing parameter of  $\zeta$  and preserved by  $\varphi$ . To match the boundary conditions prescribed by  $(T, \Omega)$ , we again quotient one exterior of the black hole with parameter period  $T$  along the flow generated by  $\xi = \zeta + \Omega \varphi$ . To match the electric potential  $\Phi$ , we also shift the Maxwell field  $A$  by  $(\Phi - \Phi_0) d\hat{t}$ .<sup>6</sup>

In this constrained saddle,  $\gamma$  is now a singular surface. For example, as before, there

<sup>5</sup>See section 6.5.2 for a discussion of these issues in higher dimensions.

<sup>6</sup>We take it to be part of the definition of the boundary conditions (and the coordinate  $\hat{t}$  on the boundary) that shifting  $A$  by  $(\Phi - \Phi_0) d\hat{t}$  in a neighbourhood of the boundary takes a configuration satisfying boundary conditions with electric potential  $\Phi_0$  to another configuration with electric potential  $\Phi$ .



is a conical singularity characterized by the opening angle around  $\gamma$ . Because generically  $\Omega \neq \Omega_0$  and  $\Phi \neq \Phi_0$ , two other types of singularities now appear on  $\gamma$ .

Let us first consider what ref. [6] dubbed, and what we will continue to call, the *helical* singularity on  $\gamma$ . Because  $\Omega \neq \Omega_0$ , the Killing vector  $\xi = \zeta + \Omega\varphi$  does not vanish on the bifurcation surface  $\gamma$  of the original black hole geometry. Consequently, the surfaces of constant time  $\hat{t}$  illustrated in red in fig. 2 are identified with a relative shift, in the  $\varphi$  direction, which remains nontrivial even as we approach  $\gamma$ . The closed orbits generated by  $\xi$  near  $\gamma$ , *e.g.* the teal curve in fig. 2, appears to move in the  $\varphi$  direction along  $\gamma$ , but only because the picture is drawn to be approximately faithful to metric angles. On the other hand, in a picture faithfully showing identified points,<sup>7</sup> the teal curve would appear as a closed loop while another curve orthogonal to slices of constant time  $\hat{t}$  would generically wind helically around  $\gamma$ . (We will find it useful in this paper to adopt this latter picture, where it is the closed teal curve of fig. 2 that hovers near a fixed “point” on  $\gamma$ .<sup>8</sup>) Some previous work which considered helical singularities (though, not under this name) in special contexts include refs. [9, 10]; the Euclidean analysis of the latter bears some resemblance to the naive Euclidean path integral calculation presented in section 4.

Due to the shift by  $(\Phi - \Phi_0)d\hat{t}$ , there is also on  $\gamma$  what we will call a *holonomic* singularity in the Maxwell field  $A$ . Figure 2 doubles as an illustration of this singularity if we reinterpret what we previously viewed as the spatial angular direction now as the fibre direction of the Maxwell principal fibre bundle. In particular, the two red surfaces over constant  $\hat{t}$  in the principal fibre bundle are identified with not only a helical shift in the  $\varphi$  direction as discussed in the previous paragraph, but also a shift in the gauge fibre direction. If we turn off the helical singularity (*e.g.*, if  $\Omega = \Omega_0$ ) to isolate the effect of the holonomic singularity, then a Wilson loop around a closed orbit of  $\xi$  infinitesimally near  $\gamma$  will be proportional to the strength of the holonomic singularity — hence the name.<sup>9</sup> Ref. [11] has previously studied holonomic singularities in  $D = 2$  dimensions.

The enlarged class of codimension-two singularities — conical, helical, and holonomic — considered in this paper, to my knowledge, has not been treated as thoroughly in literature relative to purely conical singularities.<sup>10</sup> A significant portion of this paper

---

<sup>7</sup>For example, see fig. 3. A closed loop parametrized by  $\tau$  is obtained at fixed  $\rho$  and  $y^i$ .

<sup>8</sup>More precisely, we view this teal closed curve as being contactable to a point on  $\gamma$  in a regulated version of the geometry where a small neighbourhood of  $\gamma$  is used to smooth out the singularity, as described in section 2.2. Other smooth in-fillings of the neighbourhood can lead to physically distinct singularities, labelled by other values of the helical shifts, as described in section 2.2.1, or even having no helical singularity, as sketched in fig. 11c.

<sup>9</sup>But more generically, this Wilson loop will be nonzero due to a combined effect of the helical and holonomic singularities.

<sup>10</sup>For example, refs. [9, 10] considered helical singularities in highly symmetric configurations. Ref. [11] considered holonomic singularities in  $D = 2$  dimensions resulting from a dimensional reduction of smooth  $D = 3$  configurations, so any action contribution localized on the singularity is purposely excluded. We would instead like to study conical, helical, and holonomic singularities in generic configurations that might appear in the path integral and write down an action including contributions from the singularity. This in particular requires resolving some subtleties that become apparent only when the singularity is regulated, as described in section 2.2. Further complications can arise in Lorentzian signature, as described in section 5.1.2.

will be dedicated to studying properties of these singularities in general Euclidean and Lorentzian configurations. In the presence of these new types of singularities, we must in particular revisit the definition of the Einstein-Maxwell action. Our strategy, for deducing what the action should be, will be to consider regulated configurations where the singularity on  $\gamma$  has been smoothed out over a neighbourhood of  $\gamma$ . A perhaps surprising comment is that certain configurations which seem diffeomorphic or gauge equivalent to each other away from  $\gamma$  can actually be physically distinguished by very different in-fillings of the regulated neighbourhood. Considering localized curvature contributions in the regulated neighbourhood, we will propose a definition for the action of singular configurations — see eqs. (3.1) and (5.18). Admittedly, some open questions of interpretation remain for certain infinite terms that arise in this derivation but are omitted from our proposed action. Regardless, we find that our action leads to a reasonable variational principle. Moreover, at fixed  $(\mathcal{S}, \mathcal{J}, \mathcal{Q})$ , we are able to construct constrained saddles as illustrated in fig. 2 with conical, helical, and holonomic singularities.

Continuing now our discussion of partition functions, the path integral  $Z(T, \Omega, \Phi; \mathcal{S}, \mathcal{J}, \mathcal{Q})$  over a subcontour of fixed  $(\mathcal{S}, \mathcal{J}, \mathcal{Q})$  receives a nontrivial contribution  $Z_{\text{BH}}(T, \Omega, \Phi; \mathcal{S}, \mathcal{J}, \mathcal{Q})$  from each such constrained saddle constructed from a black hole. This follows from Morse theory arguments just as in ref. [6] — see section 6.2. At leading order in the semiclassical approximation, each contribution

$$Z_{\text{LBH}}(T, \Omega, \Phi; \mathcal{S}, \mathcal{J}, \mathcal{Q}) \sim e^{iI} = e^{\mathcal{S} - iT E_{\xi, \Phi}(\mathcal{S}, \mathcal{J}, \mathcal{Q})} , \quad (1.17)$$

is given by the value of the action, where now

$$E_{\xi, \Phi}(\mathcal{S}, \mathcal{J}, \mathcal{Q}) = E(\mathcal{S}, \mathcal{J}, \mathcal{Q}) - \Omega \mathcal{J} - \Phi \mathcal{Q} , \quad (1.18)$$

$E(\mathcal{S}, \mathcal{J}, \mathcal{Q})$  is the energy of the original black hole in fig. 2 with Bekenstein-Hawking entropy  $\mathcal{S}$ , (angular) momentum  $\mathcal{J}$ , and electric charge  $\mathcal{Q}$ .

The analysis then proceeds similarly to section 1.1, but we now treat  $(\mathcal{S}, \mathcal{J}, \mathcal{Q})$  on the same footing. In particular, by integrating eq. (1.17), we obtain the contribution

$$Z_{\text{LBH}}(T, \Omega, \Phi) \sim \int d\mathcal{S} d\mathcal{J} d\mathcal{Q} e^{\mathcal{S} - iT E_{\xi, \Phi}(\mathcal{S}, \mathcal{J}, \mathcal{Q})} \quad (1.19)$$

to the path integral  $Z_{\text{L}}(T, \Omega, \Phi)$  over the full contour over Lorentzian configurations. We can further apply the integral transform (1.10) to obtain the corresponding contribution  $Z_{\text{BH}}(\beta, \Omega, \Phi)$  to the thermal partition function  $Z(\beta, \Omega, \Phi)$ . Similar to our previous treatment of  $\mathcal{S}$  in section 1.1, our prescription in this paper will be to always leave the  $(\mathcal{S}, \mathcal{Q}, \mathcal{J})$  integrals until *after* the  $T$  integral. We thus find:

$$Z_{\text{BH}}(\beta, \Omega, \Phi) \sim \int d\mathcal{S} d\mathcal{J} d\mathcal{Q} e^{\mathcal{S} - \beta E_{\xi, \Phi}(\mathcal{S}, \mathcal{J}, \mathcal{Q})} . \quad (1.20)$$

Again, these final integrals can be evaluated with saddle points corresponding to black holes with temperature  $1/\beta$ , angular velocity  $\Omega$ , and electric potential  $\Phi$ .

Note however that the relevant<sup>11</sup> saddles are now local maxima of the integrand in eq. (1.20), *i.e.* local minima of the free energy

$$F(\beta, \Omega, \Phi; \mathcal{S}, \mathcal{J}, \mathcal{Q}) = E_{\xi, \Phi}(\mathcal{S}, \mathcal{J}, \mathcal{Q}) - \frac{1}{\beta} \mathcal{S} \quad (1.21)$$

$$= E(\mathcal{S}, \mathcal{J}, \mathcal{Q}) - \Omega \mathcal{J} - \Phi \mathcal{Q} - \frac{1}{\beta} \mathcal{S} \quad (1.22)$$

with respect to the three independent variables  $(\mathcal{S}, \mathcal{J}, \mathcal{Q})$ . Alternatively, one may change variables to the more standard set of thermodynamic variables  $(E, \mathcal{J}, \mathcal{Q})$  and view  $\mathcal{S}(E, \mathcal{J}, \mathcal{Q})$  as a function giving the Bekenstein-Hawking entropy of a black hole with energy  $E$ , angular momentum  $\mathcal{J}$ , and charge  $\mathcal{Q}$ . At any rate, we recover a stronger thermodynamic stability condition relative to the analysis of ref. [6] summarized in section 1.1.

How did this happen? Relative to the previous analysis, we seem to have merely reorganized the ordering of the  $T$  integral relative to the  $\mathcal{J}$  and  $\mathcal{Q}$  integrals.<sup>12</sup> In the discussion of section 6, we will emphasize how the order of integration can be particularly important in Lorentzian path integrals evaluated using approximate saddle-point methods. Specifically, if performed *after* the integral over possibly “unstable” variables such as  $\mathcal{J}$  and  $\mathcal{Q}$ , then the integral transform from  $T$  to  $\beta$  can behave rather pathologically. For example, we will see from some toy examples how one-loop corrections to eq. (1.7) from any such unstable variable can, under the integral transform, map to a nonsensical answer differing drastically from the naive expectation (1.11). To avoid these pathologies, one should therefore perform the integral transform in  $T$  *before* the integrals over possibly unstable variables such as  $(\mathcal{S}, \mathcal{J}, \mathcal{Q})$ . An interesting question which we will leave for future work is whether saddles that are stable with respect to variations in  $(\mathcal{S}, \mathcal{J}, \mathcal{Q})$  might be unstable with respect to other variables (which one should then also integrate last in the path integral) — see section 6.5.3.

### 1.3 Overview of this paper

Let us now give an overview of the remainder of this paper. While conical, helical, and holonomic singularities will serve as important ingredients for our gravitational path integral, the latter two types of singularities might seem somewhat exotic and, to my knowledge, has not been analyzed in existing literature to a sufficient degree for our purposes. A significant portion of this paper is therefore dedicated to studying our enlarged class of codimension-two singularities. We will therefore start studying these singularities in the more modest Euclidean context in sections 2 to 4 before graduating to Lorentzian signature in sections 5 and 6.

**Section 2** is dedicated to specifying these singularities and studying their properties. In particular, conical and helical geometries are defined in section 2.1.1 while holonomic

---

<sup>11</sup>See footnote 4 and section 6.3.2.

<sup>12</sup>One might also note that we have now allowed a larger class of singularities in the path integral. However, even if the preceding analysis summarized in section 1.1 included such configurations in the path integral, without fixing  $\mathcal{J}$  and  $\mathcal{Q}$ , constrained saddles at fixed  $\mathcal{S}$  would still only have purely conical singularities.

singularities in the Maxwell configuration are defined in section 2.1.2. Some questions about whether singularity strengths and related parameters are allowed to vary around and along  $\gamma$  are discussed in section 2.1.3.

To better understand these singularities, in section 2.2, we consider a procedure for regulating them in an  $\varepsilon$ -neighbourhood  $\mathcal{N}_\varepsilon$  of the singular surface  $\gamma$ . Firstly, this demonstrates that configurations which are naively diffeomorphic or gauge equivalent to each other away from  $\gamma$  can have physically distinct internal structure within  $\mathcal{N}_\varepsilon$  when regulated. Secondly, in section 2.3, this allows us to extract localized curvature contributions, of both the geometry and Maxwell connection, from the regulated  $\mathcal{N}_\varepsilon$ .

**Section 3** is dedicated to studying the action for the codimension-two singularities introduced in section 2. Motivated by the curvature contributions found in section 2.3, we first define our proposal for the action of singular configurations in section 3.1. This action includes terms accounting for the conical singularity, previously appearing also in ref. [6], and additional terms associated to the helical and holonomic singularities. Subtleties related to the cutoff surface  $\partial\mathcal{N}_\varepsilon$ , on which some of these terms reside, are discussed in section 3.1.1.

Having specified the action, we then consider its variation in section 3.2, giving rise to equations of motions away from  $\gamma$  and boundary terms near  $\gamma$ . A Brown-York stress tensor on  $\partial\mathcal{N}_\varepsilon$  provides a convenient expression for the gravitational boundary terms here that arise in this variation. Its “time-space” component, in particular, provides a useful notion of a momentum density  $(p_{\text{BY}})_i$  along  $\gamma$ . By setting the variation of the action to zero, possibly subject to fixed constraints on  $\gamma$ , we deduce in section 3.3 conditions obeyed by saddles and constrained saddles. In particular, we will see in section 3.3.3 that fixing the area, integrated momentum density  $(p_{\text{BY}})_i$ , and integrated electric flux on a codimension-two surface  $\gamma$  leads to constrained saddles which generically have conical, helical, and holonomic singularities on  $\gamma$ .

**Section 4** then considers a naively *Euclidean* path integral calculation of the thermal partition function  $Z(\beta, \Omega, \Phi)$ . Of course, the integral over Euclidean metrics is doomed at the outset by the conformal factor problem; at the same time, this naive representation of  $Z(\beta, \Omega, \Phi)$  is also perhaps familiar to most readers. Remaining agnostic to the actual contour of integration, we will therefore use the Euclidean framework to practice constructing (constrained) saddles.

Specifically, in section 4.2.2, we will consider evaluating  $Z(\beta, \Omega, \Phi)$  by first fixing, and then later integrating over, quantities  $(\mathcal{S}, \mathcal{J}, \mathcal{Q})$  proportional to the area, integrated momentum density, and electric flux on a generically singular codimension-two surface  $\gamma$ . We then look for constrained saddles which are saddles for the intermediate integral  $Z(\beta, \Omega, \Phi; \mathcal{S}, \mathcal{J}, \mathcal{Q})$  over a subcontour of fixed  $(\mathcal{S}, \mathcal{J}, \mathcal{Q})$ . In particular, starting from a smooth Euclidean black hole, we construct conically, helically, and holonomically singular constrained saddles using a procedure analogous to fig. 2. The resulting contribution to  $Z(\beta, \Omega, \Phi)$  is eq. (1.20), but derived with complete disregard for the conformal factor problem. Of course, this is unsatisfactory.

**Section 5** therefore extends our analysis to Lorentz signature. The first step, in section 5.1, is to translate what we have learned about conical, helical, and holonomic singularities from Euclidean to Lorentz signature. As described in section 5.1.1, this is fairly straightforward when the singular surface  $\gamma$  has no lightcones in the Lorentzian configuration — indeed, this is the case for the configuration illustrated in fig. 2. For completeness, however, we also include in section 5.1.2 a fairly detailed discussion of cases where the spacetime contains lightcones for  $\gamma$ , leading to complications, for example, in evaluating the action.

The second step, in section 5.2, is to re-evaluate the thermal partition function  $Z(\beta, \Omega, \Phi)$  using a Lorentzian path integral  $Z(T, \Omega, \Phi)$ . This analysis, already summarized in section 1.2, leads to the contribution (1.19) from constrained saddles built from Lorentzian black holes as illustrated in fig. 2. Upon performing the integral transform from  $T$  to  $\beta$ , eq. (1.20) is reproduced now from a purely Lorentzian path integral without the conformal factor problem.

**Section 6** concludes this paper with a discussion. After a brief summary in section 6.1, we further flesh out in section 6.2 some of the ideas sketched above in section 1.2 concerning the thermodynamic stability of saddles relevant to the grand canonical partition function. For example, as an intermediate step, some basic Morse theory is reviewed to argue that the constrained saddles built from Lorentzian black holes do in fact contribute with nonzero weight to the path integrals  $Z(T, \Omega, \Phi; \mathcal{S}, \mathcal{J}, \mathcal{Q})$  over subcontours of fixed  $(\mathcal{S}, \mathcal{J}, \mathcal{Q})$ . Moreover, we again highlight that, by leaving the  $(\mathcal{S}, \mathcal{J}, \mathcal{Q})$  integrals for last, we are able to recover a more complete stability condition which indicates the relevance of a given black hole saddle to the final partition function  $Z(\beta, \Omega, \Phi)$ .

In section 6.3, we study toy examples firstly to explain why this order of integration is particularly important for potentially unstable variables like  $(\mathcal{S}, \mathcal{J}, \mathcal{Q})$  when using approximate saddle-point methods. Secondly, we also address the question of whether unstable saddles contribute to the path integral. The answer can depend subtly on the definition of Lefschetz thimbles (*i.e.* steepest descent contours) for stable saddles, such that, without precisely specifying the integrals along the latter, contributions from unstable saddles can sometimes become meaningless.

Section 6.4 discusses an interesting feature that arises from the equivalence of boundary conditions related by full rotations in space and around a compact Maxwell gauge group. As described in sections 4 and 5.2, from this equivalence, our construction naturally generates a sum over constrained saddles, which enforces the quantization of angular momentum and charge. This then leads to a discrete family of smooth black hole saddles for the final integrals over  $(\mathcal{S}, \mathcal{J}, \mathcal{Q})$ . For  $\text{AdS}_3$ , we identify this family as a subset of the  $\text{SL}(2, \mathbb{Z})$  black holes [12]. We also sketch how some other  $\text{SL}(2, \mathbb{Z})$  black holes might fit into our formalism by incorporating constrained saddles generated from exotic, *e.g.* CRT-twisted [13], black holes.

Finally, we end in section 6.5 with a discussion of open questions.

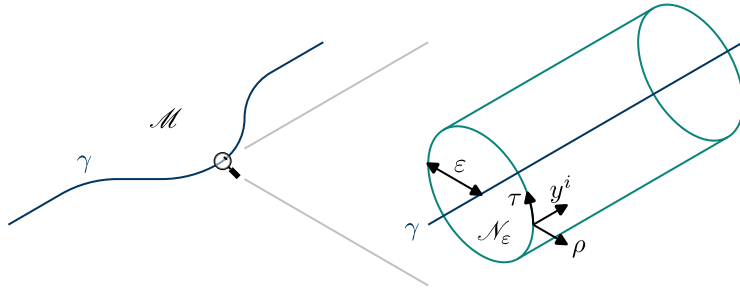


**Figure 3:** A codimension-two singularity  $\gamma$  and coordinates in its neighbourhood. Metric angles are *not* accurately depicted in this figure.

## 2 Codimension-two singularities

Let us start by specifying and studying properties of conical, helical, and holonomic singularities in Euclidean signature. (Lorentz signature will be treated later in section 5.) In section 2.1, we will first introduce these codimension-two singularities in generality, as might be found in a generic configuration included in the path integral. Then, in section 2.2, we will introduce a procedure for regulating the singularities in a small neighbourhood  $\mathcal{N}_\epsilon$  of the singular surface  $\gamma$ . This will firstly give us a better understanding of whether singular configurations which are diffeomorphic or gauge equivalent to each other away from  $\gamma$  are actually physically distinct when regulated in  $\mathcal{N}_\epsilon$ . Secondly, in section 2.3, we will be able to extract curvature contributions from the regulated  $\mathcal{N}_\epsilon$ , in preparation for defining an action for singular configurations in section 3.

### 2.1 Specifying codimension-two singularities

We will now describe the codimension-two singularities  $\gamma$  by specifying how the metric and Maxwell field are allowed to behave near  $\gamma$ .

#### 2.1.1 Conical and helical singularities

We start with codimension-two singularities of the metric. In addition to the more familiar purely conical singularities, we will consider also singularities which impart a “helical” shift upon going around the codimension-two surface. Refs. [9, 10], for example, have previously considered highly symmetric cases of these singularities constructed by cutting and gluing flat spacetime and black holes respectively, with the latter similar to the constrained saddles in section 4.2.2. Let us, however, give a general description of conical and helical singularities.

On a  $D$ -dimensional spacetime  $\mathcal{M}$ , we consider Euclidean metric configurations which are smooth, with the possible exception of a codimension-two surface  $\gamma$ . In a neighbourhood

of  $\gamma$ , we require the metric to take the form<sup>13</sup>

$$G_{AB} dX^A dX^B = d\rho^2 + g_{ab} dx^a dx^b \quad (2.1)$$

$$g_{ab} dx^a dx^b = N^2 d\tau^2 + h_{ij} (dy^i + N^i d\tau)(dy^j + N^j d\tau) . \quad (2.2)$$

As illustrated in fig. 3,  $X^A = (\rho, x^a)$  are  $D$ -dimensional spacetime coordinates, with  $\rho$  a radial geodesic coordinate<sup>14</sup> starting at  $\rho|_\gamma = 0$ ;  $x^a = (\tau, y^i)$  are coordinates on constant  $\rho$  surfaces, with  $\tau \sim \tau + 2\pi$  an angular coordinate around  $\gamma$ ; and  $y^i$  are coordinates in the remaining directions, parallel to  $\gamma$ .

Smooth metric configurations have, up to partial gauge-fixing,

$$N = \rho + \mathcal{O}(\rho^3) , \quad N^i = \mathcal{O}(\rho^2) . \quad (2.3)$$

Instead, we will also allow generically singular configurations<sup>15</sup>

$$N = \kappa \rho + (\text{subleading in } \rho) , \quad N^i = v^i + \mathcal{O}(\rho^2) . \quad (2.4)$$

Here,  $\kappa$  describes the rate of change in metric angle around  $\gamma$  with respect to  $\tau$ ; if constant,  $2\pi\kappa$  is the proper opening angle around  $\gamma$ . Meanwhile,  $v^i$  parametrizes the ‘‘helical’’ nature of the singularity, as we describe shortly. We will further require  $\lim_{\rho \rightarrow 0} h_{ij}$  to have a finite limit. In section 2.1.3, we will explain our assumptions about whether various quantities, such as  $\kappa$ ,  $v^i$ , and  $\lim_{\rho \rightarrow 0} h_{ij}$ , are allowed to depend on  $\tau$  and/or  $y^i$ .

To understand the helical nature of the singularity, note that a small closed circle around  $\gamma$ , parametrized by  $\tau \sim \tau + 2\pi$  is obtained at fixed  $\rho$  and  $y^i$ . However, even as  $\rho \rightarrow 0$ , such a path is not orthogonal to  $\gamma$  in the metric sense, as a consequence of the nontrivial shift  $N^i \rightarrow v^i$ . Relatedly, such a closed circle which shrinks towards  $\gamma$  can nonetheless retain a nonzero metric length even though the circle ‘‘contracts to a point’’ on  $\gamma$ .<sup>16</sup> A path which is metric-orthogonal to  $\gamma$  is instead one on which the pullback of  $dy^i + N^i d\tau$  vanishes. However, this latter path is no longer closed but rather winds helically around  $\gamma$ . In particular, upon moving by  $\delta\tau$  in  $\tau$  along such a path infinitesimally close to  $\gamma$ , one is displaced by  $-v^i \delta\tau$  along  $\gamma$ .

Before proceeding, let us establish some additional notation. Let us call the unit normals of the  $(D - 1) + 1$  and  $(D - 2) + 1$  decompositions in eqs. (2.1) and (2.2)

$$u = d\rho , \quad n = N d\tau , \quad (2.5)$$

<sup>13</sup>This way of decomposing the metric is inspired by ref. [10]. Whereas ref. [10] applies the ADM decomposition to a time slice, our ADM decomposition (2.2) is of a surface at constant radial separation from  $\gamma$ . Our fig. 3 can be compared with ref. [10]’s fig. 3.

<sup>14</sup>Our coordinates are Gaussian normal coordinates associated to surfaces of constant proper distance  $\rho$  from  $\gamma$  and the orthogonal geodesic vector field  $u^A = (\partial_\rho)^A$ .

<sup>15</sup>To more precisely map out the admissible forms of the small  $\rho$  expansions of metric components, one might try to generalize the analysis in the appendices of ref. [14] which considered only conical singularities.

<sup>16</sup>Topology and the notion of contractibility near  $\gamma$  will become more precise when considering a regulated version of the geometry, as described in section 2.2. In the regulated geometry, contractible cycles do shrink to zero proper size.

and write

$$G_{AB} = u_A u_B + g_{AB} = u_A u_B + n_A n_B + h_{AB}, \quad g_{ab} = n_a n_b + h_{ab}, \quad (2.6)$$

thus defining the uplifted tensors  $g_{AB}$ ,  $h_{AB}$ , and  $h_{ab}$ . These are projected down to  $g_{ab}$  and  $h_{ij}$  by

$$g^A{}_a = \frac{\partial X^A}{\partial x^a}, \quad h^a{}_i = \frac{\partial x^a}{\partial y^i}. \quad (2.7)$$

We will lower/raise indices  $(A, B, \dots)$ ,  $(a, b, \dots)$ , and  $(i, j, \dots)$  with  $G_{AB}/G^{AB}$ ,  $g_{ab}/g^{ab}$ , and  $h_{ij}/h^{ij}$  respectively. As an example,

$$n^A = G^{AB} n_B = \frac{(\partial_\tau)^A - N^A}{N} = g^A{}_a n^a. \quad (2.8)$$

We will use  $\nabla_A$ ,  $D_a$ , and  $d_i$  to respectively denote the covariant derivatives associated to  $G_{AB}$ ,  $g_{ab}$ , and  $h_{ij}$ .

We shall denote the spacetime volume form<sup>17</sup> by  $\epsilon$ , and write its interior product with a vector  $\xi^A$  as

$$\xi^A \epsilon_A = \iota_\xi \epsilon. \quad (2.9)$$

Most codimension-one surfaces we will consider are boundaries and thus have induced orientations. Our convention will be to take the volume form on  $\gamma$  and more generally codimension-two surfaces of constant  $(\rho, \tau)$  to be given by

$${}^{(D-2)}\epsilon = n^A u^B \epsilon_{AB} = \iota_u (\iota_n \epsilon), \quad (2.10)$$

so

$$\epsilon = N \, d\tau \wedge d\rho \wedge {}^{(D-2)}\epsilon. \quad (2.11)$$

### 2.1.2 Holonomic singularity

We will also consider a Maxwell field  $A$ , which we require to be smooth away from  $\gamma$ . Just as we have introduced conical and helical singularities in radially static coordinates (2.1) where  $G_{\rho a} = 0$ , let us now consider a radial gauge for the Maxwell field in which

$$u^A A_A = 0. \quad (2.12)$$

At  $\gamma$ , smoothness would ordinarily require

$$N n^a A_a = \mathcal{O}(\rho^2), \quad (2.13)$$

---

<sup>17</sup>We do not immediately see a reason why our formalism requires spacetimes to be orientable, that is possess a *globally* defined nonvanishing top form. In general,  $\epsilon$  should be interpreted as simply an instruction to integrate with a positive weight; *i.e.* whatever orientation one might *locally* assign to a piece of spacetime,  $\epsilon$  is a similarly locally defined form that is positive relative to that choice.



in analogy to having a vanishing shift (2.3). However, just as one can turn on a helical singularity (2.4), we will more generally allow an electric potential for which

$$N n^a A_a = \mu + \mathcal{O}(\rho^2) . \quad (2.14)$$

In the same way that  $v^i$  describes geometric motion along  $\gamma$ ,  $\mu$  describes motion along the fibres of the Maxwell principal bundle as one moves around  $\gamma$  in a metric-orthogonal manner. This is related to a generically nontrivial holonomy around  $\gamma$ , as quantified by an  $\varepsilon$ -size Wilson loop  $\int_{\mathcal{C}_\varepsilon} A$  encircling  $\gamma$ . However, taking  $\mathcal{C}_\varepsilon$  to be a closed circle at fixed  $\rho = \varepsilon$  and  $y^i$ , note that the value of this Wilson loop will depend on both  $\mu$  and the components of  $A$  along any helical shift  $v^i$  present on  $\gamma$ :

$$\int_{\mathcal{C}_\varepsilon} A = \int_{\mathcal{C}_\varepsilon} d\tau (\partial_\tau)^a A_a \sim \int_{\mathcal{C}_\varepsilon} d\tau (\mu + v^i A_i) . \quad (2.15)$$

We will require the components  $A_i$  along  $\gamma$  to have finite  $\rho \rightarrow 0$  limits. At any rate, for brevity, we will refer to singularities with  $\mu \neq 0$  as holonomic singularities.

Such configurations have previously appeared, for example, in  $D = 2$  dimensions in ref. [11], where they were called “KK instantons” because they arose from the dimensional reduction of smooth  $D = 3$  configurations. In that context, however, the singularities were not truly singularities in the fundamental  $D = 3$  description and are artifacts of the dimensional reduction; these are analogous to conical singularities which appear when taking orbifolds of replica-symmetric saddles computing gravitational Rényi entropies [15]. In both situations, action contributions localized to these “artificial” singularities should be excluded. Another perspective is that such singularities each occur with fixed strength. To impose the right boundary conditions on the singularity to fix this strength, terms must be added to the action, which happen to cancel the localized contributions from the singularity [11, 14].

In contrast, the conical, helical, and holonomic singularities which we will consider in this paper are somewhat less artificial. As we will describe in section 2.2, we will view each singular configuration as a limit of some smooth regulated configuration differing from the original singular configuration in some neighbourhood  $\mathcal{N}_\varepsilon$  of the singular surface  $\gamma$ . Just as the smooth configuration can appear in the path integral, weighted by an action including contributions from  $\mathcal{N}_\varepsilon$ , we will similarly allow singular configuration in the path integral, weighted by an action including contributions localized near  $\gamma$ . In the path integral, the strengths of the conical, helical, and holonomic singularities are not fixed; in fact, as sketched in section 1 and carried out in sections 4 and 5.2, we will evaluate the path integral by initially fixing quantities that are conjugate in some sense to these singularity strengths.

### 2.1.3 Approximate stationarity

Before moving on, let us address how we will allow various field components to vary around  $\gamma$ . For the most part, in this paper, we will assume a very weak notion of approximate stationarity near  $\gamma$  — namely that certain components of the metric and Maxwell field

in the  $\rho \rightarrow 0$  expansion are  $\tau$ -independent, as elaborated below. However, we will revisit some of these assumptions when considering Lorentz signature in section 5.1.

Firstly, it seems reasonable to require the induced fields  $h_{ij}$  and  $A_i$  on surfaces of constant  $(\rho, \tau)$  to have  $\tau$ -independent limits as  $\rho \rightarrow 0$ . These limits can then be understood as the induced field configurations on  $\gamma$ . A  $\tau$ -dependent induced field configuration seems highly unnatural and we will find no reason to relax the assumed  $\tau$ -independence of  $\lim_{\rho \rightarrow 0} h_{ij}, A_i$ , even when we consider Lorentzian signature in section 5.

In sections 3.2 and 3.3, it will become apparent that the volume element on surfaces of constant  $(\rho, \tau)$  is, in a certain sense, conjugate to the variable  $\kappa$ . Thus, it seems natural also to require  $\kappa(y)$  to be  $\tau$ -independent.<sup>18</sup> By analogy, we are inclined to further restrict helical shifts  $v^i(y)$  to also be  $\tau$ -independent. In doing so, we might also require the  $\mathcal{O}(\rho^2)$  term of  $N^i$  to be similarly  $\tau$ -independent, as it will later be revealed to be conjugate to the helical shift  $v^i$ . The same can be said for the holonomic singularity strength  $\mu(y)$  and its conjugate, the pullback of  $*F$  to surfaces of constant  $(\rho, \tau)$  in the  $\rho \rightarrow 0$  limit.

However, it is not immediately obvious that configurations which do not satisfy all the above assumptions of  $\tau$ -independence should be ruled out as a matter of principle. Aside from some comments on why we might want to relax some of these assumptions when considering Lorentzian signature in sections 5 and 6, we will largely leave this question for future work.

A partial list of issues that may arise in case the above stated assumptions of  $\tau$ -independence fail is as follows. If the induced fields  $h_{ij}$  and  $A_i$  are  $\tau$ -dependent near  $\gamma$ , then they must be interpolated when regulating the singularity as described in section 2.2 and potentially give additional curvature contributions in section 2.3. If  $\kappa, v^i, \mu$  or their conjugate variables are  $\tau$ -dependent, then we must refrain from trivially integrating out the  $\tau$  direction in certain equations, *e.g.* eqs. (2.36), (3.39), (3.44), (3.50), (3.52), (4.13), (4.14), (5.45) and (5.46) (but this does not seem to qualitatively alter our discussion). Moreover, in section 3.1.1, we will find that the action of a helically singular configuration is sensitive to the shape of a cutoff surface placed around  $\gamma$ , except when  $\lim_{\rho \rightarrow 0} h_{ij}, \kappa$ , and  $v^i$  are  $\tau$ -independent or when  $\lim_{\rho \rightarrow 0} h_{ij}$  is  $\tau$ -independent and  $\kappa$  is  $y^i$ -independent.

## 2.2 Regulating singularities using smooth configurations

It is worthwhile to consider smooth regulated configurations which approximate the singularities introduced in section 2.1. This will motivate the localized curvature and action contributions we will later assign to the singularities. Moreover, the regulated geometries will resolve some apparent redundancies in describing the structure of the singularities.

---

<sup>18</sup>At first sight, this might appear to be a statement purely about gauge-fixing a redundancy in the choice of parameter  $\tau$ . Given a  $\kappa(x)$  which is a function of  $x^a = (\tau, y^i)$ , one can remove the  $\tau$ -dependence of  $\kappa$  by reparametrizing  $\tau$  in a  $y^i$ -dependent manner. This reparametrization, however, does not generally map surfaces of constant  $\tau$  to each other. As we will see in section 2.2.1, a special choice of foliation by surfaces of constant  $\tau$  is picked out by the physical internal structure of a helical singularity, which becomes apparent when we regulate the singularity. Thus, under the regulation prescription we will adopt,  $y^i$ -dependent reparametrizations of  $\tau$  are not viewed as redundancies, but rather move us between physically distinct configurations.

To regulate a configuration singular on the codimension-two surface  $\gamma$ , let us consider a small neighbourhood  $\mathcal{N}_\varepsilon$  of  $\gamma$  in the spacetime  $\mathcal{M}$  — see fig. 3. The radial extent of  $\mathcal{N}_\varepsilon$  from  $\gamma$  is understood to be parametrized by a small regulator  $\varepsilon$ ; to be concrete for now, we will take  $\partial\mathcal{N}_\varepsilon$  in the singular configuration to be a surface of constant  $\rho$  of order  $\varepsilon$ .<sup>19</sup> The regulated configuration we construct will coincide with the original singular configuration outside the neighbourhood  $\mathcal{N}_\varepsilon$ , *i.e.* in  $\mathcal{M} \setminus \mathcal{N}_\varepsilon$ . However, we require the regulated configuration to be modified in  $\mathcal{N}_\varepsilon$  such that it is smooth everywhere, in particular at the centre  $\gamma$  of  $\mathcal{N}_\varepsilon$  where the original configuration was singular. Practically, this amounts to an interpolation inside  $\mathcal{N}_\varepsilon$  from the smooth behaviour (2.3) and (2.13) on  $\gamma$  to the behaviour eqs. (2.4) and (2.14) matching the original singular configuration on  $\partial\mathcal{N}_\varepsilon$ .<sup>20</sup> We will take the interpolation scale of each function of  $\rho$  to be  $\mathcal{O}(\varepsilon)$ . Moreover, we require the induced metric on  $\gamma$  in the regulated geometry to be unmodified from the  $\rho \rightarrow 0$  limit of the induced metric  $h_{ij}$  on surfaces of constant  $(\rho, \tau)$  in the original singular geometry. While trivial at first glance, this last statement can be regarded as a gauge condition, as we describe below.

### 2.2.1 Inequivalent resolutions of naively equivalent singularities

We are now in a position to discuss the question of whether singularities described by different values of  $(\kappa, v^i, \mu)$  are truly physically distinct. In light of the above described procedure for resolving singularities using regulated configurations, we will argue that this is indeed the case.

Let us consider, in the spacetime region away from  $\gamma$ , the effect of a  $y$ -dependent reparametrization of  $\tau$ . Taking the variation  $\delta_f \equiv \mathcal{L}_f \partial_\tau$ , generated by a vector  $f(y)\partial_\tau$ , we find the components of the metric (2.2) vary as

$$\delta_f N = f \partial_\tau N - N N^i \partial_i f, \quad (2.16)$$

$$\delta_f N^i = f \partial_\tau N^i + N^2 \partial^i f - N^i N^j \partial_j f, \quad (2.17)$$

$$\delta_f h_{ij} = f \partial_\tau h_{ij} + N_i \partial_j f + N_j \partial_i f. \quad (2.18)$$

In helically singular configurations, these transformations remain nontrivial as one approaches  $\gamma$ . Thus, unregulated configurations to which we ascribe different values of  $(\kappa, v^i, \lim_{\rho \rightarrow 0} h_{ij})$  may yet be related to each other by diffeomorphisms away from  $\gamma$ . (In contrast, in the absence  $v^i = 0$  of a helical singularity, eqs. (2.3) and (2.4), with definite values of  $\kappa$  and  $v^i$ , as well as  $\lim_{\rho \rightarrow 0} h_{ij}$ , are preserved by the above.)

However, we will view this as a redundancy only in the description of the unregulated configuration away from  $\gamma$  or the regulated configuration outside  $\mathcal{N}_\varepsilon$ . Let us consider the question of whether two singular configurations related by a reparametrization generated

---

<sup>19</sup>The action we will derive for singular configurations will be expressed in terms of this neighbourhood  $\mathcal{N}_\varepsilon$  of the singularity  $\gamma$ . As described in section 3.1.1, however, this action will turn out to be insensitive to the shape of  $\partial\mathcal{N}_\varepsilon$  as one moves around the  $\tau$  direction.

<sup>20</sup>Note from the interpolation in  $N$  that, setting the proper radius of  $\mathcal{N}_\varepsilon$  in the original geometry to be  $\varepsilon$ , the proper radius in the regulated geometry will generically differ (but should be of the same order). Thus, if we insist on the form (2.1) of the metric in the regulated geometry and require  $\rho$  to match continuously to the unregulated geometry at  $\partial\mathcal{N}_\varepsilon$ , then  $\gamma$  will not generically lie at  $\rho = 0$  in the regulated geometry.

by eqs. (2.16) to (2.18) are really distinct. Away from  $\gamma$ , there appears to be no physical distinction between the two configurations. However, applying our regulation procedure to these two configurations leads to distinct in-fillings of the regulated neighbourhood  $\mathcal{N}_\varepsilon$ . For example, the regulated configurations have different induced metrics on  $\gamma$  related by eq. (2.18). Our regulation procedure therefore imbues the singularity with some internal structure that distinguishes the two configurations.

Practically, we will continue to describe singularities through field components, *e.g.*  $(\kappa, v^i, \lim_{\rho \rightarrow 0} h_{ij})$ , associated to a choice of  $\tau$  foliation. Implicitly, we will always have in mind that the singularity is regulated according to our procedure for *that given  $\tau$  foliation*. For example, the induced metric on  $\gamma$  — made precise in the regulated geometry — is really the stated value of  $\lim_{\rho \rightarrow 0} h_{ij}$  and not some other metric related by eq. (2.18). With this in mind, singularities assigned different values of  $(\kappa, v^i, \lim_{\rho \rightarrow 0} h_{ij})$  related by eqs. (2.16) to (2.18) are physically distinct. In particular, in section 2.3, we will extract curvature contributions from the regulated neighbourhood  $\mathcal{N}_\varepsilon$  of  $\gamma$  and, in section 3.1, we will use these results to deduce an action for singular configurations. Singularities with different values of  $(\kappa, v^i, \lim_{\rho \rightarrow 0} h_{ij})$  related by eqs. (2.16) to (2.18) will have generically different action.

Analogous remarks can be made about certain discrete shifts of  $v^i$  that naively appear to lead to redundancies. Suppose there exists a locally Killing vector field  $w^i$ , tangential to constant  $(\rho, \tau)$  surfaces near  $\gamma$ , which generates closed orbits with parameter period  $2\pi$  — in particular,  $e^{2\pi w} \sim 1$  acts identically on tensor fields. Then, any (unregulated) configuration described by helical shift  $v^i$  on  $\gamma$  is related, in the spacetime region away from  $\gamma$ , by discrete diffeomorphisms to configurations with helical shifts  $v^i + mw^i$  for  $m \in \mathbb{Z}$ .<sup>21</sup> (Moreover, any spin structure is preserved by the diffeomorphisms relating  $v^i + 2mw^i$  for  $m \in \mathbb{Z}$ .) However, by our regulation procedure, we will regard these shifts as describing helical singularities which are resolved by physically distinct regulated geometries near  $\gamma$ . In particular, a helical singularity with shift parameter  $v^i + mw^i$  is regulated by a smooth geometry with a shift vector  $N^i$  interpolating between zero on  $\gamma$  and  $N^i \sim v^i + mw^i$  on  $\partial\mathcal{N}_\varepsilon$ .

We can make identical remarks about the Maxwell sector. The Maxwell gauge group  $G_M$  can be either compact  $\cong U(1)$  or non-compact  $\cong \mathbb{R}$ . In the former case, when  $G_M = U(1)$ , one may have naively thought that a holonomic singularity  $\mu$  is equivalent to one with  $\mu + n$  for  $n \in \mathbb{Z}$ . However, just as in the above helical discussion, our convention for regularization resolves these singularities using physically distinct smooth configurations near  $\gamma$ .

### 2.3 Curvatures for singular configurations

We now calculate various curvatures in the singular configurations introduced in section 2.1.

---

<sup>21</sup>For an illustration, see our construction of helically singular constrained saddles for the gravitational partition function in fig. 4. In fig. 4c, the two helical shifts indicated by solid and dashed green arrows describe the same identification of the red surfaces. However, under our regulation procedure, these different helical shifts lead to different contractible cycles, indicated by the solid and dashed teal curves respectively, in the regulated versions of the geometry.

### 2.3.1 Geometric curvatures

We first consider curvatures of the spacetime geometry. We start with the extrinsic curvatures of  $(D-1)$ - and  $(D-2)$ -dimensional slices foliating the geometries (2.1) and (2.2). These will be related by the Gauss-Codazzi equation to intrinsic curvature. Using the regulated geometry introduced in section 2.2, we will identify pertinent contributions to intrinsic curvature as contact terms associated to the singularity on  $\gamma$ .

We denote the extrinsic curvature of the  $(D-1)$ -dimensional constant  $\rho$  surfaces by

$$(K_u)_{AB} = \frac{1}{2}\mathcal{L}_u g_{AB} = \frac{1}{2}\mathcal{L}_u G_{AB} = \nabla_A u_B, \quad (2.19)$$

where  $\nabla_A$  denotes the covariant derivative of the metric  $G_{AB}$ . Of course,  $u^A (K_u)_{AB} = u^A (K_u)_{BA} = 0$  so no information is lost in the projection

$$(K_u)_{ab} = \frac{1}{2}\partial_\rho g_{ab}. \quad (2.20)$$

Of interest to us are two scalars constructed from this extrinsic curvature:

$$(K_u)^a{}_a = \frac{\partial_\rho N}{N} + \frac{1}{2}h^{ij}\partial_\rho h_{ij} \quad (2.21)$$

$$(K_u)^{ab}(K_u)_{ab} = \left(\frac{\partial_\rho N}{N}\right)^2 + \frac{h_{ij}\partial_\rho N^i\partial_\rho N^j}{2N^2} + \frac{1}{4}h^{ik}h^{j\ell}\partial_\rho h_{ij}\partial_\rho h_{k\ell}. \quad (2.22)$$

Each constant  $\rho$  surface is in turn foliated by constant  $\tau$  surfaces with extrinsic curvature

$$(k_n)_{ab} = \frac{1}{2}\mathcal{L}_n h_{ab}. \quad (2.23)$$

The  $(D-2)+1$  decomposition (2.2) leads to the standard formula<sup>22</sup>

$$(k_n)_{ij} = \frac{1}{2N}(\partial_\tau h_{ij} - \mathcal{L}_{\vec{N}}h_{ij}). \quad (2.24)$$

Let us turn now to the intrinsic curvature, given by the Gauss-Codazzi equation<sup>23</sup>

$$R = {}^{(D-1)}R - (K_u)^{ab}(K_u)_{ab} + (K_u)^a{}_a(K_u)^b{}_b - 2\nabla_A(u^A\nabla_B u^B). \quad (2.25)$$

A second iteration of Gauss-Codazzi gives

$${}^{(D-1)}R = {}^{(D-2)}R - (k_n)^{ij}(k_n)_{ij} + (k_n)^i{}_i(k_n)^j{}_j + 2D_a(n^b D_b n^a - n^a D_b n^b). \quad (2.26)$$

The Ricci curvatures  $R$ ,  ${}^{(D-1)}R$ , and  ${}^{(D-2)}R$  are associated to the full  $D$ -dimensional spacetime, constant  $\rho$  surfaces, and constant  $(\rho, \tau)$  surfaces respectively. The covariant derivative of  $g_{ab}$  is denoted  $D_a$ .

<sup>22</sup>To avoid confusion with the lapse, we will write the shift vector as  $\vec{N}$  when suppressing its index.

<sup>23</sup>Recall that we are currently in Euclidean signature; the corresponding Lorentzian equation has extra signs on the terms quadratic in extrinsic curvature and the normal vector, when the normal is time-like. Note also that eq. (2.25) ordinarily has a term  $2\nabla_A(u^B\nabla_B u^A)$  on the RHS, but this vanishes because our  $u^A$  is a geodesic vector field.

Let us now deduce contact terms in  $R$  associated to the conical and helical singularities on  $\gamma$ . To proceed, we consider the regulated geometry introduced in section 2.2. On this smooth regulated geometry, which we will indicate by subscript  $\text{reg}(\varepsilon)$ , let us consider the integral  $\int_{\mathcal{N}_\varepsilon} (\varepsilon R)_{\text{reg}(\varepsilon)}$  of curvature over the small neighbourhood  $\mathcal{N}_\varepsilon$  of  $\gamma$ . To write the integrand in terms of metric components, we use eqs. (2.25) and (2.26) for Ricci curvature and eqs. (2.21), (2.22) and (2.24) for extrinsic curvature. Now recall that we have required metric components to behave like eq. (2.4) in the unregulated configuration, but our regulation procedure interpolates the metric in  $\mathcal{N}_\varepsilon$  to be smooth on  $\gamma$ , as expressed in eq. (2.3). In light of all this, the terms contributing to  $\int_{\mathcal{N}_\varepsilon} (\varepsilon R)_{\text{reg}(\varepsilon)}$  that can survive the  $\varepsilon \rightarrow 0$  limit are<sup>24</sup>

$$\begin{aligned} \int_{\mathcal{N}_\varepsilon} (\varepsilon R)_{\text{reg}(\varepsilon)} \sim & -2 \int_{\partial\mathcal{N}_\varepsilon - \partial\mathcal{N}_0} (u^A \varepsilon_A \nabla_B u^B)_{\text{reg}(\varepsilon)} - \int_{\mathcal{N}_\varepsilon} \left( \varepsilon \frac{h_{ij} \partial_\rho N^i \partial_\rho N^j}{2N^2} \right)_{\text{reg}(\varepsilon)} \\ & + \int_{\mathcal{N}_\varepsilon} \left[ \varepsilon \frac{(h^{ij} h^{kl} - h^{ik} h^{jl}) \mathcal{L}_{\vec{N}} h_{ij} \mathcal{L}_{\vec{N}} h_{kl}}{4N^2} \right]_{\text{reg}(\varepsilon)}. \end{aligned} \quad (2.27)$$

We will now discuss the RHS term by term, for example, pointing out where they come from and explaining how they can survive the  $\varepsilon \rightarrow 0$  limit even though the neighbourhood  $\mathcal{N}_\varepsilon$  shrinks to zero size.

The first term of eq. (2.27) arises from the total derivative in eq. (2.25). In particular,

$$2 \int_{\partial\mathcal{N}_0} (u^A \varepsilon_A \nabla_B u^B)_{\text{reg}(\varepsilon)} \sim 4\pi \text{Area}(\gamma) \quad (2.28)$$

results from the divergence  $\nabla_B u^B$  being singular at  $\gamma$  even on smooth geometries. Here,  $\mathcal{N}_0$  is an infinitesimal neighbourhood of  $\gamma$  in the regulated geometry.<sup>25</sup> From eq. (2.19), we see that we can also write the integral on  $\partial\mathcal{N}_\varepsilon$  as

$$-2 \int_{\partial\mathcal{N}_\varepsilon} u^A \varepsilon_A \nabla_B u^B = -2 \int_{\partial\mathcal{N}_\varepsilon} u^A \varepsilon_A (K_u)^b{}_b. \quad (2.29)$$

The second term of eq. (2.27) comes from the second term in eq. (2.22) and is more subtle to interpret. Due to the regulating interpolation, the derivatives  $\partial_\rho N^i_{\text{reg}(\varepsilon)}$  become large and cause this term to diverge in the  $\varepsilon \rightarrow 0$  limit. Note, however, that the divergence is quadratic in the helical singularity parameter  $v^i$  setting the size of the shift  $N^i$ .

Let us recall that a similar situation arises for conical singularities in higher curvature theories, say with an  $R^2$  term in the Lagrangian. The resulting action diverges on conical singularities  $\gamma$  of finite strength. However, taking the action around  $\gamma$  and linearizing with respect to the singularity strength<sup>26</sup>, one can extract a linear coefficient which is finite and can be identified as the geometric entropy of the surface  $\gamma$  [16]. Conical singularities of finite

<sup>24</sup>We orient boundaries so that Stokes' theorem takes the standard form  $\int_{\mathcal{N}} d\omega = \int_{\partial\mathcal{N}} \omega$ . A minus sign  $-\partial\mathcal{N}$  indicates reversal of orientation.

<sup>25</sup>Equation (2.28) is not written as an equality at finite  $\varepsilon$  because  $\gamma$  (and thus  $\partial\mathcal{N}_0$ ) may not necessarily lie exactly at  $\rho = 0$  in the regulated geometry as commented in footnote 20.

<sup>26</sup>As ref. [16] emphasizes, linearization of the action requires greater care than naively linearizing the Lagrangian. Specifically, ref. [16] considers linearizing the difference in action between a conically singular

strength do appear in the calculation of Rényi entropies using orbifold geometries [15] and in states of fixed geometric entropy. In the former case, the singularity strength is fixed and a good variational principle is obtained from the bulk action evaluated over  $\mathcal{M} \setminus \mathcal{N}_\varepsilon$ , excluding a neighbourhood  $\mathcal{N}_\varepsilon$  of the singular surface  $\gamma$ , possibly supplemented by counterterms near  $\gamma$  [14]. Indeed, the conical singularity is an artifact of the orbifold and should not contribute to the action in the Rényi calculation [15]. In contrast, to obtain a good variational principle with fixed geometric entropy, one must perform a Legendre transform which effectively reinstates, in the action, a contribution from the conical singularity equal to the singularity strength times the geometric entropy [14].

Later in this paper, we will study path integrals where quantities conjugate to the conical, helical, and holonomic singularity strengths are fixed on  $\gamma$ , analogous to the situation of fixed geometric entropy described above. One might therefore guess that the appropriate action should only include contributions from the singularity that are *linear* in the singularity strengths. This guess will be partially justified in sections 3.2 and 3.3 by examining the variational principle that results from such an action. For now, let us simply treat the second term of eq. (2.27) by keeping only the contribution linear in the strength  $v^i$  of the helical singularity (of the original unregulated geometry). The result is:

$$- \int_{\mathcal{N}_\varepsilon} \left( \epsilon \frac{h_{ij} \partial_\rho N^i \partial_\rho N^j}{2N^2} \right)_{\text{reg}(\varepsilon)} \sim - \int_{\partial \mathcal{N}_\varepsilon} u^A \epsilon_A \frac{N_i \partial_\rho N^i}{N^2} \quad (\text{part linear in } v^i) \quad (2.32)$$

$$= -2 \int_{\partial \mathcal{N}_\varepsilon} u^A \epsilon_A (d\tau)_a N_i (K_u)^{ai}, \quad (2.33)$$

which remains finite in the  $\varepsilon \rightarrow 0$  limit, as can be seen from eq. (2.4). The linear dependence on  $v^i$  enters through the undifferentiated shift  $N^i$ .

Finally, the second line of eq. (2.27) comes from the second term of eq. (2.24). In  $D = 3$  spacetime dimensions, the codimension-two metric  $h_{ij}$  has only one component and, consequently, the numerator causes the second line of eq. (2.27) to vanish identically. This case of  $D = 3$  will be the primary focus in later sections of this paper.

---

geometry and its smooth regulated counterpart,

$$\partial_\kappa \left( \int_{\mathcal{M}} L_{\text{reg}(\varepsilon)} - \int_{\mathcal{M} \setminus \mathcal{N}_0} L \right)_{\kappa=1} = \partial_\kappa \left( \int_{\mathcal{N}_\varepsilon} L_{\text{reg}(\varepsilon)} - \int_{\mathcal{N}_\varepsilon \setminus \mathcal{N}_0} L \right)_{\kappa=1} \quad (2.30)$$

with respect to the opening angle  $2\pi\kappa$  varied from its smooth value  $2\pi$ . Due to the smoothing of the configuration,  $\partial_\kappa L_{\text{reg}(\varepsilon)}$  remains uniformly bounded over  $\mathcal{N}_\varepsilon$  as  $\kappa \rightarrow 1$ , so

$$\partial_\kappa \left( \int_{\mathcal{N}_\varepsilon} L_{\text{reg}(\varepsilon)} \right)_{\kappa=1} = \int_{\mathcal{N}_\varepsilon} (\partial_\kappa L_{\text{reg}(\varepsilon)})_{\kappa=1}. \quad (2.31)$$

However, the same is not true for the Lagrangian  $L$  of the original singular configuration. In particular, ref. [16] showed that higher curvature terms in  $L$  can be equal to  $(\kappa - 1)^2$  times integrands which become increasingly singular near  $\gamma$  until they are nonintegrable in the  $\kappa \rightarrow 1$  limit. The integration can therefore produce an inverse power of  $\kappa - 1$ , promoting the  $\mathcal{O}((\kappa - 1)^2)$  terms of  $L$  to  $\mathcal{O}(\kappa - 1)$  terms of the action.

An analogous mechanism does not appear to be at play in the current calculation, but perhaps a more careful analysis is warranted.

However, let us also comment briefly on the case of  $D > 3$ , where this term does not vanish identically. For  $D > 3$ , the integrand would in fact generically diverge like  $1/\rho$  at  $\gamma$ , were it not for the regulation  $\text{reg}(\varepsilon)$  which interpolates the integrand to zero on  $\gamma$ . If we view this interpolation as a fuzzy cutoff for the integral at some  $\rho = \varepsilon'$  between 0 and  $\varepsilon$ , then the term on the second line of eq. (2.27) merely shifts the cutoff surface for its counterpart integrated over  $\mathcal{M} \setminus \mathcal{N}_\varepsilon$ :

$$\begin{aligned} & \int_{\mathcal{M}=\mathcal{N}_\varepsilon+(\mathcal{M}\setminus\mathcal{N}_\varepsilon)} \left[ \epsilon \frac{(h^{ij}h^{kl} - h^{ik}h^{jl})\mathcal{L}_{\vec{N}}h_{ij}\mathcal{L}_{\vec{N}}h_{kl}}{4N^2} \right]_{\text{reg}(\varepsilon)} \\ & \sim \int_{\mathcal{M}\setminus\mathcal{N}_{\varepsilon'}} \epsilon \frac{(h^{ij}h^{kl} - h^{ik}h^{jl})\mathcal{L}_{\vec{N}}h_{ij}\mathcal{L}_{\vec{N}}h_{kl}}{4N^2}. \end{aligned} \quad (2.34)$$

The fact that the second line of eq. (2.27) remains *finite* in the  $\varepsilon \rightarrow 0$  limit simply reflects the fact that the above is *logarithmically divergent* in the  $\varepsilon' \rightarrow 0$  limit. How should we handle this potential divergence in  $\int_{\mathcal{M}\setminus\mathcal{N}_\varepsilon} \epsilon R$  as  $\varepsilon \rightarrow 0$ ? Should we perhaps only allow those helical singularities for which

$$(h^{ij}h^{kl} - h^{ik}h^{jl})\mathcal{L}_v h_{ij}\mathcal{L}_v h_{kl} = 0 \quad (2.35)$$

on  $\gamma$ ? We will leave these questions for future work and retreat to cases where eq. (2.35) is satisfied, as in  $D = 3$ .

In summary, we argue that the natural analogue of  $\int_{\mathcal{M}} \epsilon R$  in the presence of the conically and helically singular surface  $\gamma$  is  $\int_{\mathcal{M}\setminus\mathcal{N}_\varepsilon} \epsilon R$  plus the contributions (2.28), (2.29) and (2.33) accounting for contact terms from the singularity. Aside from the above derivation, we will see in sections 3 and 4 how the incorporation of such contact terms in the gravitational action leads to a reasonable variational principle and thermodynamically intuitive interpretations of the gravitational partition function.

### 2.3.2 Maxwell field strength

It is relatively straightforward to also deduce a contact term in the Maxwell field strength  $F = dA$  resulting from eq. (2.15):

$$\int_{\mathcal{D}_\varepsilon} F = \int_{\partial\mathcal{D}_\varepsilon} A \sim 2\pi(\mu + v^i A_i). \quad (2.36)$$

Here,  $\mathcal{D}_\varepsilon$  is an  $\varepsilon$ -disk punctured by  $\gamma$  (with orientation chosen so that  $\int_{\partial\mathcal{D}_\varepsilon} d\tau = 2\pi$ ). Clearly,  $F$  possesses a  $\delta$ -function contact term at  $\gamma$  in its orthogonal plane.

We would also like to understand how to integrate the squared field strength  $\int_{\mathcal{M}} F \wedge *F$  on such singular configurations. The naive integral diverges because the integrand contains a squared  $\delta$ -function, but this pathology can be treated analogously to eq. (2.32), where we linearized with respect to the strength of the singularity. Let us again consider an  $\varepsilon$ -regulated configuration as described in section 2.2. Writing out

$$F \wedge *F = \frac{1}{2} \epsilon F_{AB} F^{AB} = \epsilon \left[ (n^a \partial_\rho A_a)^2 + n^a n^b h^{ij} F_{ai} F_{bj} + h^{ij} \partial_\rho A_i \partial_\rho A_j + \frac{1}{2} F_{ij} F^{ij} \right] \quad (2.37)$$



in radial gauge eq. (2.12), we again recognize the dangerous first term as a squared  $\rho$ -derivative of the interpolated field  $A_{\text{reg}(\varepsilon)}$  in the regulated configuration. As in the helical case, linearization with respect to the (unregulated) singularity strength, here  $\mu$  in eq. (2.14), produces the desired result:

$$\int_{\mathcal{N}_\varepsilon} (F \wedge *F)_{\text{reg}(\varepsilon)} \sim 2 \int_{\partial \mathcal{N}_\varepsilon} A \wedge *F . \quad (\text{part linear in } \mu) \quad (2.38)$$

Actually, in writing eq. (2.38), we have made an assumption analogous to eq. (2.35), namely that the second term on the RHS of eq. (2.37) is sufficiently tame near  $\gamma$  that  $\int_{\mathcal{M} \setminus \mathcal{N}_\varepsilon} \epsilon n^a n^b h^{ij} F_{ai} F_{bj}$  converges as  $\varepsilon \rightarrow 0$ . This can be understood as the physical statement that the electric field  $n^a F_{ai}$  on constant time  $\tau$  surfaces does not diverge like  $\rho^{-1}$  or worse as  $\rho \rightarrow 0$ . (Moreover, note that the normal electric field  $n^A u^B F_{AB} = \mathcal{O}(\rho^0)$ , which is the relevant component of the field strength on the RHS of eq. (2.38), is finite by virtue of eqs. (2.4), (2.8) and (2.14).)

### 3 Action for singular configurations

In section 2, we have specified a class of codimension-two singularities which we want to include in the gravitational path integral. The weight of each configuration in the path integral is of course determined by an action. Our goal in this section will firstly be to define an action for singular configurations and secondly, by varying the action, to determine sufficient conditions that pick out saddles and constrained saddles for the path integral.

#### 3.1 Proposal for the action

Making use of the curvature contact terms suggested in section 2.3 for the types of singularities described in section 2.1 on the codimension-two surface  $\gamma$ , we now propose an action for Einstein-Hilbert-Maxwell theory including such singularities. Again we denote the full  $D$ -dimensional Euclidean spacetime by  $\mathcal{M}$  and an  $\varepsilon$ -neighbourhood of  $\gamma$  by  $\mathcal{N}_\varepsilon$ . Then the action we propose is

$$I = \int_{\mathcal{M} \setminus \mathcal{N}_\varepsilon} (L_{\text{EH}} + L_{\text{M}}) + \int_{\partial \mathcal{M}} L_{\partial \mathcal{M}} - \frac{\text{Area}(\gamma)}{4G_{\text{N}}} + \int_{-\partial \mathcal{N}_\varepsilon} (L_{\text{GH}} + L_{\text{hel}} + L_{\text{hol}}) , \quad (3.1)$$

where we will now define each term on the RHS.

The first integral contains the standard bulk Einstein-Hilbert and Maxwell Lagrangian densities,

$$L_{\text{EH}} = -\frac{1}{16\pi G_{\text{N}}}(R - 2\Lambda)\epsilon , \quad L_{\text{M}} = \frac{1}{2g_{\text{M}}^2} F \wedge *F . \quad (3.2)$$

We allow also for a spacetime boundary where a boundary Lagrangian  $L_{\partial \mathcal{M}}$  resides. Restricted to a set of boundary conditions to be specified later, we assume that the bulk  $\mathcal{M} \setminus \mathcal{N}_\varepsilon$  and boundary  $\partial \mathcal{M}$  actions give a good variational principle away from  $\gamma$ . In particular, surface terms resulting from the variation cancel on  $\partial \mathcal{M}$ . Of primary interest

to us are the remaining terms of eq. (3.1) which correspond directly to the contact terms we deduced in section 2.3.

Together with the area term, the integral of the Gibbons-Hawking Lagrangian density

$$L_{\text{GH}} = -\frac{1}{8\pi G_{\text{N}}} u^A \epsilon_A (K_u)^b{}_b \quad (3.3)$$

over  $-\partial \mathcal{N}_\varepsilon$  gives the action of the conical singularity at  $\gamma$ , as described by eqs. (2.27) to (2.29). These terms have already made an appearance in this context, for example in ref. [6]<sup>27</sup>. For later reference, as  $\rho \rightarrow 0$ , we have where .

The next term in eq. (3.1) has Lagrangian density

$$L_{\text{hel}} = -\frac{1}{8\pi G_{\text{N}}} u^A \epsilon_A (d\tau)^a N^i (K_u)_{ai} = -d\tau \wedge (p_{\text{BY}})_i N^i, \quad (3.4)$$

where we will later interpret the dual vector density on surfaces of constant  $(\rho, \tau)$ ,

$$(p_{\text{BY}})_i = -\frac{1}{8\pi G_{\text{N}}} (D-2)\epsilon (K_u)^{ab} n_a h_{bi}, \quad (3.5)$$

as a momentum density. (Recall, that  $(D-2)\epsilon$  is the volume form on surfaces of constant  $(\rho, \tau)$ , as introduced in eq. (2.10).) We have shown in eqs. (2.27) and (2.33) how this contact term in the action arises from a direct evaluation of the Einstein-Hilbert action on a regulated helical singularity. Ref. [10] suggested an identical term, evaluated on a time slice, for the purposes of obtaining a good variational principle when fixing  $(p_{\text{BY}})_i$ . We will make use of some of these results in section 3.2, where the connection to angular momentum will also become clear.

One might worry about the diffeomorphism invariance of the action, given the explicit appearance of  $\tau$  and  $N^i$  in eq. (3.4). Firstly, recall from section 2.2.1 that a choice of constant- $\tau$ -foliation near a helical singularity  $\gamma$  can be viewed as part of the specification of the physical internal structure of the singularity. That is, different choices of constant- $\tau$  surfaces lead to physically distinct configurations through our procedure for regulating the singularity. Secondly, on  $\partial \mathcal{N}_\varepsilon$ , note that diffeomorphisms along each surface of constant  $\tau$  can be dressed to  $\gamma$  by following radial geodesics orthogonal to  $\gamma$ ; in particular, over a given point on  $\gamma$ , a circle  $\mathcal{C}_\varepsilon \subset \mathcal{N}_\varepsilon$  is unambiguously picked out by these radial geodesics. The shift vector  $N^i$  is the projection of the tangent  $\partial_\tau$  of this circle onto surfaces of constant  $\tau$ . The only possible remaining redundancies are reparametrizations of the circle  $\mathcal{C}_\varepsilon$ , which correspond to purely  $\tau$ -dependent reparametrizations  $\tau \mapsto f(\tau)$ . We have already implicitly fixed this redundancy (up to a constant) by requiring the lapse  $N(y)$  to be constant in  $\tau$ . But, even if we had not, the combination  $d\tau_a N^i$  would be invariant under such reparametrizations regardless. On a cutoff surface  $\partial \mathcal{N}_\varepsilon$  at constant proper separation from  $\gamma$ , the Lagrangian density eq. (3.4) is thus unambiguously defined. (We will explore the possibility of other choices of cutoff surfaces in section 3.1.1.)

Finally, the last term in eq. (3.1) with Lagrangian density

$$L_{\text{hol}} = -\frac{1}{2g_{\text{M}}} A \wedge *F \quad (3.6)$$

---

<sup>27</sup>See section 5 for more direct comparison to [6] in Lorentzian signature.

corresponds to the contact term eq. (2.38) resulting from the generically nontrivial holonomic singularity (2.14) around  $\gamma$ .

### 3.1.1 (In)dependence on the cutoff shape

As initially defined in section 2.2, the neighbourhood  $\mathcal{N}_\varepsilon$  around the singularity  $\gamma$  has been chosen thus far to be a solid tube of constant proper radius from  $\gamma$  as measured by  $\rho$ . What about other choices  $\tilde{\mathcal{N}}_\varepsilon$ , where the cutoff surface  $\partial\tilde{\mathcal{N}}_\varepsilon$  is not a surface of constant  $\rho$ ? In particular, suppose instead that  $\partial\tilde{\mathcal{N}}_\varepsilon$  is a surface of constant  $\tilde{\rho}$  of order  $\varepsilon$ , where the new coordinate  $\tilde{\rho}$  is related to  $\rho$  by

$$\rho = \tilde{\rho} e^{f(x)}, \quad (3.7)$$

for some function  $f(x)$  of  $x^a = (\tau, y^i)$ . We would like to understand whether the action (3.1) is sensitive to the choice of  $f$ . We will find below that, provided that  $f$  is a function of only  $\tau$  (*i.e.* is constant in  $y^i$ ) in some neighbourhood of each connected component of  $\gamma$ , the action is insensitive to the choice of  $f$  in the  $\varepsilon \rightarrow 0$  limit. This can become particularly useful in the Lorentzian context where it might be more natural to consider a cutoff surface  $\partial\tilde{\mathcal{N}}_\varepsilon$  at non-constant proper separation from  $\gamma$ .

As we will explicitly see below, the surface integral  $\int_{-\partial\tilde{\mathcal{N}}_\varepsilon}$  in the action (3.1) converges in the  $\varepsilon \rightarrow 0$  limit, for arbitrary  $f$  and the class of singularities allowed on  $\gamma$  as described in section 2.1. If we restrict to configurations with finite action per finite area on  $\gamma$ , then the bulk integral  $\int_{\mathcal{M} \setminus \tilde{\mathcal{N}}_\varepsilon}$  should therefore also converge in the  $\varepsilon \rightarrow 0$  limit. Moreover, from our study of curvatures in section 2.3, it becomes apparent that the  $\varepsilon \rightarrow 0$  limit of these bulk terms, should it exist, is insensitive to the choice of  $f$ . We need therefore only consider the  $f$ -dependence of the surface terms on  $\partial\tilde{\mathcal{N}}_\varepsilon$  which is now a surface of constant  $\tilde{\rho}$ .

To be explicit, let  $\tilde{u}^A$ ,  $\tilde{g}_{ab}$ ,  $\tilde{g}^{ab}$ , and  $(\tilde{K}_{\tilde{u}})_{ab}$  respectively be the unit normal, induced metric, its inverse, and extrinsic curvature on surfaces of constant  $\tilde{\rho}$ . Using the same  $\tau$  coordinate as before, we obtain a  $(D-2)+1$  decomposition of  $\tilde{g}_{ab}$  analogous to eq. (2.2), in terms of a lapse  $\tilde{N}$ , shift  $\tilde{N}^i$ , and  $(D-2)$ -dimensional metric  $\tilde{h}_{ij}$ .

Consider first the gravitational surface terms. The Gibbons-Hawking and helical surface Lagrangian densities on  $-\partial\tilde{\mathcal{N}}_\varepsilon$  are taken to be

$$\tilde{L}_{\text{GH}} = -\frac{1}{8\pi G_{\text{N}}} \tilde{u}^A \epsilon_A \tilde{g}^{ab} (\tilde{K}_{\tilde{u}})_{ab}, \quad (3.8)$$

$$\tilde{L}_{\text{hel}} = -\frac{1}{8\pi G_{\text{N}}} \tilde{u}^A \epsilon_A (d\tau)_a \tilde{g}^{ab} \tilde{N}^i (\tilde{K}_{\tilde{u}})_{bi}. \quad (3.9)$$

We want to compare these densities with the  $f=0$  case intended in eqs. (3.3) and (3.4) on a surface  $-\partial\mathcal{N}_\varepsilon$  of constant proper separation  $\rho$  from  $\gamma$ . To do so, it is helpful to pull back all densities to a common space  $S^1 \times \gamma$  with coordinates  $x^a = (\tau, y^i)$ :

$$\begin{array}{ccc} S^1 \times \gamma & \xrightarrow{\phi_\varepsilon} & \partial\mathcal{N}_\varepsilon \\ & \downarrow \tilde{\phi}_\varepsilon & \\ & \partial\tilde{\mathcal{N}}_\varepsilon & \end{array} \quad (3.10)$$

We will denote the respective pullbacks by  $\phi_\varepsilon^*$  and  $\tilde{\phi}_\varepsilon^*$ . For brevity, we will write  $\phi_{\varepsilon \rightarrow 0}^* = \lim_{\varepsilon \rightarrow 0} \phi_\varepsilon^*$  and  $\tilde{\phi}_{\varepsilon \rightarrow 0}^* = \lim_{\varepsilon \rightarrow 0} \tilde{\phi}_\varepsilon^*$ .

With the original choice of cutoff surface  $\partial \mathcal{N}_\varepsilon$  at constant proper separation from  $\gamma$ , we find

$$\phi_{\varepsilon \rightarrow 0}^* L_{\text{GH}} = \frac{1}{8\pi G_{\text{N}}} \kappa \, d\tau \wedge {}^{(D-2)}\epsilon , \quad (3.11)$$

$$\phi_{\varepsilon \rightarrow 0}^* L_{\text{hel}} = -v^i \, d\tau \wedge (p_{\text{BY}})_i . \quad (3.12)$$

(Here,  ${}^{(D-2)}\epsilon$  as introduced in eq. (2.10) is the volume form on surfaces of constant  $(\rho, \tau)$ , implicitly evaluated above at  $\rho \rightarrow 0$ , thus giving the volume form on  $\gamma$ . Similarly,  $(p_{\text{BY}})_i$  is implicitly the  $\rho \rightarrow 0$  limit of the momentum density eq. (3.5). These are then interpreted in the obvious way as forms on  $S^1 \times \gamma$  in the above RHSs.) However, with a more general cutoff surface  $\partial \tilde{\mathcal{N}}_\varepsilon$ ,

$$\tilde{\phi}_{\varepsilon \rightarrow 0}^* \tilde{L}_{\text{GH}} = \phi_{\varepsilon \rightarrow 0}^* \left( L_{\text{GH}} - \frac{u^A \epsilon_A \rho}{8\pi G_{\text{N}}} \left\{ \frac{1}{2} n^a \partial_a f n^b \partial_b \log [1 + (\rho n^c \partial_c f)^2] - D_a D^a f \right\} \right) \quad (3.13)$$

$$\begin{aligned} \tilde{\phi}_{\varepsilon \rightarrow 0}^* \tilde{L}_{\text{hel}} = \phi_{\varepsilon \rightarrow 0}^* \left( L_{\text{hel}} - \frac{u^A \epsilon_A \rho}{16\pi G_{\text{N}}} \left\{ n^a \partial_a f \frac{N^i}{N} \partial_i \log [1 + (\rho n^c \partial_c f)^2] \right. \right. \\ \left. \left. - N^i \partial_i \frac{n^a \partial_a f}{N} - \frac{N^a h_{ab}}{N} \mathcal{L}_n (h^{bc} \partial_c f) \right\} \right) , \end{aligned} \quad (3.14)$$

where  $\mathcal{L}_\bullet$  denotes a Lie derivative.

In the absence of a helical singularity, in the  $\varepsilon \rightarrow 0$  limit, the Gibbons-Hawking action  $\int_{-\partial \tilde{\mathcal{N}}_\varepsilon} \tilde{L}_{\text{GH}}$  becomes insensitive to  $f(x)$  and the helical action  $\int_{-\partial \tilde{\mathcal{N}}_\varepsilon} \tilde{L}_{\text{hel}}$  vanishes. To see the insensitivity of  $\int_{-\partial \tilde{\mathcal{N}}_\varepsilon} \tilde{L}_{\text{GH}}$ , consider the terms in braces in eq. (3.13), of which the second is already manifestly a total derivative. Meanwhile, using the identity

$$\frac{d}{dx} [F(x) - \arctan F(x)] = \frac{1}{2} F(x) \log [1 + F^2(x)] , \quad (3.15)$$

applied with  $F = \rho n^c \partial_c f$ , the other term can be recast, to non-vanishing order, as a total  $\tau$ -derivative that integrates to zero over the  $S^1$  circle.<sup>28</sup> This is necessarily true only because  $N n^a \sim (\partial_\tau)^a$  when the helical shift  $v^i$  vanishes.

In the presence of a helical singularity, we must combine the first terms in the braces on the RHSs of eqs. (3.13) and (3.14) to obtain a total  $\tau$ -derivative. Together, the sum of eqs. (3.13) and (3.14) can be expressed as

$$\begin{aligned} \tilde{\phi}_{\varepsilon \rightarrow 0}^* \left( \tilde{L}_{\text{GH}} + \tilde{L}_{\text{hel}} \right) = \phi_{\varepsilon \rightarrow 0}^* \left( L_{\text{GH}} + L_{\text{hel}} - \frac{u^A \epsilon_A}{8\pi G_{\text{N}}} \left\{ -\frac{1}{N} \partial_\tau \arctan (\rho n^c \partial_c f) \right. \right. \\ \left. \left. + \rho \partial_a f D_b \frac{n^a N^b}{N} \right\} \right) , \end{aligned} \quad (3.16)$$

<sup>28</sup>As below, we have used the fact that  $\sqrt{\det g}/N = \sqrt{\det h}$  becomes  $\tau$ -independent as  $\rho \rightarrow 0$ .

where we have used the fact that  $h_{ij}$  and thus  $\sqrt{\det g}/N = \sqrt{\det h}$  are  $\tau$ -independent as  $\rho \rightarrow 0$ . Also because of this fact, the first term in the braces gives a non-contributing total  $\tau$ -derivative. However, for generic  $f(x)$ , the remaining extraneous term seems to contribute an unwanted mismatch between  $\int_{-\partial\tilde{\mathcal{N}}_\varepsilon}(\tilde{L}_{\text{GH}} + \tilde{L}_{\text{hel}})$  and  $\int_{-\partial\mathcal{N}_\varepsilon}(L_{\text{GH}} + L_{\text{hel}})$ .

This mismatch disappears when  $f$ , in some neighbourhood of each connected component of  $\gamma$ , is a function only of  $\tau$  and not the directions  $y^i$  along  $\gamma$ . To see this, we express the extraneous term as

$$-\frac{u^A \epsilon_A \rho}{8\pi G_{\text{N}}} \partial_a f D_b \frac{n^a N^b}{N} = -\frac{\rho}{8\pi G_{\text{N}}} \frac{u^A \epsilon_A}{N} \partial_a f \left( N^b D_b n^a + n^a d_i N^i \right), \quad (3.17)$$

where  $d_i$  is the covariant derivative associated to  $h_{ij}$ . On the RHS, the first term vanishes because  $n^a$  is a unit normal so  $N^b D_b n^a$  is tangential to surfaces of constant  $\tau$ . The second term, involving  $n^a \partial_a f(\tau) = \partial_\tau f(\tau)/N$  for each connected component of  $\gamma$ , again contributes a total  $\tau$ -derivative, provided  $d_i N^i/N$  is also  $\tau$ -independent at leading order in the  $\rho \rightarrow 0$  limit. Alternatively, this term is a total  $y^i$ -derivative to finite order if  $N$  is invariant under the flow generated by  $N^i$  at leading order as  $\rho \rightarrow 0$  (*i.e.*  $N^i \partial_i N$  vanishes faster than  $\rho$ ). Thus, we conclude that, given the  $\tau$ -independence of  $\lim_{\rho \rightarrow 0} h_{ij}$ ,  $\kappa$ , and  $v^i$  or given the  $\tau$ -independence of  $\lim_{\rho \rightarrow 0} h_{ij}$  and the shift invariance  $v^i \partial_i \kappa = 0$ , the surface terms  $\int_{-\partial\tilde{\mathcal{N}}_\varepsilon}(\tilde{L}_{\text{GH}} + \tilde{L}_{\text{hel}})$  of the action are insensitive to the time profile  $f(\tau)$  of each connected component of the cutoff surface  $\partial\tilde{\mathcal{N}}_\varepsilon$ .

Finally, let us consider the Maxwell surface term  $\int_{-\partial\tilde{\mathcal{N}}_\varepsilon} L_{\text{hol}}$ , where the Lagrangian density  $L_{\text{hol}}$  is again given by eq. (3.6). We simply have

$$\tilde{\phi}_{\varepsilon \rightarrow 0}^* L_{\text{hol}} = \phi_{\varepsilon \rightarrow 0}^* L_{\text{hol}} = -\frac{1}{g_{\text{M}}^2} \mu \, d\tau \wedge *F, \quad (3.18)$$

provided, as previously mentioned below eq. (2.38), the electric field  $n^a F_{ai}$  does not diverge like  $\rho^{-1}$  or worse as  $\rho \rightarrow 0$ . (On the RHS,  $*F$  is implicitly understood in the  $\rho \rightarrow 0$  limit and viewed as a form on  $S^1 \times \gamma$  in the obvious way.) Thus,  $\int_{-\partial\tilde{\mathcal{N}}_\varepsilon} L_{\text{hol}}$  is insensitive, in the  $\varepsilon \rightarrow 0$  limit, to the profile  $f(x)$  of the cutoff surface  $\partial\tilde{\mathcal{N}}_\varepsilon$ .

In summary, assuming  $\lim_{\rho \rightarrow 0} h_{ij}$  is  $\tau$ -independent as required for  $\gamma$  to have a well-defined induced metric, we altogether have

$$\begin{aligned} & \tilde{\phi}_{\varepsilon \rightarrow 0}^* \left( \tilde{L}_{\text{GH}} + \tilde{L}_{\text{hel}} + L_{\text{hol}} \right) \\ &= d\tau \wedge \left[ \frac{\kappa}{8\pi G_{\text{N}}} \, {}^{(D-2)}\epsilon - v^i (p_{\text{BY}})_i - \frac{\mu}{g_{\text{M}}^2} *F - \frac{f'(\tau) d_i v^i}{8\pi G_{\text{N}} \kappa} \, {}^{(D-2)}\epsilon \right] \end{aligned} \quad (3.19)$$

for any profile  $f(\tau)$  of the cutoff surface  $\partial\tilde{\mathcal{N}}_\varepsilon$  with arbitrary dependence only on time  $\tau$ . We conclude that, if  $\kappa$  and  $v^i$  are also  $\tau$ -independent or if  $\kappa$  is invariant under the helical shift  $v^i$ , then the last term above is a total derivative and any time profile  $f(\tau)$  for each connected component of the cutoff surface  $\partial\tilde{\mathcal{N}}_\varepsilon$  can be used to evaluate the action (3.1), without altering the value of the action. This fact will be useful when we eventually turn to Lorentzian signature in section 5. For the sake of simplicity, however, for now we will return to working with cutoff surfaces  $\partial\mathcal{N}_\varepsilon$  at constant proper separation  $\rho$  from the singularity  $\gamma$ .

### 3.2 Variation of the action

We will now evaluate the variation of the action eq. (3.1). In the process, conjugacy between various quantities on  $\partial\mathcal{N}_\varepsilon$  will become apparent. A surface stress tensor, as well as angular momentum and electric charge densities here, will be introduced.

Varying the bulk Lagrangians,

$$\delta(L_{\text{EH}} + L_{\text{M}}) = (E_{\text{EHM}})^{AB}\delta G_{AB} + (E_{\text{M}})^A\delta A_A + \text{d}(\theta_{\text{EH}} + \theta_{\text{M}}) \quad (3.20)$$

produces the Einstein-Hilbert-Maxwell equations of motion (as densities)  $E_{\text{EHM}}$  and  $E_{\text{M}}$ , together with surface terms. As previously mentioned, surface terms at  $\partial\mathcal{M}$  cancel in variations subject to boundary conditions,

$$\int_{\partial\mathcal{M}} (\theta_{\text{EH}} + \theta_{\text{M}} + \delta L_{\partial\mathcal{M}}) = 0. \quad (3.21)$$

Meanwhile, on  $\partial\mathcal{N}_\varepsilon$ , we have the standard result

$$\pi_{\partial\mathcal{N}_\varepsilon}\theta_{\text{EH}} + \delta L_{\text{GH}} = -\frac{1}{2}u^A\epsilon_A(T_{\text{BY}})^{ab}\delta g_{ab}, \quad (3.22)$$

where the surface, *i.e.* Brown-York, stress tensor is given by<sup>29</sup>

$$(T_{\text{BY}})^{ab} = -\frac{1}{8\pi G_{\text{N}}}\left[(K_u)^{ab} - g^{ab}(K_u)^c{}_c\right]. \quad (3.23)$$

From a radial evolution perspective, eq. (3.22) is the standard Einstein-Hilbert presymplectic potential density, so the coefficient of  $\delta g_{ab}$  there is understood as the canonical momentum of the induced metric  $g_{ab}$  on  $\partial\mathcal{N}_\varepsilon$ . Note that presymplectic potential densities related by field space exact one-forms, *e.g.*  $\delta L_{\text{GH}}$ , lead to the same presymplectic density  $\omega = \delta\theta$  (where  $\delta$  is the field space exterior derivative).

We will find it helpful to apply the  $(D-2)+1$  decomposition (2.2) to eq. (3.22) [10]:

$$\pi_{\partial\mathcal{N}_\varepsilon}\theta_{\text{EH}} + \delta L_{\text{GH}} = \text{d}\tau \wedge [e_{\text{BY}}\delta N + (p_{\text{BY}})_i\delta N^i] - \frac{1}{2}u^A\epsilon_A T^{ij}\delta h_{ij} \quad (3.24)$$

where the surface energy and (angular) momentum densities are given by<sup>30</sup>

$$e_{\text{BY}} = {}^{(D-2)}\epsilon (T_{\text{BY}})^{ab}n_a n_b = \frac{1}{8\pi G_{\text{N}}} {}^{(D-2)}\epsilon (K_u)^i{}_i \quad (3.25)$$

and, as in eq. (3.5),

$$(p_{\text{BY}})^i = {}^{(D-2)}\epsilon (T_{\text{BY}})^{ab}n_a h_b^i = -\frac{1}{8\pi G_{\text{N}}} {}^{(D-2)}\epsilon (K_u)^{ab}n_a h_b^i, \quad (3.26)$$

<sup>29</sup>Note that we are currently in Euclidean signature — *c.f.* eq. (5.14). The signs in eqs. (3.22) and (3.23) are because  $u^A$  is directed radially outward, so the orientation on  $-\partial\mathcal{N}_\varepsilon$  as part of  $\partial(\mathcal{M}\setminus\mathcal{N}_\varepsilon)$  is  $-u^A\epsilon_A$ .

<sup>30</sup>Our extrinsic curvature  $K_u$  is the negative of the extrinsic curvature  $K$  in ref. [10], because the subscript reminds us that  $K_u$  is defined using the vector  $u$  which, near  $\gamma$ , points *into* the spacetime region  $\mathcal{M}\setminus\mathcal{N}_\varepsilon$ . Our  $e_{\text{BY}}$  and  $p_{\text{BY}}$  are thus equal to  $-{}^{(D-2)}\epsilon = u^A n^B \epsilon_{AB}$  times the  $q$  and  $j$  defined in ref. [10]'s eq. (2.9) and (2.10). When comparing our eq. (3.30) to ref. [10]'s eq. (4.3), one should be wary of the orientation  $-u^A\epsilon_A$  of  $-\partial\mathcal{N}_\varepsilon$ .

where  $(^{D-2})\epsilon$  is the volume form on surfaces of constant  $(\rho, \tau)$ , as defined in eq. (2.10). The variation of the above can be easily combined with eq. (3.24):

$$\pi_{\partial\mathcal{N}_\epsilon}\theta_{\text{EH}} + \delta L_{\text{GH}} + \delta L_{\text{hol}} = d\tau \wedge [e_{\text{BY}} \delta N - \delta(p_{\text{BY}})_i N^i] - \frac{1}{2}u^A \epsilon_A (T_{\text{BY}})^{ij} \delta h_{ij}. \quad (3.27)$$

For the Maxwell field, the presymplectic potential density is

$$\theta_{\text{M}} = \frac{1}{g_{\text{M}}^2} \delta A \wedge *F, \quad (3.28)$$

or equivalently

$$\theta_{\text{M}} + \delta L_{\text{hol}} = -\frac{1}{g_{\text{M}}^2} A \wedge \delta(*F), \quad (3.29)$$

which both reproduce the usual conjugacy between the vector potential and the electric field on codimension-one surfaces.

Collecting together eqs. (3.20), (3.21), (3.27) and (3.29), the variation of the action (3.1) is given by

$$\begin{aligned} \delta I = & \int_{\mathcal{M} \setminus \mathcal{N}_\epsilon} [(E_{\text{EHM}})^{AB} \delta G_{AB} + (E_{\text{M}})^A \delta A_A] - \frac{\delta \text{Area}(\gamma)}{4G_{\text{N}}} \\ & + \int_{-\partial\mathcal{N}_\epsilon} \left\{ d\tau \wedge [e_{\text{BY}} \delta N - \delta(p_{\text{BY}})_i N^i] - \frac{1}{2}u^A \epsilon_A (T_{\text{BY}})^{ij} \delta h_{ij} - \frac{1}{g_{\text{M}}^2} A \wedge \delta(*F) \right\}. \end{aligned} \quad (3.30)$$

We have a good variational principle if the variation of the action reduces only to equations of motion while all other terms vanish when appropriate “boundary” conditions are imposed, in this context, on  $\partial\mathcal{N}_\epsilon$  in the  $\epsilon \rightarrow 0$  limit or  $\gamma$ .<sup>31</sup> In particular, as we will note in section 3.3.2, taking the  $\epsilon \rightarrow 0$  limit, the  $\int_{-\partial\mathcal{N}_\epsilon} d\tau \wedge e_{\text{BY}} \delta N$  term above vanishes and the  $\int_{-\partial\mathcal{N}_\epsilon} u^A \epsilon_A (T_{\text{BY}})^{ij} \delta h_{ij}$  term becomes proportional to  $\int_\gamma \delta (^{D-2})\epsilon$  where again  $(^{D-2})\epsilon$  is the volume form on  $\gamma$ . Therefore, we can say we have a good variational principle at fixed  $(^{D-2})\epsilon$ ,  $(p_{\text{BY}})_i$ , and  $*F$  along  $\gamma$ . Alternatively, in section 3.3.3, we will see that the surface terms in eq. (3.30) vanish also if we fix the area, integrated momentum density, and integrated electric flux on  $\gamma$ , and the singularity strengths satisfy some constancy conditions (3.57) to (3.59).<sup>32</sup>

### 3.3 Conditions for saddles and constrained saddles

We would now like to deduce conditions that must be satisfied by saddles of the action (3.1) by requiring that its variation (3.30) vanishes. Obviously, saddles must solve the bulk

<sup>31</sup>Recall we are assuming that we already have boundary conditions on  $\partial\mathcal{M}$  which make the variation surface terms there vanish, as written in (3.21).

<sup>32</sup>In this paper, we are not necessarily restricting our path integrals to be over configurations with constant singularity strengths. Rather, if we call the constancy conditions (3.57) to (3.59) “equations of motion”, we can also claim to have a good variational principle at fixed area, integrated momentum density, and integrated electric flux on  $\gamma$ . (As described in section 4, path integrals which fix these integrated quantities will come into play in our analysis of the gravitational partition function.)

gravitational and Maxwell equations of motion away from  $\mathcal{N}_\varepsilon$ ,

$$E_{\text{EHM}} = 0, \quad E_{\text{M}} = 0. \quad (3.31)$$

We would also like to understand the saddle-point conditions implied by the other terms of eq. (3.30) near the possibly singular surface  $\gamma$ . We will be further interested in constrained saddles where certain quantities are fixed near  $\gamma$ , thus restricting the set of possible field variations there.

### 3.3.1 Equations of motion near $\gamma$

Before proceeding, let us observe that some nontrivial conditions on  $\gamma$  and its embedding into (constrained) saddles can already be obtained from the bulk equations of motion (3.31). For example, let us consider the components of the gravitational equations of motion corresponding to “momentum constraints” on constant  $\rho$  surfaces. Let us take the expression (3.23) for the Brown-York stress tensor to define  $(T_{\text{BY}})^{ab}$  on any surface of small constant  $\rho$  in terms of the induced metric  $g_{ab}$  and extrinsic curvature  $(K_u)_{ab}$  of the surface. Then, the momentum constraints are equivalent to the conservation of  $(T_{\text{BY}})^{ab}$ ,

$$D_a (T_{\text{BY}})^{ab} = 0, \quad (3.32)$$

where again  $D_a$  is the covariant derivative associated to the metric  $g_{ab}$  on constant  $\rho$  surfaces. Let us focus on the component

$$n_a D_b (T_{\text{BY}})^{ab} = \frac{1}{8\pi G_{\text{N}}} \left[ h^{ij} \partial_\rho (k_n)_{ij} + \frac{1}{2} \partial_\rho h^{ij} (k_n)_{ij} + \frac{1}{2} d_i \frac{\partial_\rho N^i}{N} - \frac{\partial_\rho N^i \partial_i N}{N^2} \right] \quad (3.33)$$

written out here for a generically off-shell configuration, in terms of the  $(D-2)+1$  decomposition (2.2) of  $g_{ab}$  and the extrinsic curvature (2.24) of constant  $(\rho, \tau)$  slices. Again,  $d_i$  is the covariant derivative associated to  $h_{ij}$ . The first two terms of eq. (3.33) generically diverge in the  $\rho \rightarrow 0$  limit while the latter terms are  $\mathcal{O}(\rho^0)$ . To be explicit, let us write

$$h_{ij}(\rho, \tau, y) = h_{ij}^0(y) + h'_{ij}(\rho, \tau, y), \quad \lim_{\rho \rightarrow 0} h'_{ij}(\rho, \tau, y) = 0, \quad (3.34)$$

and use  $(h^0)^{ij}$  to denote the inverse of  $h_{ij}^0$  (against the prevailing convention of raising indices using  $h^{ij}$ ). Let us suppose that  $h'_{ij}$  generically vanishes slower than  $\rho^2$  as  $\rho \rightarrow 0$ , so that the latter two terms in eq. (3.33) can be neglected in the following. Then, we find

$$\begin{aligned} n_a D_b (T_{\text{BY}})^{ab} &= \frac{1}{8\pi G_{\text{N}}} \left\{ \frac{\partial_\rho N}{2N^2} (h^0)^{ij} \mathcal{L}_{\vec{N}} h_{ij}^0 - \frac{\partial_\rho N}{2N^2} \left[ (h^0)^{ij} (\partial_\tau - \mathcal{L}_{\vec{N}}) h'_{ij} + (h^0)^{ik} (h^0)^{j\ell} h'_{k\ell} \mathcal{L}_{\vec{N}} h_{ij}^0 \right] \right. \\ &\quad \left. + \frac{1}{2N} \left[ (h^0)^{ij} \partial_\rho (\partial_\tau - \mathcal{L}_{\vec{N}}) h'_{ij} + \frac{1}{2} (h^0)^{ik} (h^0)^{j\ell} \partial_\rho h'_{k\ell} \mathcal{L}_{\vec{N}} h_{ij}^0 \right] + \dots \right\}. \end{aligned} \quad (3.35)$$

The first term, of order  $\rho^{-2}$ , is dominant over all other terms at small  $\rho$ . The remaining terms on the RHS’s first line and the displayed terms on the last line are respectively of



order  $\rho^{-2} h'_{ij}$  and  $\rho^{-1} \partial_\rho h'_{ij}$ ; which of the two is larger is contingent on the  $\rho$ -dependence of  $h'_{ij}$ , but at least one of the two is larger than the omission  $\dots$ . The vanishing of eq. (3.35) to leading order implies that the helical shift  $N^i \sim v^i$  of  $\gamma$  is divergence-free:

$$0 = \frac{1}{2} (h^0)^{ij} \mathcal{L}_v h_{ij}^0 = d_i v^i . \quad (3.36)$$

Let us also consider for a moment  $v^i = 0$ , *i.e.* non-helical singularities, and suppose that  $h_{ij}$  has a small  $\rho$  expansion with first subleading term  $h'_{ij} = f_1(\rho, y) h_{ij}^1(\tau, y) + \dots$  for some  $f_1$  and  $h_{ij}^1$ . (*E.g.* for a power law expansion, as considered in ref. [14],  $f_1 = \rho^s$  for some  $s > 0$  possibly dependent on the strength of the conical singularity.) Then, we see that, the vanishing of eq. (3.35) generically<sup>33</sup> implies that  $(h^0)^{ij} \partial_\tau h_{ij}^1 = 0$ , which reproduces the well known extremality condition for the area of a conically singular surface  $\gamma$ .<sup>34</sup> More generally, in the presence of a nontrivial helical singularity, at least just from examining the component (3.33) alone, it appears that the helical shift  $v^i$  will muddle this would-be extremality condition.

We leave for future work a thorough analysis of conditions on  $\gamma$  implied by other bulk equations of motion.

### 3.3.2 Surface terms under unconstrained variations

Let us move on to the saddle-point conditions implied by the other terms in eq. (3.30). Firstly, we note that the lapse term

$$\int_{-\partial\mathcal{N}_\varepsilon} d\tau \wedge e_{\text{BY}} \delta N \sim 0 \quad (3.37)$$

in eq. (3.30) vanishes as  $\varepsilon \rightarrow 0$  automatically as a consequence of  $N = \mathcal{O}(\rho)$  and  $h_{ij} = \mathcal{O}(\rho^0)$ . The remaining terms in eq. (3.30) are

$$-\frac{\delta \text{Area}(\gamma)}{4G_{\text{N}}} = -\frac{1}{8G_{\text{N}}} \int_\gamma^{(D-2)} \epsilon h^{ij} \delta h_{ij} , \quad (3.38)$$

$$-\int_{-\partial\mathcal{N}_\varepsilon} d\tau \wedge \delta(p_{\text{BY}})_i N^i \sim -2\pi \int_\gamma \delta(p_{\text{BY}})_i v^i , \quad (3.39)$$

$$-\frac{1}{2} \int_{-\partial\mathcal{N}_\varepsilon} u^A \epsilon_A (T_{\text{BY}})^{ij} \delta h_{ij} \sim \frac{1}{16\pi G_{\text{N}}} \int_{-\partial\mathcal{N}_\varepsilon} u^A \epsilon_A (K_u)^c{}_c h^{ij} \delta h_{ij} \quad (3.40)$$

$$\sim -\frac{1}{16\pi G_{\text{N}}} \int_{-\partial\mathcal{N}_\varepsilon} u^A \epsilon_A n^a n^b (K_u)_{ab} h^{ij} \delta h_{ij} \quad (3.41)$$

$$= -\frac{1}{16\pi G_{\text{N}}} \int_{-\partial\mathcal{N}_\varepsilon} u^A \epsilon_A \frac{\partial_\rho N}{N} h^{ij} \delta h_{ij} \quad (3.42)$$

$$\sim \frac{1}{8G_{\text{N}}} \int_\gamma^{(D-2)} \epsilon \kappa h^{ij} \delta h_{ij} , \quad (3.43)$$

<sup>33</sup>In the special smooth case,  $\partial_\rho N \sim 1$  and  $f_1(\rho) = \rho$ , so the relevant terms in eq. (3.35) automatically cancel.

<sup>34</sup>*C.f.* ref. [14]'s eqs. (A.64) and (A.65).

and

$$-\frac{1}{g_M^2} \int_{-\partial \mathcal{N}_\epsilon} A \wedge \delta(*F) \sim -\frac{2\pi}{g_M^2} \int_\gamma \mu \delta(*F) . \quad (3.44)$$

For unconstrained variations  $\delta h_{ij}$ ,  $\delta(p_{BY})_i$ , and  $\delta(*F)$ , requiring the terms (3.38)+(3.43), (3.39), and (3.44) to vanish respectively lead to the saddle point conditions

$$\kappa = 1 , \quad v^i = 0 , \quad \mu = 0 . \quad (3.45)$$

Thus, unsurprisingly, unconstrained saddles are smooth at  $\gamma$ .

### 3.3.3 Constrained saddles

However, we are also interested in constrained saddles where certain quantities, which we will denote by  $\mathcal{C}^{(\alpha)}$ , near  $\gamma$  are fixed. For such saddles, the variation of the action  $\delta I$  need only vanish for constrained variations preserving the fixed quantities,  $\delta \mathcal{C}^{(\alpha)} = 0$ . Equivalently, for each constrained saddle, there exist constant Lagrange multipliers  $\lambda_{(\alpha)}$ , such that all (unconstrained) variations from the saddle satisfy

$$\delta I + \lambda_{(\alpha)} \delta \mathcal{C}^{(\alpha)} = 0 . \quad (3.46)$$

One quantity which we would like to fix is the area of  $\gamma$ ,

$$\mathcal{C}^{(1)} = \text{Area}(\gamma) , \quad (3.47)$$

whose unconstrained variation is given by eq. (3.38).

We would also like to fix some notion of (angular) momentum on  $\gamma$ . To construct such a quantity from  $(p_{BY})_i$  defined in eq. (3.26), we must choose a vector with which to contract this dual-vector density. In  $D = 3$  spacetime dimensions, a natural choice is the unit-norm vector

$$\chi^i = ({}^{(D-2)}\epsilon)^i = h^{ij} ({}^{(D-2)}\epsilon)_j . \quad (3.48)$$

which serves also as the einbein on  $\gamma$ ,

$$h_{ij} = \chi_i \chi_j . \quad (3.49)$$

Using  $(p_{BY})_i$  and  $\chi^i$ , we construct the quantity<sup>35</sup>

$$\mathcal{C}^{(2)} = \int_\gamma (p_{BY})_i \chi^i , \quad (3.50)$$

which we would like to fix on  $\gamma$ . The unconstrained variation of this quantity is

$$\delta \mathcal{C}^{(2)} = \int_\gamma \left[ \delta(p_{BY})_i \chi^i - \frac{1}{2} (p_{BY})_i \chi^i h^{jk} \delta h_{jk} \right] . \quad (3.51)$$

---

<sup>35</sup>Note that  $(p_{BY})_i \chi^i$  is a top form on  $\gamma$  — see eq. (3.26).

In higher dimensions, it is less clear what vector(s) we should contract with  $(p_{\text{BY}})_i$  to construct fixed quantities that lead to desirable saddle-point conditions, *e.g.* as described below. Let us therefore restrict all discussion of fixed (angular) momentum to  $D = 3$ , at least for now.

Lastly, for the Maxwell field, we would also like to fix the electric charge enclosed by  $\gamma$ , as measured by Gauss's law,

$$\mathcal{C}^{(3)} = \int_{\gamma} *F . \quad (3.52)$$

From eq. (3.46), we see that fixing the quantities (3.47), (3.50) and (3.52) weakens the saddle-point conditions at  $\gamma$  from eq. (3.45) to now

$$0 = \frac{\kappa - 1}{8G_{\text{N}}} + \frac{\lambda_{(1)}}{2} - \frac{\lambda_{(2)}}{2} \iota_{\chi}(p_{\text{BY}})_i \chi^i , \quad (3.53)$$

$$0 = -2\pi v^i + \lambda_{(2)} \chi^i , \quad (3.54)$$

$$0 = -2\pi\mu + \lambda_{(3)} , \quad (3.55)$$

for arbitrary constants  $\lambda_{(\alpha)}$ . As previously,  $\iota$  denotes an interior product, *e.g.* for  $\chi$  which we have defined in  $D = 3$ ,

$$\iota_{\chi} \left( {}^{(D-2)}\epsilon \right) = \chi^i \chi_i = 1 . \quad (3.56)$$

The second condition can be used to eliminate  $\lambda_{(2)}$  from the first. Also making use of eqs. (3.48) and (3.49), these saddle-point conditions can be succinctly expressed as

$$\kappa - 8\pi G_{\text{N}} \iota_{\chi}(p_{\text{BY}})_i v^i = \text{constant} , \quad (3.57)$$

$$\chi_i v^i = \text{constant} , \quad (3.58)$$

$$\mu = \text{constant} . \quad (3.59)$$

These saddle-point conditions will be satisfied by the constrained saddles to be constructed in section 4.2.2 from black holes.

## 4 Thermal partition function

As described in the introduction in section 1, a goal of this paper is to better understand the gravitational path integral, in particular, as applied to calculate the analogue of a thermal partition function  $Z(\beta, \Omega, \Phi)$ . More precisely, if the gravitational theory is holographically dual to a theory on its boundary, then in this boundary theory,

$$Z(\beta, \Omega, \Phi) = \text{tr} \left( e^{-\beta H_{\xi, \Phi}} \right) \quad (4.1)$$

is the grand canonical partition, where

$$H_{\xi, \Phi} = H - \Omega J - \Phi Q , \quad (4.2)$$

$H$  is the Hamiltonian generating evolution in a static time direction  $\zeta$ ,  $J$  is the (angular) momentum generating translation or rotation in a spatial direction  $\varphi$ , and  $Q$  is electric charge.

In section 4.1, we will describe a naively Euclidean path integral representation of  $Z(\beta, \Omega, \Phi)$ . Of course, the integral over Euclidean metrics is plagued by the conformal factor problem. Remaining agnostic to what the precise contour of integration might be, we will use this Euclidean setup merely to practice constructing (constrained) saddles, in preparation for the better defined Lorentzian calculation in section 5.2. Specifically, we will practice evaluating the path integral in section 4.2 by first fixing then later integrating quantities  $(\mathcal{S}, \mathcal{J}, \mathcal{Q})$  proportional to the area, integrated momentum density, and electric flux on a generically singular codimension-two surface  $\gamma$ . We will construct conically, helically, and holonomically singular constrained saddles for the intermediate integral at fixed  $(\mathcal{S}, \mathcal{J}, \mathcal{Q})$ , allowing us to evaluate the path integral by saddle-point methods. Many of the techniques used in this section will reappear in the Lorentzian calculation of section 5.2.

#### 4.1 Specifying the Euclidean path integral

To give a partial description of the configurations which we would like to include in our gravitational path integral, we might say the following. At the spacetime boundary,  $\partial\mathcal{M}$ , the configurations will be required to satisfy certain boundary conditions, to be specified below. Within the interior of the spacetime  $\mathcal{M}$ , we integrate over configurations which are smooth apart from a (possibly disconnected) codimension-two surface  $\gamma$ . On  $\gamma$ , we allow singularities of the types introduced in section 2.1 for Euclidean signature. But, are we really integrating over all such real Euclidean spacetimes  $\mathcal{M}$ ? Unfortunately, such an integral is ill-defined because of the conformal factor problem [1]: the Euclidean action is unbounded below on this choice of integration contour. We will leave the precise contours of the path integral unspecified for now, but revisit this question in sections 5 and 6.

Turning a temporary blind eye to this issue, let us continue by describing the boundary conditions at the spacetime boundary  $\partial\mathcal{M}$  relevant for the grand canonical partition function eq. (4.1). The induced geometry on  $\partial\mathcal{M}$  is fixed and possesses at least two Killing vectors  $-i\zeta$  and  $\varphi$  interpreted as generating Euclidean time evolution and spatial translation (or rotation). (To be consistent with later notation, we have introduced  $\zeta$  as a Lorentzian time Killing vector, hence the factor of  $-i$ .) Moreover, we require the boundary conditions of all fields to be invariant under these Killing symmetries. The parameters  $\beta$  and  $\Omega$  do not influence the local rigid structure of  $\partial\mathcal{M}$  but instead enter as follows. We require  $\partial\mathcal{M}$  to have topology  $Y \times S^1$ , where the constant sections  $Y$  and fibres  $S^1$  need not be metric-orthogonal. The Killing vector  $\varphi$  is tangent to constant sections  $Y$  while the  $S^1$  fibres are the orbits of

$$-i\xi = -i\zeta - i\Omega\varphi, \quad (4.3)$$

such that  $e^{-i\beta\xi} \sim 1$  (acting on integer-spin fields) completes one orbit. To obtain boundary conditions for a real Euclidean metric,  $\Omega$  can be taken to be imaginary; on the other hand, real  $\Omega$  describes a physical angular velocity, *e.g.* for a physical Lorentzian black hole or to

give  $Z(\beta, \Omega, \Phi)$  a standard thermodynamic interpretation. It will be useful to introduce a time coordinate  $\hat{\tau} \sim \hat{\tau} + \beta$  starting at zero on a given constant section  $Y$  of  $\partial\mathcal{M}$  and evolving as the Killing parameter of  $-i\zeta$  (and thus also  $-i\xi$ ). We will further denote the orbital period of  $\varphi$  by  $\text{Period}(\varphi)$ , so that  $e^{\text{Period}(\varphi)\varphi} \sim 1$  (acting on integer-spin fields). Then we say that  $\varphi$  generates a rotation if such a finite  $\text{Period}(\varphi)$  exists; otherwise  $\varphi$  generates translation.

The Maxwell field  $A$  will also be subject to boundary conditions on  $\partial\mathcal{M}$ . Sidestepping the possibly nontrivial analysis of field asymptotics<sup>36</sup> near  $\partial\mathcal{M}$ , we will simply assume boundary conditions which lead to a good variational principle in the sense of eq. (3.21). We require that the boundary conditions for  $A$  be parametrized by a number  $\Phi$ , with the interpretation of an electric potential that is fixed on  $\partial\mathcal{M}$ . We demand, for example, that a trivial configuration  $A = 0$  near  $\partial\mathcal{M}$  satisfies these boundary conditions with  $\Phi = 0$  and that shifting the time component of the Maxwell field  $A \mapsto A + \hat{\mu} d\hat{\tau}$  leads to a configuration satisfying boundary conditions with a shifted potential  $\Phi \mapsto \Phi + i\hat{\mu}$ . Moreover, we will also assume that  $\Phi$  enters into the value of the boundary Hamiltonian in the manner befitting a fixed potential ensemble, *e.g.* as in eq. (4.21) below. It will be convenient below to write the size of the Maxwell gauge group  $G_M$  as  $\text{Period}(G_M)$ , *e.g.*

$$\text{Period}(G_M) = \begin{cases} 2\pi & \text{if } G_M = U(1) \\ +\infty & \text{if } G_M = \mathbb{R} \end{cases} . \quad (4.4)$$

Are boundary conditions specified by different values of  $\Omega$  or  $\Phi$  inequivalent? For translation or non-compact  $G_M \cong \mathbb{R}$ , yes seems to be the most natural answer. However, when  $\varphi$  generates rotation, one might expect that inequivalent boundary conditions are specified by  $\Omega$  only up to shifts by  $\frac{2\pi i}{\beta \Delta_J}$  for some  $\Delta_J$ .<sup>37</sup> For example, if states of the theory are all invariant under one full rotation  $e^{\text{Period}(\varphi)\varphi}$ , then one would expect

$$\Delta_J = \frac{2\pi}{\text{Period}(\varphi)} . \quad (4.5)$$

If two full rotations  $e^{2\text{Period}(\varphi)\varphi}$  are required, then one would instead expect

$$\Delta_J = \frac{1}{2} \frac{2\pi}{\text{Period}(\varphi)} . \quad (4.6)$$

This would be the case, for example, if the gravitational theory has a dual boundary description in which fermions have anti-periodic Neveu-Schwarz identification around orbits of  $\varphi$ .<sup>38</sup>

For compact  $G_M \cong U(1)$ , we might similarly consider inequivalent boundary conditions to be specified by  $\Phi \bmod \frac{2\pi i}{\beta \Delta_Q}$ , where one might most naturally expect

$$\Delta_Q = \frac{2\pi}{\text{Period}(G_M)} . \quad (4.7)$$

<sup>36</sup>See *e.g.* [17] for some analysis in asymptotically AdS spacetimes.

<sup>37</sup>Boundary conditions that are equivalent under this relation with  $\Delta_J$  given by eqs. (4.5) and (4.6) respectively are related by the  $T$  and  $T^2$  modular transformation of the boundary torus  $\partial\mathcal{M}$ .

<sup>38</sup>The partition function eq. (4.1), without any fermion-parity  $(-1)^F$  insertion, implicitly has Neveu-Schwarz conditions for fermions around the orbits generated by  $-i\xi$ .

We will regard the equivalences

$$\Omega \sim \Omega + \frac{2\pi i m}{\beta \Delta_J} \quad (m \in \mathbb{Z}) \quad (4.8)$$

$$\Phi \sim \Phi + \frac{2\pi i n}{\beta \Delta_Q} \quad (n \in \mathbb{Z}) \quad (4.9)$$

between boundary conditions as assumptions about how the path integral should be formulated. (Depending on whether one wishes to ignore or make these assumptions, the notation used later can be interpreted with  $m$  or  $n$  set to zero or taking arbitrary integer values.) Assuming the equivalence(s), we will conversely find that the path integral quantizes angular momentum and/or charge with spacing  $\Delta_J$  and  $\Delta_Q$  respectively.

For simplicity, we focus on pure Einstein-Maxwell theory with a cosmological constant. In section 6, we will touch on some of the challenges associated to the inclusion of other matter fields, for the most part leaving these extensions for future work.

## 4.2 Saddle-point evaluation

We now construct saddles of the path integral which, as described in section 3.3, extremize the action, possibly subject to constraints on  $\gamma$ . We do not claim that the list of saddles below is exhaustive. Moreover, we will refrain from arguing whether the saddles actually contribute to a saddle-point approximation of the path integral, leaving such an analysis to sections 5 and 6. For now, we simply assume they do and study their potential contributions to the grand canonical partition function.

### 4.2.1 Empty thermal saddle

One somewhat trivial saddle is given by an empty stationary background, periodically identified along a stationary flow to produce the nowhere degenerate  $S^1$ . The Maxwell background  $A = -i\Phi d\hat{\tau}$  is flat, with the time coordinate  $\hat{\tau}$  extended into the bulk. The surface  $\gamma = \emptyset$  is trivial for this saddle.

The action for this stationary background is proportional to  $\beta$  and independent of  $\Omega$  and  $\Phi$ . The leading, classical contribution of this saddle to the grand canonical partition function is therefore  $e^{-\beta E}$  for some  $E$ , interpreted as the background energy of this saddle. Perturbative fluctuations around this saddle describe the thermal QFT grand canonical ensemble on this empty background. Writing the QFT grand canonical partition function, *e.g.* including gravitons to one loop, as  $Z_{\text{th}}^{\text{QFT}}(\beta, \Omega, \Phi)$ , the corrected gravitational partition function is

$$Z_{\text{th}}(\beta, \Omega, \Phi) = e^{-\beta E} Z_{\text{th}}^{\text{QFT}}(\beta, \Omega, \Phi) . \quad (4.10)$$

### 4.2.2 Black hole saddles

As is well known, charged rotating black holes are possible smooth saddles when considering the path integral of the grand canonical partition function  $Z(\beta, \Omega, \Phi)$ . However, it is instructive to dissect the calculation of the path integral slightly. In particular, let us imagine first integrating over everything with the exception of certain fixed quantities

$(\mathcal{S}, \mathcal{J}, \mathcal{Q})$  on a singular codimension-two surface  $\gamma$  and, only at the end, integrating over those initially fixed quantities. That is, we write

$$Z(\beta, \Omega, \Phi) = \int d\mathcal{S} d\mathcal{J} d\mathcal{Q} Z(\beta, \Omega, \Phi; \mathcal{S}, \mathcal{J}, \mathcal{Q}) . \quad (4.11)$$

where  $Z(\beta, \Omega, \Phi; \mathcal{S}, \mathcal{J}, \mathcal{Q})$  is the integral over a codimension-three subcontour of fixed  $(\mathcal{S}, \mathcal{J}, \mathcal{Q})$  in the full contour of the path integral  $Z(\beta, \Omega, \Phi)$ . The quantities whose integrals we would like to leave until the end are

$$\mathcal{S} = \frac{\text{Area}(\gamma)}{4G_{\text{N}}} , \quad (4.12)$$

$$\mathcal{J} = -i \frac{\text{Area}(\gamma)}{\text{Period}(\varphi)} \int_{\gamma} (p_{\text{BY}})_i \chi^i , \quad (4.13)$$

$$\mathcal{Q} = -\frac{i}{g_{\text{M}}^2} \int_{\gamma} *F , \quad (4.14)$$

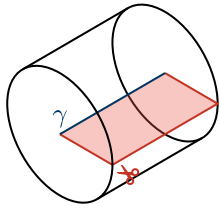
which are related to the  $\mathcal{C}^{(\alpha)}$ , introduced in eqs. (3.47), (3.50) and (3.52), by rescaling so that they can be equated to a black hole's Bekenstein-Hawking entropy, (angular) momentum, and charge below. For definiteness, we have taken  $\varphi$  and  $\chi$  to point in the same direction.<sup>39</sup> The factors of  $-i$  in eqs. (4.13) and (4.14) ensure that the RHSs coincide with the standard real values of angular momentum and charge when evaluated on a Lorentzian black hole with real angular velocity  $\Omega$  and potential  $\Phi$ . (The Lorentzian expressions (5.45) and (5.46) for  $\mathcal{J}$  and  $\mathcal{Q}$  are related to eqs. (4.13) and (4.14) above by the Wick rotations (5.12) and (5.17) of quantities on the RHSs.)

We may now look for potential saddles for the subcontour path integral  $Z(\beta, \Omega, \Phi; \mathcal{S}, \mathcal{J}, \mathcal{Q})$ . As described in section 3.3, such constrained saddles must satisfy eqs. (3.57) to (3.59) on  $\gamma$  in addition to equations of motion away from  $\gamma$ . We can construct such constrained saddles as follows.

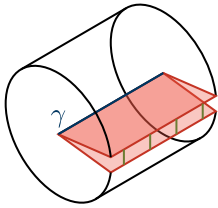
First, we start with a smooth stationary black hole solution with Bekenstein-Hawking entropy (*i.e.* horizon area), (angular) momentum, and electric charge set to the prescribed values of  $(\mathcal{S}, \mathcal{J}, \mathcal{Q})$  fixed in the integral  $Z(\beta, \Omega, \Phi; \mathcal{S}, \mathcal{J}, \mathcal{Q})$ . While (angular) momentum and charge are ordinarily evaluated on  $\partial\mathcal{M}$ , it is straightforward to see that evaluating eqs. (4.13) and (4.14) on the bifurcation surfaces of stationary black holes reproduces the values obtained from standard definitions on  $\partial\mathcal{M}$ .<sup>40</sup> We require this initial configuration to satisfy boundary conditions on  $\partial\mathcal{M}$  with some parameters  $(\beta_0, \Omega_0, \Phi_0)$  possibly differing from the desired values  $(\beta, \Omega, \Phi)$ . We will now correct this mismatch.

<sup>39</sup>This statement is meaningful when  $\gamma$  can be homologically related to a boundary time slice  $Y$  by a preferred class of continuous deformations. We anticipate that this will be true in Lorentz signature for certain cases where  $\gamma$  is homologically related to a boundary time slice  $Y$  by spatial surfaces of bulk codimension one.

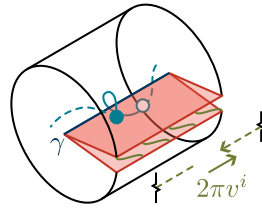
<sup>40</sup>We have in mind here situations where  $\gamma$  is homologically related to a boundary time slice  $Y$  by a surface of bulk codimension one, which is preserved by the Killing vector  $\varphi$  extended into the bulk and coincides with a surface of constant  $\tau$  (or  $t$  in Lorentz signature, as will be considered in section 5) near  $\gamma$ . In more general situations, *e.g.* for arbitrary  $\text{SL}(2, \mathbb{Z})$  black holes [12] discussed in section 6.4, eqs. (4.13), (4.14), (5.45) and (5.46) might not correspond precisely to the standard definitions of (angular) momentum and charge on  $\partial\mathcal{M}$ .



(a) First, we cut open the spacetime along a stationary time slice which is preserved by the bulk extension of the boundary Killing vector  $\varphi$  generating spatial translation or rotation. For rotation, the front and back faces of the solid cylinder are identified.



(b) The top and bottom faces of the cut are initially identified in the trivial manner, as indicated by the green threads connecting identified points of the two red faces.



(c) However, we can instead resew the top and bottom faces with a shift  $2\pi v^i$ . The solid teal curve, drawn as winding helically around  $\gamma$ , is now a closed curve, because the empty and filled endpoints are identified. The strength of the helical singularity at the bifurcation surface  $\gamma$  is given by  $v^i$ . When the front and back faces of the solid cylinder are identified, different  $v^i$ , *e.g.* corresponding to the shifts shown as solid and dashed arrows, can lead to configurations that agree away from  $\gamma$ . However, when regularized as described in section 2.2, these configurations become distinct in a neighbourhood of  $\gamma$ . In particular, they have different contractible cycles, as illustrated by the solid and dashed teal curves.

**Figure 4:** A cut, shift, and resew procedure on a stationary spacetime with a bifurcation surface  $\gamma$ . By an appropriate choice of the shift, it is possible to ensure that the boundary co-rotating Killing vector  $-i\xi$  in eq. (4.3) has closed orbits on the spacetime boundary  $\partial\mathcal{M}$  (and the bulk extension of  $-i\xi$  also has closed orbits, *e.g.* the solid teal curve in (c)).

Let  $\hat{\tau}$  be the bulk stationary time extending the boundary time introduced in section 4.1. Then, to satisfy the periodicity prescribed by  $\beta$ , we set by hand  $\hat{\tau} \sim \hat{\tau} + \beta$ . This induces a conical singularity with opening angle

$$2\pi\kappa = 2\pi\frac{\beta}{\beta_0} \quad (4.15)$$

around the bifurcation surface  $\gamma$ .

To produce the shift prescribed by  $\Omega$ , we can perform a cut, shift, and resew procedure illustrated in fig. 4. First, we cut open the spacetime along a stationary time slice, then relatively shift the two faces of the cut, and finally reidentify the two faces so that closed orbits are generated with period  $\beta$  by the desired co-rotating vector  $-i\xi$ , given by (4.3), on  $\partial\mathcal{M}$ . This introduces a helical singularity on  $\gamma$  with shift *e.g.*

$$v^i = \frac{\beta}{2\pi i}(\Omega - \Omega_0)\varphi^i, \quad (4.16)$$

where we have extended the Killing vector  $\varphi$ , previously introduced on  $\partial\mathcal{M}$  in section 4.1, now into the bulk. When boundary conditions (4.8) are treated as equivalent for  $m \in \mathbb{Z}$ ,



one can make other choices for the shift, turning on any

$$v^i = \left[ \frac{\beta}{2\pi i} (\Omega - \Omega_0) + \frac{m}{\Delta_J} \right] \varphi^i . \quad (m \in \mathbb{Z}) \quad (4.17)$$

These different shifts lead to configurations which are diffeomorphic to each other away from  $\gamma$  — see fig. 4c — but have helical singularities on  $\gamma$  which are physically distinct, as evident upon regularization — see section 2.2.

Finally, to match the prescribed electric potential  $\Phi$  on  $\partial\mathcal{M}$ , we can shift the Maxwell field  $A \mapsto A - i(\Phi - \Phi_0)d\hat{\tau}$ . Doing so turns on a holonomic singularity with strength

$$\mu = \frac{\beta}{2\pi i} (\Phi - \Phi_0) . \quad (4.18)$$

If boundary conditions (4.9) are equivalent for  $n \in \mathbb{Z}$ , we can further shift  $A$  by arbitrary integer multiples of  $\frac{2\pi}{\beta\Delta_Q} d\hat{\tau}$ , giving

$$\mu = \frac{\beta}{2\pi i} (\Phi - \Phi_0) + \frac{n}{\Delta_Q} . \quad (n \in \mathbb{Z}) \quad (4.19)$$

At last, we have some configuration(s) satisfying the desired boundary conditions specified by  $(\beta, \Omega, \Phi)$  at  $\partial\mathcal{M}$  and reproducing the fixed values of  $(\mathcal{S}, \mathcal{J}, \mathcal{Q})$  on  $\gamma$ . Equations of motion are satisfied away from  $\gamma$ , because the original smooth back hole is a solution. Moreover, we see from eqs. (4.15), (4.17) and (4.19) and the bulk Killing symmetry  $\varphi$  that (3.57) to (3.59) on  $\gamma$  are satisfied. Thus, we have indeed constructed constrained saddle(s) which are saddles for the integral  $Z(\beta, \Omega, \Phi; \mathcal{S}, \mathcal{J}, \mathcal{Q})$ , or rather many constrained saddles labelled by integer  $m$  and/or  $n$  if the equivalences (4.8) and/or (4.9) between boundary conditions are assumed.

To evaluate the saddle-point contribution to this integral, we must calculate the action (3.1) on the constrained saddle. It is helpful to first consider the original smooth black hole with parameters  $(\beta_0, \Omega_0, \Phi_0)$ , where the combination of terms

$$\int_{\mathcal{M} \setminus \mathcal{N}_\epsilon} (L_{\text{EH}} + L_{\text{M}}) + \int_{\partial\mathcal{M}} L_{\partial\mathcal{M}} + \int_{-\partial\mathcal{N}_\epsilon} L_{\text{GH}} \sim \beta_0 E_{\zeta + \Omega_0 \varphi, \Phi_0}(\mathcal{S}, \mathcal{J}, \mathcal{Q}) \quad (4.20)$$

is given by the value

$$E_{\zeta + \Omega_0 \varphi, \Phi_0}(\mathcal{S}, \mathcal{J}, \mathcal{Q}) = E(\mathcal{S}, \mathcal{J}, \mathcal{Q}) - \Omega_0 \mathcal{J} - \Phi_0 \mathcal{Q} \quad (4.21)$$

of the boundary Hamiltonian generating time evolution and translation or rotation with (angular) velocity  $\Omega_0$  in the presence of an electric potential  $\Phi_0$ . Here,  $E(\mathcal{S}, \mathcal{J}, \mathcal{Q})$  is the energy of the system with respect to just the time evolution. The modifications undergone from this smooth black hole to construct our constrained saddle should not locally modify the Lagrangian densities appearing in eq. (4.20). The only change in the value to eq. (4.20) results from the adjustment of the time period  $\beta_0 \mapsto \beta$ . Thus, for our constrained saddle,

$$\int_{\mathcal{M} \setminus \mathcal{N}_\epsilon} (L_{\text{EH}} + L_{\text{M}}) + \int_{\partial\mathcal{M}} L_{\partial\mathcal{M}} + \int_{-\partial\mathcal{N}_\epsilon} L_{\text{GH}} \sim \beta E_{\zeta + \Omega_0 \varphi, \Phi_0}(\mathcal{S}, \mathcal{J}, \mathcal{Q}) . \quad (4.22)$$

With eqs. (4.17) and (4.19), we can also evaluate other terms in the action (3.1):

$$\int_{-\partial\mathcal{N}_\varepsilon} L_{\text{hel}} \sim -2\pi \int_\gamma v^i (p_{\text{BY}})_i = \left[ \beta (\Omega_0 - \Omega) - \frac{2\pi i m}{\Delta_J} \right] \mathcal{J} \quad (4.23)$$

$$\int_{-\partial\mathcal{N}_\varepsilon} L_{\text{hol}} \sim -\frac{2\pi}{g_{\text{M}}^2} \int_\gamma \mu * F = \left[ \beta (\Phi_0 - \Phi) - \frac{2\pi i n}{\Delta_Q} \right] \mathcal{Q}. \quad (4.24)$$

In the first line, we have used eq. (3.4) and

$$\varphi^i = \frac{\text{Area}(\gamma)}{\text{Period}(\varphi)} \chi^i \quad (4.25)$$

on  $\gamma$ . Altogether, the action (3.1) of our constrained saddle evaluates to

$$I = \beta E_{\xi, \Phi}(\mathcal{S}, \mathcal{J}, \mathcal{Q}) - \mathcal{S} - 2\pi i m \frac{\mathcal{J}}{\Delta_J} - 2\pi i n \frac{\mathcal{Q}}{\Delta_Q}. \quad (4.26)$$

where

$$E_{\xi, \Phi}(\mathcal{S}, \mathcal{J}, \mathcal{Q}) = E(\mathcal{S}, \mathcal{J}, \mathcal{Q}) - \Omega \mathcal{J} - \Phi \mathcal{Q}. \quad (4.27)$$

The contribution of each such saddle to the subcontour path integral  $Z(\beta, \Omega, \Phi; \mathcal{S}, \mathcal{J}, \mathcal{Q})$  is perturbatively given by  $e^{-I}$ , with the above value of  $I$ , corrected multiplicatively by the partition function of perturbative quantum fluctuations, which we will write as

$$Z_{\text{BH}}^{\text{QFT}} \left( \beta, \Omega + \frac{2\pi i m}{\beta \Delta_J}, \Phi + \frac{2\pi i n}{\beta \Delta_Q}; \mathcal{S}, \mathcal{J}, \mathcal{Q} \right). \quad (4.28)$$

Including the final integrals over  $(\mathcal{S}, \mathcal{J}, \mathcal{Q})$ , and summing over  $m$  and  $n$  as needed, the contribution to the full integral (4.11) becomes

$$\sum_{m, n} Z_{\text{BH}} \left( \beta, \Omega + \frac{2\pi i m \mathcal{J}}{\beta \Delta_J}, \Phi + \frac{2\pi i n \mathcal{Q}}{\beta \Delta_Q} \right), \quad (4.29)$$

where

$$Z_{\text{BH}}(\beta, \Omega, \Phi) = \int d\mathcal{S} d\mathcal{J} d\mathcal{Q} e^{\mathcal{S} - \beta E_{\xi, \Phi}(\mathcal{S}, \mathcal{J}, \mathcal{Q})} Z_{\text{BH}}^{\text{QFT}}(\beta, \Omega, \Phi; \mathcal{S}, \mathcal{J}, \mathcal{Q}). \quad (4.30)$$

The latter takes the expected form for a grand canonical ensemble of states with energies  $E$ , (angular) momenta  $\mathcal{J}$ , electric charges  $\mathcal{Q}$ , and density  $e^{\mathcal{S}}$ , with corrections from quantum fluctuations.<sup>41</sup>

When  $\varphi$  generates translation, the sum  $\sum_m$  has only the trivial  $m = 0$  term. For rotation, if all  $m \in \mathbb{Z}$  saddles are included, then the sum over these saddles leads to a discrete angular momentum spectrum. To see this, note that the summed contribution (4.29) to the partition function is periodic in imaginary values of  $\Omega$  as required by eq. (4.8). Therefore, taking the inverse Laplace transform in  $-\Omega$  (*i.e.* inverse Fourier transform in  $-i\Omega$ ), we

---

<sup>41</sup>Recall that  $E$  can be regarded as a function of  $(\mathcal{S}, \mathcal{J}, \mathcal{Q})$ ; alternatively, one can regard  $\mathcal{S}$  as a function of  $(E, \mathcal{J}, \mathcal{Q})$ .

conclude that the thermodynamically conjugate variable, angular momentum, must have a discrete spectrum with spacing  $\Delta_J$ . To see this more directly in a toy calculation, let us naively neglect quantum fluctuations by dropping  $Z_{\text{BH}}^{\text{QFT}}$ . Then, the sum over  $m$  becomes a Dirac comb

$$\sum_{m=-\infty}^{\infty} e^{2\pi i m \mathcal{J} / \Delta_J} = \sum_{j=-\infty}^{\infty} \delta\left(\frac{\mathcal{J}}{\Delta_J} - j\right), \quad (4.31)$$

selecting discrete values of  $\mathcal{J} \in \Delta_J \mathbb{Z}$ .<sup>42</sup>

If the Maxwell gauge group  $G_M$  is compact and we sum over all  $n \in \mathbb{Z}$ , then charge is similarly quantize as expected with spacing  $\Delta_Q$ .

## 5 Lorentzian formulation

In this section, we turn now to configurations in Lorentzian signature. Our goal will be twofold. Firstly, we would like to characterize and assign an action to conical, helical, and holonomic singularities on a codimension-two surface  $\gamma$  in a Lorentzian spacetime. In section 5.1, we will be partially successful in this respect, leaving for future work some open challenges introduced by the presence of lightcones.

We will nonetheless be able to progress towards our second goal in section 5.2, evaluating the gravitational thermal partition function  $Z(\beta, \Omega, \Phi)$  using a Lorentzian path integral. This calculation, as already sketched in section 1.2, closely parallels the calculation of ref. [6], but, like the naive Euclidean calculation of section 4, employs constrained saddles containing the more general types of codimension-two singularities studied in this paper. The final answer for black hole contributions to  $Z(\beta, \Omega, \Phi)$  is again eqs. (4.29) and (4.30), but derived now from a Lorentzian path integral free from the conformal factor problem. This result and its advantages over the previous analysis of [6] will be discussed in section 6.

### 5.1 Codimension-two singularities

In Lorentzian signature, the singular codimension-two surface  $\gamma$  can be timelike or spacelike.<sup>43</sup> In the former case, we do not expect any novelties relative to our preceding Euclidean discussion, apart from the fact that  $h_{ij}$  in eq. (2.2) is now Lorentzian as opposed to Euclidean. (See, *e.g.* ref. [9], which treats special cases of time-like conical and helical singularities constructed by cutting and gluing flat spacetime.) From here on, we will try to understand the situation where  $\gamma$  is a spacelike surface.

The primary challenges that arise when studying spacelike  $\gamma$  occur when the spacetime possesses lightcones that emanate from  $\gamma$ . Thus, it will be easier to start in section 5.1.1 to consider spacetimes where such lightcones do not exist — see fig. 5. In fact, this will

---

<sup>42</sup>Of course, this is only a toy calculation since  $Z_{\text{BH}}^{\text{QFT}}$  is a multiplicative correction to each saddle, so dropping this factor to perform the sum  $\sum_m$  is unjustified; moreover,  $\mathcal{J}$  captures only the angular momentum of the background. We expect the more general argument following from the periodicity in  $\Omega$  to hold even when the quantum corrections  $Z_{\text{BH}}^{\text{QFT}}$  are included.

<sup>43</sup>The possibility of a null  $\gamma$  is perhaps more subtle.



(a)  $\gamma$  spacelike separated from nearby points in the spacetime  $\mathcal{M}$ . (b)  $\gamma$  timelike separated from nearby points.

**Figure 5:** The spacetime  $\mathcal{M}$  (shaded) near a spacelike singularity  $\gamma$  with no lightcones. The red surfaces are identified. The would-be lightcones (grey lines) lie beyond the spacetime  $\mathcal{M}$ . Similar to fig. 3,  $\rho$  or  $\underline{\rho}$  is a proper radial coordinate coming out from  $\gamma$ ,  $t$  is a boost angle coordinate with some period, say  $2\pi$ , and  $y^i$  are coordinates along the directions of  $\gamma$ . Additional cases are obtained by rotating (a) and (b) by  $\pi$ .

be the situation directly relevant to our construction of Lorentzian constrained saddles for the thermal partition function in section 5.2. In section 5.1.2, we will address some of the subtleties that arise in the presence of lightcones; however, these issues do not arise in the saddles used in section 5.2 so uninterested readers are free to skip section 5.1.2 directly to section 5.2.

### 5.1.1 Spacelike $\gamma$ with no lightcones

When no lightcones emanate from the singular codimension-two surface  $\gamma$ , the singularity can still be characterized in almost the same manner as in section 2.1, except that  $\tau$  in eq. (2.2) should be traded for a boost angle  $t$ . Pictorially, the spacetime near  $\gamma$  can be illustrated as in fig. 5, as we now describe.

The fact that the spacetime possesses no lightcones emanating from  $\gamma$  indicates that the spacetime near  $\gamma$  does not span infinite proper boost angles. Thus, the (possibly improper) boost angle coordinate  $t$  can be taken to be periodically identified with some constant period, say  $2\pi$ , much like the Euclidean angle  $\tau$  of section 2.1. Topologically, a neighbourhood of  $\gamma$  is thus again given by  $\gamma$  times a disk, as illustrated in fig. 3. However, the causal structure is better exhibited by the Penrose diagrams in fig. 5. Note, in particular, that closed curves are parametrized by  $t$  at fixed proper spacelike separation  $\rho$  or timelike separation  $\underline{\rho}$  from  $\gamma$  and fixed coordinates  $y^i$  along the directions of  $\gamma$ . Moreover, these circles degenerate at  $\gamma$ , where the causal structure becomes singular.

For the purposes of translating equations from previous sections to Lorentzian signature, the boost angle  $t$  can roughly be viewed<sup>44</sup> as a Wick rotation of the Euclidean angle

<sup>44</sup>This is not to say that an arbitrary real Euclidean spacetime necessarily becomes a real Lorentzian spacetime under this wick rotation. This is true for only certain (*e.g.* static) spacetimes or in conjunction with the analytic continuation of other parameters (*e.g.* eq. (5.2) for stationary spacetimes).

$\tau$ :

$$\tau = i t \tag{5.1}$$

It will be convenient to refer to some Lorentzian quantities by reusing the same symbols previously introduced in Euclidean signature. For example, the relation between the Euclidean (E) and Lorentzian (L) unit normals, lapses, and shifts with respect to  $\tau$  and  $t$  are:

$$n_E = N_E d\tau = i N_L dt = i n_L, \quad N_E = N_L, \quad N_E^i = -i N_L^i, \tag{5.2}$$

From here on, we will work primarily with Lorentzian objects and omit subscripts except when explicitly comparing Lorentzian and Euclidean quantities. In case  $\gamma$  is timelike separated from nearby points as in fig. 5b, we also rotate the proper radial coordinate

$$\rho = i \underline{\rho}. \tag{5.3}$$

The unit normals respectively to surfaces of constant  $\underline{\rho}$  and  $t$ , and the lapse with respect to  $t$  will be similarly be underlined in case  $\gamma$  is timelike separated from nearby points as in fig. 5a:

$$u = d\rho = i d\underline{\rho} = i \underline{u}, \quad n = N dt = i \underline{N} dt = i \underline{n}, \quad N = i \underline{N}. \tag{5.4}$$

As in section 2.1.1, we can characterize the conical and helical nature of the singularity  $\gamma$  by examining metric (2.1) near  $\gamma$  in radially static gauge,

$$G_{AB} dX^A dX^B = d\rho^2 + g_{ab} dx^a dx^b = -d\underline{\rho}^2 + g_{ab} dx^a dx^b. \tag{5.5}$$

The induced metric  $g_{ab}$  on surfaces of constant proper radius  $\rho$  or  $\underline{\rho}$  now reads

$$g_{ab} dx^a dx^b = -N^2 dt^2 + h_{ij} (dy^i + N^i dt)(dy^j + N^j dt) \tag{5.6}$$

$$= \underline{N}^2 dt^2 + h_{ij} (dy^i + N^i dt)(dy^j + N^j dt). \tag{5.7}$$

Again, we can consider small  $\rho$  or  $\underline{\rho}$  behaviour of the lapse  $N$  or  $\underline{N}$  and shift  $N^i$  as in eq. (2.4):

$$\begin{aligned} N &= \kappa \rho + (\text{subleading in } \rho), & N^i &= v^i + \mathcal{O}(\rho^2) = v^i + \mathcal{O}(\underline{\rho}^2). \\ \underline{N} &= \kappa \underline{\rho} + (\text{subleading in } \underline{\rho}), \end{aligned} \tag{5.8}$$

Similar to in section 2.1.1, the conical nature of the singularity is determined by  $\kappa$  which describes the passage of proper hyperbolic angle around  $\gamma$  per coordinate time  $t$ . If constant,  $2\pi \kappa$  is the total opening angle when the period of  $t$  is taken to be  $2\pi$ . More generally, we will allow  $\kappa$  to depend on  $t$  or  $y^i$  below. Meanwhile, the strength of the helical singularity is parametrized by  $v^i$  as before, which also might depend on  $t$  and/or  $y^i$ . (In section 5.1.2, we will explain why we might want to relax some of the assumptions described in section 2.1.3 forbidding  $t$ -dependence.)

As previously mentioned in section 2.1.1, the degenerate limit  $\varepsilon \rightarrow 0$  of a closed circle  $\mathcal{C}_\varepsilon$ , at fixed  $\rho, \rho = \varepsilon$  and  $y^i$ , can retain a finite length, because the metric registers the path  $\mathcal{C}_\varepsilon$  as moving in a direction along  $\gamma$  (even though, topologically, it is not). Since this is a spacelike length even in the current Lorentzian context, there is a sort of ergo region near  $\gamma$ , where  $\partial_t$  is spacelike. (Figure 5 may be misleading in this respect, because  $\partial_t$  has a finite projection  $N^i \sim v^i$  onto the directions orthogonal to the page.)

The holonomic singularity of the Maxwell field  $A$  is again characterized by the leading behaviour of the electric potential near  $\gamma$  as in eq. (2.14),

$$[(\partial_t)^a - N^a] A_a = \mu + \mathcal{O}(\rho^2) . \quad (5.9)$$

The holonomic singularity strength  $\mu$ , possibly a function of  $t$  and/or  $y^i$ , again enters into the Wilson loop  $\int_{\mathcal{C}_\varepsilon} A$  on a small circle  $\mathcal{C}_\varepsilon$  now parametrized by  $t$ .

Let us now consider the action for such singular configurations. Because the causal structure breaks down at  $\gamma$ , the strategy used in sections 2.3 and 3.1 to derive the action by smoothing out the singularity would now likely involve complex regulated configurations. Rather than deriving the Lorentzian action from scratch in this way, we will instead simply analytically continue the Euclidean answer (3.1).

For clarity, let us state some additional conventions for Wick rotation. We will adopt the conventional relations between Euclidean and Lorentzian Lagrangian densities and actions,

$$L_E = -i L_L , \quad I_E = -i I_L , \quad (5.10)$$

where the factor of  $i$  comes from the continuation (5.1) of the volume form,

$$\epsilon_E = N d\tau \wedge d\rho \wedge {}^{(D-2)}\epsilon = i N dt \wedge d\rho \wedge {}^{(D-2)}\epsilon = i \epsilon_L . \quad (5.11)$$

Also because of this Wick rotation of the volume form,

$$*_E = i *_L . \quad (5.12)$$

Due to the signs in eq. (5.1), the Euclidean and Lorentzian stress tensors, *e.g.* the Brown-York stress tensors on surfaces of constant  $\rho$ , are related by<sup>45</sup>

$$(T_{\text{EBY}})^{ab} = -(T_{\text{LBY}})^{ab} , \quad (5.13)$$

so that, in Lorentzian signature, an extra sign appears in eq. (3.23)<sup>46</sup>

$$(T_{\text{BY}})^{ab} = \frac{1}{8\pi G_N} \left[ (K_u)^{ab} - g^{ab} (K_u)^c{}_c \right] = \frac{i}{8\pi G_N} \left[ (K_{\underline{u}})^{ab} - g^{ab} (K_{\underline{u}})^c{}_c \right] . \quad (5.14)$$

<sup>45</sup>To understand equations such as eq. (5.13), it is important to be consistent with the tensor indices. For example,  $(T_{\text{EBY}})^{\tau\tau} = -(T_{\text{LBY}})^{\tau\tau} = (T_{\text{LBY}})^{tt}$ .

<sup>46</sup>Recall our convention for orientations as described in footnote 29. This carries over to our Lorentzian setting as described below eq. (5.23).

Due to the Wick rotation (5.4), this is imaginary for spacelike surfaces of constant  $\underline{\rho}$  as indicated in the last expression. However, the momentum density on surfaces of constant  $(\rho, t)$  or  $(\underline{\rho}, t)$ ,

$$(p_{\text{BY}})^i = {}^{(D-2)}\epsilon (T_{\text{BY}})^{ab} n_a h_b^i = \frac{1}{8\pi G_{\text{N}}} {}^{(D-2)}\epsilon (K_u)^{ab} n_a h_b^i \quad (5.15)$$

$$= {}^{(D-2)}\epsilon (T_{\text{BY}})^{ab} i \underline{n}_a h_b^i = -\frac{1}{8\pi G_{\text{N}}} {}^{(D-2)}\epsilon (K_{\underline{u}})^{ab} \underline{n}_a h_b^i, \quad (5.16)$$

is always real. From eqs. (5.2) and (5.13), we see that the relation between the Euclidean momentum density (3.26) and its Lorentzian counterpart (to which we implicitly refer above and elsewhere in this section) is

$$(p_{\text{EY}})^i = -i (p_{\text{LY}})^i. \quad (5.17)$$

With these conventions, the Lorentzian action is given by

$$I = \int_{\mathcal{M} \setminus \mathcal{N}_\varepsilon} (L_{\text{EH}} + L_{\text{M}}) + \int_{\partial \mathcal{M}} L_{\partial \mathcal{M}} - i \frac{\text{Area}(\gamma)}{4G_{\text{N}}} + \int_{-\partial \mathcal{N}_\varepsilon} (L_{\text{GH}} + L_{\text{hel}} + L_{\text{hol}}), \quad (5.18)$$

where now

$$L_{\text{EH}} = \frac{1}{16\pi G_{\text{N}}} (R - 2\Lambda) \epsilon, \quad L_{\text{M}} = -\frac{1}{2g_{\text{M}}^2} F \wedge *F, \quad (5.19)$$

and

$$L_{\text{GH}} = \frac{1}{8\pi G_{\text{N}}} u^A \epsilon_A g^{ab} (K_u)_{ab} = -\frac{1}{8\pi G_{\text{N}}} \underline{u}^A \epsilon_A g^{ab} (K_{\underline{u}})_{ab}, \quad (5.20)$$

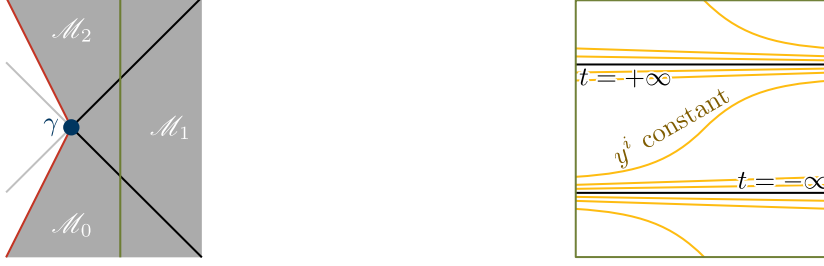
$$L_{\text{hel}} = \frac{1}{8\pi G_{\text{N}}} u^A \epsilon_A (dt)_a g^{ab} N^i (K_u)_{bi} = -\frac{1}{8\pi G_{\text{N}}} \underline{u}^A \epsilon_A (dt)_a g^{ab} N^i (K_{\underline{u}})_{bi}, \quad (5.21)$$

$$= -dt \wedge (p_{\text{BY}})_i N^i \quad (5.22)$$

$$L_{\text{hol}} = \frac{1}{g_{\text{M}}^2} A \wedge *F. \quad (5.23)$$

As in the Euclidean case,  $\mathcal{N}_\varepsilon$  is a neighbourhood of  $\gamma$  such that  $\partial \mathcal{N}_\varepsilon$  is a surface of constant proper radius  $\rho$  or  $\underline{\rho}$  of order  $\varepsilon$  from  $\gamma$  — see fig. 5. Note that the *vectors*  $u^A$  and  $\underline{u}^A$  point respectively outward from and into  $\mathcal{N}_\varepsilon$ , *i.e.* into and outward from  $\mathcal{M} \setminus \mathcal{N}_\varepsilon$ . The orientation of  $\partial \mathcal{N}_\varepsilon$  is therefore given by  $u^A \epsilon_A$  and  $-\underline{u}^A \epsilon_A$ ; the opposite orientation applies to  $\partial(\mathcal{M} \setminus \mathcal{N}_\varepsilon) = -\partial \mathcal{N}_\varepsilon$  appearing in eq. (5.18).

More generally, as described in section 3.1.1, there are certain cases where we can alternatively work with other choices of the excised neighbourhood  $\mathcal{N}_\varepsilon$  and cutoff surface  $\partial \tilde{\mathcal{N}}_\varepsilon$ . In particular, if the singularity is nonhelical, *i.e.*  $v^i = 0$ , then there is full freedom to choose the profile of  $\mathcal{N}_\varepsilon$  to be given by  $\rho = \tilde{\rho} e^{f(x)}$  or  $\underline{\rho} = \tilde{\underline{\rho}} e^{f(t)}$  for fixed  $\tilde{\rho}$  and  $\tilde{\underline{\rho}}$  of order  $\varepsilon$  and any function  $f$  of  $x^a = (t, y^i)$ . If the singularity is helical, then, around each connected component of  $\gamma$ , we can still choose an arbitrary function  $f(t)$  but only of  $t$ , provided  $\lim_{\rho, \underline{\rho} \rightarrow 0} h_{ij}$ ,  $\kappa$ , and  $v^i$  are  $t$ -independent or provided  $\lim_{\rho, \underline{\rho} \rightarrow 0} h_{ij}$  is  $t$ -independent



(a) Spacetime  $\mathcal{M}$  (shaded) constructed by gluing together wedges  $\mathcal{M}_i$ . The red surfaces are identified.

(b) A timelike surface (green in previous panel) passing through lightcones near  $\gamma$ . This illustration depicts angles measured by the metric at least approximately. Surfaces of constant  $t$  are exactly horizontal. A surface of constant  $y^i$  is drawn for the case of a constant nontrivial helical shift  $v^i$  and periodically identified  $y^i$ .

**Figure 6:** A spacetime with lightcones emanating from a codimension-two singular surface  $\gamma$ .

and  $\kappa$  is  $y^i$ -independent. The cutoff surface terms in the action (3.1) is then given by  $\int_{-\partial\tilde{\mathcal{N}}_\epsilon} (L_{\text{GH}} + L_{\text{hel}} + L_{\text{hol}})$  where the Gibbons-Hawking and helical Lagrangian densities are

$$\tilde{L}_{\text{GH}} = \frac{1}{8\pi G_{\text{N}}} \tilde{u}^A \epsilon_A \tilde{g}^{ab} (\tilde{K}_{\tilde{u}})_{ab} = -\frac{1}{8\pi G_{\text{N}}} \tilde{u}^A \epsilon_A \tilde{g}^{ab} (\tilde{K}_{\tilde{u}})_{ab}, \quad (5.24)$$

$$\tilde{L}_{\text{hel}} = \frac{1}{8\pi G_{\text{N}}} \tilde{u}^A \epsilon_A (dt)_a \tilde{g}^{ab} \tilde{N}^i (\tilde{K}_{\tilde{u}})_{bi} = -\frac{1}{8\pi G_{\text{N}}} \tilde{u}^A \epsilon_A (dt)_a \tilde{g}^{ab} \tilde{N}^i (\tilde{K}_{\tilde{u}})_{bi}, \quad (5.25)$$

while  $L_{\text{hol}}$  remains the same as in eq. (5.23). As in section 3.1.1, the induced metric  $\tilde{g}_{ab}$ , its inverse  $\tilde{g}^{ab}$ , and the shift vector  $\tilde{N}^i$  in eq. (5.21) are understood as being defined on the chosen surface  $\partial\tilde{\mathcal{N}}_\epsilon$ . We have also written the spacelike and timelike unit normals of  $\partial\tilde{\mathcal{N}}_\epsilon$  respectively as  $\tilde{u}_A = \tilde{u}_{\underline{A}}$  and  $\tilde{u}_A$ .

### 5.1.2 Lightcones and resulting complications

Let us now consider more general configurations that contain lightcones for the singular codimension-two surface  $\gamma$ . Below, we will describe a procedure for constructing such configurations in a neighbourhood of each connected component of  $\gamma$ . We then have in mind that the full spacetime  $\mathcal{M}$  is an extension of these neighbourhoods which is smooth with the exception of  $\gamma$  (and possibly its lightcones, as we will later describe).

In a neighbourhood of a given connected component of  $\gamma$ , there can be any even number  $\mathcal{N} \geq 0$  of lightcone components meeting at  $\gamma$ . The case of  $\mathcal{N} = 0$  has already been treated in section 5.1.1. Configurations with  $\mathcal{N} > 0$  in this neighbourhood can be constructed by a gluing procedure similar to that described in ref. [6]. However, the pieces of spacetime that we sew together are  $(\mathcal{N} + 1)$ -many wedges  $\mathcal{M}_i$ , each of which is the decompactified limit of a spacetime described in section 5.1.1. That is, in each  $\mathcal{M}_i$ , we relax the periodic identification of  $t$ . Instead, in  $\mathcal{M}_0$ , the range of  $t$  is taken to be a semi-infinite line from a finite value  $t_0$  to  $+\infty$ ; in each  $\mathcal{M}_{0 < i < \mathcal{N}}$ ,  $t$  takes values on an infinite line; finally, in  $\mathcal{M}_{\mathcal{N}}$ ,



$t$  again lies on a semi-infinite line from  $-\infty$  to a finite value  $t_{\mathcal{N}}$ .<sup>47</sup> These wedges are then sewn together along the lightcones where  $\text{Re } t = \pm\infty$ ; as we will later see, at least in certain situations, it is helpful to view the semi-infinite or infinite lines of  $t$  for different wedges to have imaginary offsets relative to each other. Finally, we identify the surface  $t = t_0$  in  $\mathcal{M}_0$  with  $t = t_{\mathcal{N}}$  in  $\mathcal{M}_{\mathcal{N}}$ . In this procedure,  $\gamma$  must be spacelike and timelike separated from nearby points respectively in  $\mathcal{M}_{\text{even } i}$  and  $\mathcal{M}_{\text{odd } i}$ , or vice versa. This in particular implies that  $\mathcal{N}$  must be even. In the resulting spacetime within a neighbourhood of  $\gamma$ , the number of connected lightcone components meeting at  $\gamma$  is  $\mathcal{N}$ . A case with  $\mathcal{N} = 2$  is illustrated in fig. 6a.

The possible outputs of the above procedure describe the configurations we consider only in a neighbourhood of a each component of  $\gamma$ . As already mentioned, we envision the configuration on the full spacetime  $\mathcal{M}$  to be an extension of these neighbourhoods. In principle, we see no reason to require  $\mathcal{N}$  to be identical for all connected components of  $\gamma$ .<sup>48</sup> We also see no reason to rule out nontrivial connections and identifications between the wedges associated to various connected components of  $\gamma$  through the full spacetime  $\mathcal{M}$ .

**Lightcone singularities.** As previously hinted, the treatment of such configurations can be subtle due to complications that arise from the lightcones emanating from  $\gamma$ . One issue is whether these spacetimes are singular on the lightcones. For example, the presence of a helical shift  $v^i$  can pose a threat at  $\text{Re } t = \pm\infty$  if the configuration, *e.g.* the induced metric  $h_{ij}$  on surfaces of constant  $\rho$  or  $\underline{\rho}$  and  $t$ , near  $\gamma$  is not invariant under the shift, *e.g.*  $\mathcal{L}_v h_{ij} \neq 0$ . To see the problem, suppose the metric  $\lim_{\rho, \underline{\rho} \rightarrow 0} h_{ij}$  on  $\gamma$  is not shift-invariant due to some inhomogeneity near some value of  $y^i$ . On nearby surfaces of fixed  $\rho$  or  $\underline{\rho}$  and  $t$ , the induced metric  $h_{ij}$  should have a similar inhomogeneity whose motion follows a worldline of fixed  $y^i$ . Over time  $\delta t$ , the metric will register this worldline as moving by some amount  $v^i \delta t$  in the directions  $y^i$  along  $\gamma$ . Near a lightcone,  $t$  grows arbitrarily large, so the worldline runs infinitely rapidly along the  $y^i$  directions if  $v^i$  is not turned off — see fig. 6b. Due to this effect, the metric near the lightcone can vary arbitrarily rapidly. To avoid such singularities, one might therefore want to consider  $t$ -dependent helical shifts  $v^i$  that turn off sufficiently quickly as  $\text{Re } t \rightarrow \pm\infty$ . On the other hand, one might allow these lightcone singularities, in which case one might expect a nontrivial contribution to the action from the lightcones.

A somewhat similar effect occurs for the Maxwell field. Consider a path normal to surfaces of constant  $t$  passing near  $\gamma$ , *e.g.* a vertical line in fig. 6b. Close to  $\gamma$ , parallel transport on the principal bundle along this path includes a motion  $\int_t^{t+\delta t} A = \mu \delta t$  in the fibre direction for every increment  $\delta t$  of boost time. However, this does *not* give rise to a physical singularity on the lightcone. One way to see this is simply by changing to

---

<sup>47</sup>As we have implicitly assumed before,  $\kappa$  is required to be finite, so infinite proper boost angles are only reached at infinite  $t$ .

<sup>48</sup>As constructed through our procedure, the spacetimes we consider are real and have Lorentzian signature, with the possible exception of a codimension-two surface  $\gamma$  where the causal structure can break down. However, if one further allows complex geometries, then there also does not seem to be a reason to forbid  $\mathcal{N}$  from varying within a connected component of  $\gamma$ .

a gauge in which the Wilson line  $\int A$  between different points along the path remains finite even as one crosses the lightcone. Perhaps more conceptually, the fibre direction is homogeneous just like the gauge group. So, in analogy to the previous paragraph, there is no “inhomogeneity” that is dragged infinitely rapidly in the fibre direction as we cross the lightcone.

**The action: a first pass.** Let us now turn to a discussion of the action for a configuration constructed from the gluing procedure described above. We expect the action for such configurations to again be given by eq. (5.18), where now  $\mathcal{M}$  is the full spacetime resulting from the gluing and extension procedure. A rough<sup>49</sup> argument for this is that the action near each connected component of  $\gamma$  should be a sum of the actions for the wedges  $\mathcal{M}_i$ , with the exception of the area term. We keep only one copy of the area term even as more wedges are sewn together, because, in a sense, it represents the  $2\pi$  opening angle around  $\gamma$  of a *smooth* configuration. This notion is made precise in eq. (2.28) when considering configurations where the would-be singularity on  $\gamma$  has been regulated. Several subtleties remain however, all related to the presence of lightcones.

Firstly, if the lightcones emanating from  $\gamma$  are singular as described previously, then there may be contributions to the action associated to these lightcone singularities. Secondly, if we take as before the cutoff surface  $\partial\mathcal{N}_\varepsilon$  in the action eq. (5.18) to be a surface of constant proper radius  $\rho$  and  $\underline{\rho}$ , then this cutoff surface will run far away from  $\gamma$  in terms of affine distance along the lightcones. In particular, the lightcones are part of the excised neighbourhood  $\mathcal{N}_\varepsilon$  of  $\gamma$ .

Rather than a bug, we suggest viewing this as a possible feature of the action which accounts for possible contributions from lightcone singularities. This suggestion is motivated by the fact that the Euclidean action, which analytically continues to our Lorentzian action (5.18), was derived in sections 2.3 and 3 by considering the regulated configurations described in section 2.2. Our procedure for constructing these regulated configuration involves interpolating various field components, *e.g.* the shift  $N^i$ , from values matching the unregulated singular configuration on  $\partial\mathcal{N}_\varepsilon$  to a behaviour at  $\rho = 0$  consistent with a smooth configuration. Now, in our current Lorentzian context, the locus of  $\rho = 0$  includes not only  $\gamma$  but also the lightcones. Thus, it is natural to guess that the area and cutoff surface  $\partial\mathcal{N}_\varepsilon$  terms in the action eq. (5.18), roughly speaking, account for the action  $\int_{\mathcal{N}_\varepsilon} (L_{\text{EH}} + L_{\text{M}})_{\text{reg}(\varepsilon)}$  of a configuration that is regulated to be smooth on the locus of  $\rho = 0$ , which includes both  $\gamma$  and the lightcones in the singular configuration. (The possibly singular causal structure at  $\gamma$  means the full regulation procedure likely involves complex geometries; however, to regulate just the helical shift which is responsible for the type of lightcone singularity described in reference to fig. 6b, a real interpolation of the shift  $N^i$  as a function of  $\rho$  would seem to suffice.) We leave a more careful analysis of this intuition for future work.

Setting aside this issue, in the remainder of this section, we would like to highlight the fact that the cutoff surface terms in the action receive an imaginary “pole” contribution for

---

<sup>49</sup>However, we will argue later that there are “pole” contributions to the cutoff surface  $\partial\mathcal{N}_\varepsilon$  terms of the action, which can be viewed as a consequence of the gluing between the wedges.

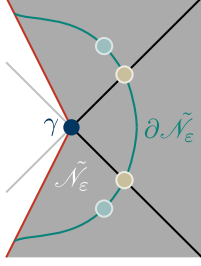


**Figure 7:** A neighbourhood  $\tilde{\mathcal{N}}_\varepsilon$  of  $\gamma$  in the spacetime constructed by gluing in fig. 6a. The cutoff surface  $\partial\tilde{\mathcal{N}}_\varepsilon$  remains everywhere affinely close to  $\gamma$ . Highlighted by dots on  $\partial\tilde{\mathcal{N}}_\varepsilon$  are surfaces that play important roles in the cutoff surface terms of the action: the light blue dots are surfaces where  $\partial\tilde{\mathcal{N}}_\varepsilon$  becomes null; the beige dots are the intersection of  $\partial\tilde{\mathcal{N}}_\varepsilon$  with lightcones emanating from  $\gamma$ , where  $\text{Re } t = \pm\infty$ .

every lightcone component emanating from  $\gamma$ . This is true even if the lightcones themselves are smooth.

**Crossing a lightcone.** To make progress, we will find it helpful to restrict our attention to certain configurations in which we have the freedom, as described around eqs. (5.24) and (5.25), to choose a cutoff surface  $\partial\tilde{\mathcal{N}}_\varepsilon$  which is everywhere affinely close to  $\gamma$  — see fig. 7. We will now argue that, given certain simplifying assumptions, such a choice is possible; in the process, we will also better understand how the boost time contours of neighbouring wedges are joined together.

From here on, we will firstly assume that the lightcones are in fact smooth, *e.g.* because of symmetries or because the shift  $v^i$  turns off sufficiently quickly at  $\text{Re } t \rightarrow \pm\infty$  as discussed previously. Secondly, we will require  $\kappa$  for each connected component of  $\gamma$  to only be a function of  $t$  and not  $y^i$ . Finally, we will assume that that  $N/\rho = \underline{N}/\underline{\rho}$  quickly approaches  $\kappa$  as we approach any lightcone (near but finitely separated from  $\gamma$ ).<sup>50</sup>

As argued in section 3.1.1 and reviewed around eqs. (5.24) and (5.25), the profile of each connected component of the cutoff surface  $\partial\tilde{\mathcal{N}}_\varepsilon$  can be taken to be given by  $\rho = \tilde{\rho} e^{f(t)}$  or  $\underline{\rho} = \tilde{\underline{\rho}} e^{f(t)}$  for fixed  $\tilde{\rho}$  and  $\tilde{\underline{\rho}}$  of order  $\varepsilon$  and an arbitrary function  $f(t)$ . It is helpful to view this surface as a worldline moving in an effective two-dimensional geometry,

$$ds_\perp^2 = d\rho^2 - N^2 d\tau^2 = -d\underline{\rho}^2 + \underline{N}^2 d\tau^2 . \quad (5.27)$$

<sup>50</sup>It is perhaps sufficient to merely require  $N/\rho = \underline{N}/\underline{\rho}$  to quickly become independent of  $y^i$  as we approach the lightcone. Then, one can consider the curvature of the effective two-dimensional metric eq. (5.27),

$${}^{(2)}R = -\frac{2}{N} \partial_\rho^2 N = \frac{2}{\underline{N}} \partial_{\underline{\rho}}^2 \underline{N} . \quad (5.26)$$

As we approach a smooth lightcone, given that  $N \rightarrow 0$  but the above should remain finite, we then expect  $N - \kappa\rho$  to vanish no slower than  $\rho^2 N$ , *i.e.*  $\rho^3$ . In particular, the “subleading” terms in eq. (5.8) are truly smaller than the  $\kappa$  terms as we approach a lightcone, even though one might have initially feared that the “subleading” terms could be enhanced by  $\text{Re } t \rightarrow \pm\infty$ .

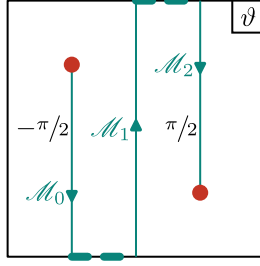


**Figure 8:** The contour traced out by the proper Euclidean angle  $\vartheta$  or the proper hyperbolic angle  $-i\vartheta = \int^t dt' \kappa(t')$ , for the spacetime in fig. 6a. The red points correspond to the identified red surfaces in fig. 6a. The dashed lines indicate that the contour is completed by segments taken to infinity.

In particular, the lapse  $\tilde{N}$  on  $\partial\tilde{\mathcal{N}}_\varepsilon$  is the einbein of a worldline in this effective geometry. Near any given lightcone, by assumption,  $N/\rho = \underline{N}/\underline{\rho}$  and thus the above effective metric quickly become independent of  $y^i$ , so the problem truly becomes two-dimensional.

To cross lightcones affinely near (but finitely separated from) a given connected component of  $\gamma$ , it is helpful to consider Kruskal coordinates

$$z = \rho e^{i\vartheta}, \quad \bar{z} = \rho e^{-i\vartheta}, \quad (5.28)$$

where the proper Euclidean angle  $\vartheta$ , or equivalently the proper hyperbolic angle  $-i\vartheta$ , is defined (up to an integration constant) by

$$d\vartheta = \kappa d\tau = i\kappa dt. \quad (5.29)$$

Using these coordinates, eq. (5.27) can be expressed as

$$ds_\perp^2 = dz d\bar{z} + [(\kappa\rho)^2 - N^2] dt^2. \quad (5.30)$$

The first term is manifestly smooth, while  $(\kappa\rho)^2 - N^2$  vanishes quickly as we approach the lightcone such that the second term is also smooth.<sup>51</sup>

To cross a lightcone at  $\text{Re } t = +\infty$  or  $\text{Re } t = -\infty$  respectively, we therefore want to take  $z \rightarrow 0$  while keeping  $\bar{z}$  finite or take  $\bar{z} \rightarrow 0$  while keeping  $z$  finite. This can be achieved for a connected component of  $\partial\tilde{\mathcal{N}}_\varepsilon$  by choosing its time profile  $f(t)$  to behave like  $\pm i\vartheta = \mp \int^t dt' \kappa(t')$  asymptotically at  $\text{Re } t = \pm\infty$ .

Before proceeding, let us remark that the Kruskal coordinates (5.28),

$$z = \rho e^{i\vartheta} = i\underline{\rho} e^{i\vartheta}, \quad \bar{z} = \rho e^{-i\vartheta} = i\underline{\rho} e^{-i\vartheta}, \quad (5.31)$$

also tell us how to relate the contours of  $t$  or  $\vartheta$  in neighbouring wedges. In particular,  $\vartheta$  jumps by  $\pi/2$  when moving from spacelike to timelike separation from  $\gamma$  across a lightcone at  $\text{Re } t = +\infty$  and when moving from timelike to spacelike separation from  $\gamma$  across a

<sup>51</sup>From footnote 50, we expect  $(\kappa\rho)^2 - N^2$  to vanish no slower than  $\rho^4$  as we approach the lightcone. Meanwhile,  $\kappa^2 \rho^2 dt = z d\bar{z} - \bar{z} dz$ .

lightcone at  $\text{Re } t = -\infty$ . The contour traced out by  $\vartheta$  when going around near a connected component of  $\gamma$  in the full spacetime  $\mathcal{M}$  thus consists of semi-infinite and infinite lines for the wedges  $\mathcal{M}_i$ , joined by segments at  $\text{Im } \vartheta = \pm\infty$ , *i.e.*  $\text{Re } t = \pm\infty$ . This is illustrated in fig. 8 for the spacetime of fig. 6a.

**The action: surface terms revisited.** We have argued above that, for configurations satisfying certain simplifying assumptions<sup>52</sup>, the cutoff surface  $\partial\mathcal{N}_\varepsilon$  can be chosen to be affinely close to  $\gamma$ , as illustrated in fig. 7. With this picture in mind, let us revisit the terms  $\int_{-\partial\mathcal{N}_\varepsilon} (L_{\text{GH}} + L_{\text{hel}} + L_{\text{hol}})$  in the action integrated over this cutoff surface.

A first comment is that the Gibbons-Hawking Lagrangian density (5.24) pulled back to  $\partial\mathcal{N}_\varepsilon$  has a pole wherever  $\partial\mathcal{N}_\varepsilon$  becomes null — see fig. 7. While the volume form on  $-\partial\mathcal{N}_\varepsilon$  vanishes here, the trace of the extrinsic curvature  $\tilde{g}^{ab}(\tilde{K}_{\tilde{u}})_{ab}$  diverges even more strongly. This can be understood as the result of the extrinsic curvature  $(\tilde{K}_{\tilde{u}})_{ab}$  being defined in terms of a unit-normalized normal  $\tilde{u}^A$ . By rewriting the extrinsic curvature and induced volume form on  $-\partial\mathcal{N}_\varepsilon$  in terms of a smoothly varying but non-normalized normal, it can be shown that the residue of the pole is proportional to the volume form on the codimension-one section of  $\partial\mathcal{N}_\varepsilon$  where  $\partial\mathcal{N}_\varepsilon$  is null. A prescription for going around the pole can then be obtained by rotating the contour of Lorentzian time slightly towards the negative imaginary direction.<sup>53</sup> This analysis has been carried out previously, *e.g.* as described in refs. [6, 8, 18], and we will refrain from repeating it.

The upshot is that the Gibbons-Hawking action should be understood as a principal value (PV) integral plus a (half) residue contribution from the pole:

$$\int_{-\partial\mathcal{N}_\varepsilon} \tilde{L}_{\text{GH}} \sim \text{PV} \int_{-\partial\mathcal{N}_\varepsilon} \tilde{L}_{\text{GH}} + \frac{i}{16G_{\text{N}}} \sum_{\text{connected } \gamma_\ell \subset \gamma} \mathcal{N}_\ell \text{Area}(\gamma_\ell), \quad (5.32)$$

where the sum is over connected components  $\gamma_\ell$  of  $\gamma$ . Above, in the  $\varepsilon \rightarrow 0$  limit intended in the relation  $\sim$ , we have equated the area element along sections of  $\partial\mathcal{N}_\varepsilon$  where  $\partial\mathcal{N}_\varepsilon$  is null to the area element along  $\gamma$ . From the discussion in section 2.2.1,<sup>54</sup> we expect this to be valid in the presence of helical singularities if (each connected component of) the section of  $\partial\mathcal{N}_\varepsilon$  tends to a surface of constant  $t$ . This is indeed true in the current case where (near each connected component of  $\gamma$ )  $\kappa(t)$  depends only on  $t$  and the profile of  $\partial\mathcal{N}_\varepsilon$  is specified by a function  $f(t)$  also only of  $t$  — see eq. (5.27).

The aforementioned pole on sections where  $\partial\mathcal{N}_\varepsilon$  becomes null appears only when considering the component of the extrinsic curvature normal to said section. Other compo-

<sup>52</sup>We will continue to assume that the geometry to be smooth away from  $\gamma$ , even on the lightcones, and  $\kappa$  is a function only of  $t$  near each connected component of  $\gamma$ .

<sup>53</sup>Very roughly speaking, if matter fields are placed on the spacetime, then their evolution with respect to a Lorentzian time  $u$  is generated by the contour-ordered exponential  $\exp(-i \int_{\mathfrak{T}} du H^{\text{QFT}}(u))$  where  $\hat{H}^{\text{QFT}}$  is the matter Hamiltonian and  $\mathfrak{T}$  is the time contour. Whereas ordinary Lorentzian time evolution involves  $\mathfrak{T}$  along the real line, our prescription slightly rotates  $\mathfrak{T}$  so that  $du$  along it is slightly negative imaginary. This effectively adds a mild exponential damping to high energy fluctuations. In contrast, the opposite prescription gives a dangerous exponential enhancement of such fluctuations.

<sup>54</sup>The function  $f$  in section 2.2.1 should not be confused with the function  $f$  in section 3.1.1 and mentioned below.

nents, *e.g.* the ones appearing in the helical term (5.25), diverge, if at all, no faster than the induced volume form vanishes on sections where  $\partial\mathcal{N}_\varepsilon$  becomes null.

However, there are somewhat similar poles in the helical and holonomic terms (5.23) and (5.25), located on the intersection of  $\partial\mathcal{N}_\varepsilon$  and the lightcones — see fig. 7. With  $\text{Re } t \rightarrow \pm\infty$  here, the helical and holonomic Lagrangian densities diverge because of the appearance of  $dt$  explicit in eq. (5.25) and implicit in the Maxwell potential  $A$  as described by eq. (5.9). The proper angle contour illustrated in fig. 8 provides a prescription for going around these poles. Specifically, the vertical and horizontal segments of fig. 8 give the principal value and pole contributions to the integrals of the helical and holonomic surface terms (5.21) and (5.23) over  $-\partial\mathcal{N}_\varepsilon$ .

In fact, the proper angle contour gives an integration prescription for all the surface terms on  $\partial\mathcal{N}_\varepsilon$ , including reproducing eq. (5.32). Continuing eq. (3.19) to Lorentz signature, we find that the pullback of  $\tilde{L}_{\text{GH}} + \tilde{L}_{\text{hel}} + L_{\text{hol}}$  to  $\partial\mathcal{N}_\varepsilon$  in the  $\varepsilon \rightarrow 0$  limit is equivalent, up to a total derivative, to a density on  $S^1 \times \gamma$  given by

$$\begin{aligned} \tilde{\phi}_{\varepsilon \rightarrow 0}^* \left( \tilde{L}_{\text{GH}} + \tilde{L}_{\text{hel}} + L_{\text{hol}} \right) &= dt \wedge \left[ -\frac{\kappa}{8\pi G_{\text{N}}} {}^{(D-2)}\epsilon - v^i (p_{\text{BY}})_i + \frac{1}{g_{\text{M}}^2} \mu * F \right] \\ &+ (\text{total derivative}) \end{aligned} \quad (5.33)$$

$$\begin{aligned} &= i d\vartheta \wedge \left[ \frac{1}{8\pi G_{\text{N}}} {}^{(D-2)}\epsilon + \frac{v^i}{\kappa} (p_{\text{BY}})_i - \frac{1}{g_{\text{M}}^2} \frac{\mu}{\kappa} * F \right] \\ &+ (\text{total derivative}) . \end{aligned} \quad (5.34)$$

The combinations  $v^i/\kappa$  and  $\mu/\kappa$  give the helical and holonomic shifts per proper hyperbolic angle. The  $\vartheta$  integral over the  $S^1$  is to be performed over the contour illustrated in fig. 8. We see that the horizontal segments of the contour, where the pullback of  $d\vartheta$  is real, gives an imaginary contribution to the cutoff surface terms in the Lorentzian action:

$$\begin{aligned} \text{Im} \int_{-\partial\mathcal{N}_\varepsilon} (\tilde{L}_{\text{GH}} + \tilde{L}_{\text{hel}} + L_{\text{hol}}) \\ \sim \sum_{\text{connected } \gamma_\ell \subset \gamma} \left\{ \frac{\mathcal{N}_\ell \text{Area}(\gamma_\ell)}{16G_{\text{N}}} + \frac{\pi}{2} \sum_{i=1}^{\mathcal{N}_\ell} \int_{\gamma_\ell^i} \left[ \frac{v^i}{\kappa} (p_{\text{BY}})_i - \frac{1}{g_{\text{M}}^2} \frac{\mu}{\kappa} * F \right] \right\} , \end{aligned} \quad (5.35)$$

where  $\gamma_\ell^i$  is the section of  $S^1 \times \gamma_\ell$  corresponding to the  $i$ -th lightcone component emanating from  $\gamma_\ell$ . (If the terms in the square brackets are  $t$ - or  $\vartheta$ -independent, as we sometimes assumed in our Euclidean calculations, then the sum just gives a multiplicative factor of  $\mathcal{N}_\ell$  like for the area term.)

In summary, we see that the cutoff surface terms in the action acquire imaginary contributions (5.35). To deduce eq. (5.35), we focused on configurations which are smooth on the lightcones of  $\gamma$  and satisfy some simplifying assumptions which allowed us to consider a cutoff surface  $\partial\mathcal{N}_\varepsilon$  which is everywhere affinely close to  $\gamma$ , as illustrated in fig. 7. Because this cutoff surface itself crosses over the lightcones, it is natural to include the horizontal real (imaginary) segments of the (hyperbolic) angle contour fig. 8 which give rise to the pole contributions.

However, we expect that, even when working with a cutoff surface  $\partial\mathcal{N}_\varepsilon$  which asymptotes to but naively never crosses the lightcones, the correct prescription for evaluating the Lorentzian action should nonetheless implicitly include similar pole contributions. After all, in the special cases where we were allowed to choose cutoff surfaces  $\partial\tilde{\mathcal{N}}_\varepsilon$  which do cross lightcones, we ought to be able to get the same answer by treating the original cutoff surface  $\partial\mathcal{N}_\varepsilon$  with a consistent prescription. Another reason is that, the Lorentzian action for a smooth configuration with  $\mathcal{N} = 4$  ought to be purely real with no special contributions near  $\gamma$ . In order to cancel the explicitly imaginary area term in the action (5.18), the cutoff surface terms on  $\partial\mathcal{N}_\varepsilon$  must also have imaginary contributions. We will leave to future work a more thorough analysis of imaginary contributions to the Lorentzian action.

## 5.2 Thermal partition function

As described in the introduction in section 1 and briefly mentioned in section 4.1, an obstacle of the Euclidean analysis in section 4 is the conformal factor problem [1]. Given the sickness of the gravitational path integral contour over purely Euclidean configurations, this raises the question of what the right integration contour should be. We will adopt the perspective that the fundamental starting point should be the Lorentzian gravitational path integral with a contour over real Lorentzian configurations. Using such a Lorentzian path integral in this section, we will reevaluate the grand canonical partition function  $Z(\beta, \Omega, \Phi)$ .

As emphasized in ref. [6], to recover the expected thermodynamic contributions from the analogue of Euclidean black holes, it is important to include configurations in the Lorentzian path integral which are at least conically singular on codimension-two surface  $\gamma$ . We will extend this analysis to include helical and holonomic singularities. Thus, we include in our path integral all Lorentzian configurations which are smooth apart from  $\gamma$  (and possibly the lightcones of  $\gamma$ ), on which we allow singularities of the kind described in section 5.1. Including this broader class of singularities leads to a richer set of constrained saddles, as we have already seen in section 4 in Euclidean signature. Consequently, we will find a larger set of stability conditions for a given saddle to contribute to the partition function  $Z(\beta, \Omega, \Phi)$ , beyond the positivity of specific heat found in ref. [6]. (In section 6, we will provide a Morse theory explanation for why these additional conditions were not visible from the analysis of ref. [6].)

Let us briefly review our strategy for evaluating  $Z(\beta, \Omega, \Phi)$ , which was already explained in section 1 and closely parallels ref. [6]. First, using saddle-point methods, we will evaluate a Lorentzian path integral  $Z_L(T, \Omega, \Phi)$  with real Lorentzian boundary conditions specified by parameters  $(T, \Omega, \Phi)$  as we elaborate in section 5.2.1. Such an integral has the quantum mechanical interpretation of a trace

$$Z_L(T, \Omega, \Phi) = \text{tr} \exp(-i T H_{\zeta+\Omega\varphi, \Phi}) , \quad (5.36)$$

Here,  $H_{\zeta+\Omega\varphi, \Phi}$  is the same Hamiltonian as in eq. (4.1). Naively, the thermal partition function  $Z(\beta, \Omega, \Phi)$  is simply an analytic continuation of  $Z_L(T, \Omega, \Phi)$ . Unfortunately, the trace (5.36) does not converge to a function, but rather gives a distribution in  $T$ . However,

we can nonetheless recover  $Z(\beta, \Omega, \Phi)$  through an integral transform of  $Z_L(T, \Omega, \Phi)$ ,

$$Z(\beta, \Omega, \Phi) = \int_{-\infty}^{\infty} dT f_\beta(T) Z_L(T, \Omega, \Phi) . \quad (5.37)$$

The kernel  $f_\beta(T)$  is chosen such that

$$e^{-\beta E} g_{E_0}(E) = \int_{-\infty}^{\infty} dT f_\beta(T) e^{-i T E} . \quad (5.38)$$

for some function  $g_{E_0}(E)$  evaluating to 1 for  $E \geq E_0$ , where  $E_0$  is a lower bound on the eigenvalues of  $H_{\zeta+\Omega\varphi, \Phi}$ . For example, we can take<sup>55</sup>

$$f_\beta(T) = -\frac{1}{2\pi i} \frac{e^{E_0(-\beta+iT)}}{T+i\beta} . \quad (5.39)$$

In section 6, we will discuss the validity of the integral transform (5.37) in conjunction with saddle point methods applied to approximate the path integral.

### 5.2.1 Boundary conditions

The Lorentzian path integral  $Z_L(T, \Omega, \Phi)$  is a function of three parameters  $(T, \Omega, \Phi)$  specifying boundary conditions at the spacetime boundary  $\partial\mathcal{M}$  essentially identical to those described in section 4.1 up to Wick rotation.

Again, we require the induced geometry on  $\partial\mathcal{M}$  to be fixed and to possess two Killing vectors  $\zeta$  and  $\varphi$ , under which all boundary conditions are required to be invariant. The main difference relative to section 4.1 is that the Killing vector  $\zeta$  here is timelike and related by Wick rotation to its Euclidean counterpart  $-i\zeta$ . As before, we require  $\partial\mathcal{M}$  to have topology  $Y \times S^1$ , where the spacial constant sections  $Y$  need not be metric-orthogonal to the  $S^1$  fibres. The constant sections  $Y$  are preserved by  $\varphi$  while the fibres  $S^1$  are the orbits of the Killing vector

$$\xi = \zeta + \Omega\varphi , \quad (5.40)$$

such that  $e^{T\xi}$  (acting on integer-spin fields) completes one orbit. Notice that a real Lorentzian boundary geometry is obtained from taking real  $T$  and  $\Omega$ , in contrast to the Euclidean case where  $\Omega$  was required to be imaginary to specify a real boundary. Let us refer to the boundary Killing time parameter of  $\zeta$  as  $\hat{t}$ , which is constant on constant sections  $Y$  and is periodically identified  $\hat{t} \sim \hat{t} + T$ .

The boundary conditions for the Maxwell field  $A$  are the same as described in section 4.1. In particular, they are parametrized by an electric potential  $\Phi$  which has the following properties:  $\Phi = 0$  for configurations which are trivial  $A = 0$  near  $\partial\mathcal{M}$ ; a shift  $A \mapsto A + \hat{\mu} d\hat{t}$  in the gauge potential shifts the electric potential  $\Phi \mapsto \Phi + \hat{\mu}$ ; and  $\Phi$  enters into the boundary Hamiltonian in the expected manner for a fixed potential ensemble as we will later specify.

---

<sup>55</sup>The sign in eq. (5.39) is due to the fact that the real integration contour in eq. (5.38), completed at infinity in the lower half plane, forms a *clockwise* contour around the pole at  $T = -i\beta$ .



As in eqs. (4.8) and (4.9), when  $\varphi$  generates rotation or the Maxwell gauge group is compact, we expect that values for the angular velocity  $\Omega$  or electric potential  $\Phi$  related by

$$\Omega \sim \Omega + \frac{2\pi m}{T \Delta_J} \quad (m \in \mathbb{Z}) \quad (5.41)$$

$$\Phi \sim \Phi + \frac{2\pi n}{T \Delta_Q} \quad (n \in \mathbb{Z}) \quad (5.42)$$

lead to equivalent boundary conditions. (Otherwise, refraining from imposing these equivalence relations,  $m$  and  $n$  can be interpreted as being set to zero in the following.)

### 5.2.2 Saddle-point evaluation

Let us now consider saddles for the path integral  $Z_L(T, \Omega, \Phi)$  and constrained saddles for its subcontour integrals.

An example of a saddle with a trivial singular surface  $\gamma = \emptyset$  is the empty thermal saddle described in section 4.2.1, Wick rotated to Lorentzian signature in the obvious way. Analogous to eq. (4.10), we expect a perturbative contribution of

$$Z_{L\text{th}}(T, \Omega, \Phi) = e^{-iT E} Z_{L\text{th}}^{\text{QFT}}(T, \Omega, \Phi) \quad (5.43)$$

from this saddle, for some constant  $E$  and corrections  $Z_{L\text{th}}^{\text{QFT}}(T, \Omega, \Phi)$  from quantum fluctuations, *e.g.* one-loop gravitons. Performing the integral transform (5.37) on the above, we expect to recover the contribution, which we called  $Z_{\text{th}}(\beta, \Omega, \Phi)$  in eq. (4.10), to the thermal partition function  $Z(\beta, \Omega, \Phi)$ . This is clear by virtue of eq. (5.38), if we ignore the quantum corrections  $Z_{L\text{th}}^{\text{QFT}}(T, \Omega, \Phi)$  and  $Z_{\text{th}}^{\text{QFT}}(\beta, \Omega, \Phi)$ , or given that  $Z_{L\text{th}}^{\text{QFT}}(T, \Omega, \Phi)$  itself takes the form of an oscillatory trace (5.36), *e.g.* now over a QFT Hilbert space.

More interesting are the Lorentzian analogues of Euclidean black holes. As emphasized by ref. [6], in the absence of singularities  $\gamma$  where the causal structure breaks down, it is hard to imagine how one would obtain contributions to the Lorentzian path integral analogous to Euclidean black holes that have contractible boundary time circles. However, as described in eq. (3.45), saddles that are stationary under all unconstrained variations are not expected to possess a nontrivial singular surface  $\gamma$ . Thus, as in ref. [6], we are again led to consider *constrained* saddles analogous to those constructed in section 4.2.2.<sup>56</sup>

Analogous to the Euclidean case described there, these constrained saddles are saddles for path integrals  $Z_L(T, \Omega, \Phi; \mathcal{S}, \mathcal{J}, \mathcal{Q})$  over subcontours of fixed

$$\mathcal{S} = \frac{\text{Area}(\gamma)}{4G_{\text{N}}} , \quad (5.44)$$

$$\mathcal{J} = -\frac{\text{Area}(\gamma)}{\text{Period}(\varphi)} \int_{\gamma} (p_{\text{BY}})_i \chi^i , \quad (5.45)$$

$$\mathcal{Q} = \frac{1}{g_{\text{M}}^2} \int_{\gamma} *F . \quad (5.46)$$

<sup>56</sup>As in section 4.2.2, we will in fact find a family of constrained saddles labelled by integers  $m$  and  $n$ . While the boundary time circle is contractible in constrained saddles with  $m = 0$ , we will find other constrained saddles with  $m \neq 0$  where the time circle is instead homologous to some number of copies of  $\gamma$ .

These quantities will be equated to the Bekenstein-Hawking entropy, (angular) momentum, and electric charge of a black hole shortly.<sup>57</sup> The path integral  $Z_L(T, \Omega, \Phi)$  over the full contour of Lorentzian configurations is obtained by formally including the integrals over  $(\mathcal{S}, \mathcal{J}, \mathcal{Q})$ :

$$Z_L(T, \Omega, \Phi) = \int d\mathcal{S} d\mathcal{J} d\mathcal{Q} Z_L(T, \Omega, \Phi; \mathcal{S}, \mathcal{J}, \mathcal{Q}). \quad (5.47)$$

However, as written above,  $Z_L(T, \Omega, \Phi)$  fails to converge to a function, which is consistent with the observation noted below eq. (5.36) that  $Z_L(T, \Omega, \Phi)$  instead has the interpretation of a distribution with respect to  $T$ . Practically, this means that any integral over  $T$ , *e.g.* the integral transform (5.37), should be performed before the integrals over  $(\mathcal{S}, \mathcal{J}, \mathcal{Q})$ .

A brief technical comment is that, as in our Euclidean analysis, it will be sufficient, for our discussion of the partition function, to include or consider in our path integral only configurations where the quantities  $(\kappa, v^i, \mu)$  and  $\lim_{\rho \rightarrow 0}(h_{ij}, (p_{BY})_i, (*F)_{i_1 \dots i_{D-2}})$ , describing the configuration near singularity  $\gamma$ , are constant with respect to hyperbolic time  $t$ . In particular, the constrained saddles we will construct shortly are highly symmetric and include no lightcones for  $\gamma$  where one might want to turn off the helical shift to avoid lightcone singularities as described in section 5.1.2. More generally, however, one may wish to allow  $(\kappa, v^i, \mu)$  and  $\lim_{\rho \rightarrow 0}((p_{BY})_i, (*F)_{i_1 \dots i_{D-2}})$  to vary with respect to  $t$ . When including such configurations in the path integral, an extra average over  $t$  should be included in certain equations, *e.g.* eqs. (3.50), (3.52), (3.57), (5.45) and (5.46), without significantly altering our results. (In particular, the configurations constructed below will continue to be constrained saddles.)

Let us now construct constrained saddles which are saddles for the subcontour integral  $Z_L(T, \Omega, \Phi; \mathcal{S}, \mathcal{J}, \mathcal{Q})$ . To contribute to this subcontour integral, these configurations must satisfy the boundary conditions parametrized by  $(T, \Omega, \Phi)$  on the spacetime boundary  $\partial\mathcal{M}$  and have the prescribed values of  $(\mathcal{S}, \mathcal{J}, \mathcal{Q})$  on  $\gamma$ . Moreover, as described in section 3.3, constrained saddles must satisfy the bulk equations of motion away from  $\gamma$  and also eqs. (3.57) to (3.59) appropriately Wick-rotated on  $\gamma$ .

Similar to the Euclidean construction of section 4.2.2, the starting point is a smooth Lorentzian stationary black hole solution whose Bekenstein-Hawking entropy, (angular) momentum, and electric charge are set to the given values of  $(\mathcal{S}, \mathcal{J}, \mathcal{Q})$ . Again, for a stationary black hole, it is straightforward to see that evaluating eqs. (5.45) and (5.46) on the bifurcation surface reproduces the values of (angular) momentum and electric charge obtained from standard definitions on  $\partial\mathcal{M}$ .<sup>58</sup> We further require this initial configuration to satisfy boundary conditions on one of its boundaries  $Y \times \mathbb{R}$  which are locally similar to those imposed by the path integral  $Z_L(T, \Omega, \Phi)$  — for example, we require the black hole to have boundary Killing vectors  $\zeta$  and  $\varphi$  which we then expect to extend into the bulk.

---

<sup>57</sup>The sign in eq. (5.45) results from the fact that the surface (angular) momentum density  $(p_{BY})_i$  was defined on  $-\partial\mathcal{N}_\epsilon$  while viewing this surface as an internal boundary of the spacetime  $\mathcal{M} \setminus \mathcal{N}_\epsilon$ . In contrast, for black hole solutions, we would like to equate  $\mathcal{J}$  to the usual notion of (angular) momentum defined on the outer boundary  $\partial\mathcal{M}$ . While the surface  $-\partial\mathcal{N}_\epsilon$  has orientation  $-u^A \epsilon_A$ , the surface  $\partial\mathcal{M}$  instead has orientation  $\tilde{u}^A \epsilon_A$ , where  $\tilde{u}$  is the outward normal to  $\partial\mathcal{M}$ .

<sup>58</sup>See footnote 40.

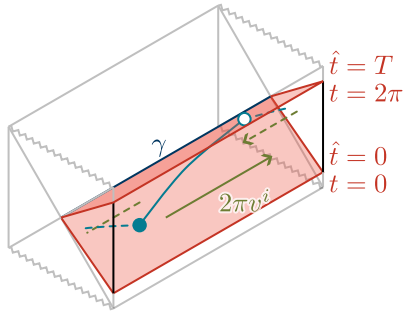


**Figure 9:** A conically and helically singular constrained saddle. Illustrated in grey is a stationary black hole spacetime. When the spatial Killing vector  $\varphi$  generates rotation (as opposed to translation), the front and back faces (where the Penrose diagram is drawn) are identified. The spacetime of the constrained saddle resides between the two red surfaces of constant time. These surfaces are identified with a relative shift  $2\pi v^i$ , *e.g.* represented by the solid green arrow. In particular, the points marked by empty and filled circles are identified, so the solid teal curve connecting these points is closed. When the helical shift  $v^i$  of  $\gamma$  is as illustrated by the solid arrow, the solid teal curve is contractible when the singularity is regularized — see section 2.2. Other choices of helical shift, *e.g.* the dashed arrow, can give configurations that are diffeomorphic to this one away from  $\gamma$  before regularization, but, upon regularization, have different contractible cycles, *e.g.* the dashed teal curve.

However, in this black hole solution, the periodic identification  $\hat{t} \sim \hat{t} + T$  is relaxed, the boundary limit of the horizon generating Killing vector is given by  $\zeta + \Omega_0 \varphi$  for some  $\Omega_0$  possibly differing from  $\Omega$ , and the electric potential  $\Phi_0$  might differ from  $\Phi$ . We will now correct these mismatches by making the bifurcation surface  $\gamma$  singular, as illustrated in fig. 9

Firstly, extending the boundary stationary time  $\hat{t}$  into the bulk, we can simply impose by hand  $\hat{t} \sim \hat{t} + T$  and consider a fundamental domain of this identification in one exterior of the black hole. This produces a spacetime of the kind illustrated in fig. 5a with no lightcones for  $\gamma$ . The metric near  $\gamma$  is given by eq. (5.6) where, taking  $t \sim t + 2\pi$  proportional to  $\hat{t}$ , the leading coefficient  $\kappa = \kappa_0 T/2\pi$  of the lapse (5.8) is determined by the horizon surface gravity  $\kappa_0$  of the black hole (as conventionally defined with respect to  $\hat{t}$ ). The hyperbolic opening angle of the now conically singular surface  $\gamma$  is then given by

$$2\pi \kappa = T \kappa_0 , \quad (5.48)$$

analogous to eq. (4.15).

When we identify the bulk surfaces  $\hat{t} = 0$  and  $\hat{t} = T$ , there is a freedom to relatively shift the surfaces along the Killing vector  $\varphi$  extended into the bulk. We can use this freedom to ensure that the Killing vector  $\xi$ , given in eq. (5.40) for the prescribed value of  $\Omega$  or any of its representatives under the equivalence relation (5.41), has closed orbits with period  $T$ . This introduces a helical singularity on  $\gamma$ , such that the helical shift in eq. (5.8)

is given by

$$v^i = \left[ \frac{T}{2\pi}(\Omega - \Omega_0) + \frac{m}{\Delta_J} \right] \varphi^i, \quad (m \in \mathbb{Z}) \quad (5.49)$$

analogous to eq. (4.17). As illustrated in fig. 9, these different  $v^i$  lead to configurations which are diffeomorphic to each other away from  $\gamma$ , but are physically distinct in the way they are regulated on  $\gamma$  — see section 2.2.

Finally, to attain the electric potential  $\Phi$  prescribed by the boundary conditions or a representative under (5.42), we can shift the Maxwell field,

$$A \mapsto A + \left( \Phi - \Phi_0 + \frac{2\pi n}{T \Delta_Q} \right) d\hat{t}. \quad (n \in \mathbb{Z}) \quad (5.50)$$

This turns on a holonomic singularity with strength

$$\mu = \frac{T}{2\pi}(\Phi - \Phi_0) + \frac{n}{\Delta_Q}. \quad (n \in \mathbb{Z}) \quad (5.51)$$

analogous to eq. (4.19).

We now have some configuration(s) satisfying the boundary conditions prescribed by  $(\beta, \Omega, \Phi)$  at  $\partial\mathcal{M}$  and having the fixed values of  $(\mathcal{S}, \mathcal{J}, \mathcal{Q})$  on  $\gamma$ . Equations of motion are satisfied away from  $\gamma$ , as in the original black hole solution, and the constrained saddle-point conditions (3.57) to (3.59) are satisfied on  $\gamma$ , as can be seen from eqs. (5.48), (5.49) and (5.51) together with the bulk Killing symmetry  $\varphi$ . Thus, we have successfully constructed constrained saddle(s) which are saddles for the subcontour integral  $Z(T, \Omega, \Phi; \mathcal{S}, \mathcal{J}, \mathcal{Q})$ , completely analogous to the Euclidean constrained saddles obtained in section 4.2.2.

The action (5.18) for these Lorentzian constrained saddles is calculated in nearly identical fashion to that section. The bulk and Gibbons-Hawking terms evaluate to

$$\int_{\mathcal{M} \setminus \mathcal{N}_\epsilon} (L_{\text{EH}} + L_{\text{M}}) + \int_{\partial\mathcal{M}} L_{\partial\mathcal{M}} + \int_{-\partial\mathcal{N}_\epsilon} L_{\text{GH}} \sim -T(E - \Omega_0 \mathcal{J} - \Phi_0 \mathcal{Q}), \quad (5.52)$$

where

$$E_{\zeta + \Omega_0 \varphi, \Phi_0}(\mathcal{S}, \mathcal{J}, \mathcal{Q}) = E(\mathcal{S}, \mathcal{J}, \mathcal{Q}) - \Omega_0 \mathcal{J} - \Phi_0 \mathcal{Q} \quad (5.53)$$

is the value of the boundary Hamiltonian generating the evolution  $\zeta + \Omega_0 \varphi$  with an electric potential  $\Phi_0$  in the original black hole solution. The helical and holonomic singularities on  $\gamma$  as described by eqs. (5.49) and (5.51) do not affect eq. (5.48), but instead enter into the action through the helical and holonomic terms:

$$\int_{-\partial\mathcal{N}_\epsilon} L_{\text{hel}} \sim -2\pi \int_{\gamma} v^i (p_{\text{BY}})_i = \left[ T(\Omega - \Omega_0) + \frac{2\pi m}{\Delta_J} \right] \mathcal{J}, \quad (5.54)$$

$$\int_{-\partial\mathcal{N}_\epsilon} L_{\text{hol}} \sim \frac{2\pi}{g_{\text{M}}^2} \int_{\gamma} \mu * F = \left[ T(\Phi - \Phi_0) + \frac{2\pi n}{\Delta_Q} \right] \mathcal{Q}, \quad (5.55)$$

where we have used eqs. (5.45) and (5.46). The action (5.18) evaluated for our constrained saddles is thus

$$I = -T E_{\xi, \Phi}(\mathcal{S}, \mathcal{J}, \mathcal{Q}) - i \mathcal{S} + 2\pi m \frac{\mathcal{J}}{\Delta_J} + 2\pi n \frac{\mathcal{Q}}{\Delta_Q} . \quad (5.56)$$

where

$$E_{\xi, \Phi}(\mathcal{S}, \mathcal{J}, \mathcal{Q}) = E(\mathcal{S}, \mathcal{J}, \mathcal{Q}) - \Omega \mathcal{J} - \Phi \mathcal{Q} \quad (5.57)$$

Summing over  $m$  and  $n$  as needed (or picking only  $m = 0$  or  $n = 0$ ), the contribution of these constrained saddle(s) to the Lorentzian path integral  $Z_L(T, \Omega, \Phi)$  is given by the analogue of eq. (4.29),

$$\sum_{m, n} Z_{\text{LBH}} \left( T, \Omega + \frac{2\pi m}{T \Delta_J}, \Phi + \frac{2\pi n}{T \Delta_Q} \right) , \quad (5.58)$$

where

$$Z_{\text{LBH}}(T, \Omega, \Phi) = \int d\mathcal{S} d\mathcal{J} d\mathcal{Q} e^{\mathcal{S} - i T E_{\xi, \Phi}(\mathcal{S}, \mathcal{J}, \mathcal{Q})} Z_{\text{LBH}}^{\text{QFT}}(T, \Omega, \Phi; \mathcal{S}, \mathcal{J}, \mathcal{Q}) , \quad (5.59)$$

and  $Z_{\text{LBH}}^{\text{QFT}}(T, \Omega, \Phi; \mathcal{S}, \mathcal{J}, \mathcal{Q})$  denotes the quantum corrections to the saddle-point evaluation of  $Z_{\text{BH}}(T, \Omega, \Phi; \mathcal{S}, \mathcal{J}, \mathcal{Q})$ . The integral (5.59) does not converge, because of the exponentially enhanced integrand at large  $\mathcal{S}$ , just as the oscillatory trace (5.36) over infinitely many states does not converge. Rather, as anticipated below eqs. (5.36) and (5.47), eq. (5.59) gives a distribution over  $T$  and the integrals displayed here should really be performed last, *e.g.* after the integral transform (5.37). Similar to the empty thermal saddle, we expect that the integral transform of eq. (5.59) will recover the Euclidean result eq. (4.30) for the black hole contribution to the grand canonical partition function  $Z(\beta, \Omega, \Phi)$ .

## 6 Discussion

### 6.1 Summary

In this paper, we have considered a class of singularities on codimension-two surfaces  $\gamma$ , in Einstein-Maxwell theory possibly with a cosmological constant, which generalizes conical singularities. In particular, as described in section 2, the helical and holonomic types of singularities involve shifts along  $\gamma$  and along the fibres of the Maxwell principal bundle as one winds around  $\gamma$  in a metric-orthogonal and connection-horizontal manner. Having given a prescription for regulating singularities with smooth configurations, we studied the curvature contributions of these singularities and subsequently, in section 3, proposed an action for singular configurations. We then studied constrained saddles, which have stationary action under variations that fix, on a codimension-two surface  $\gamma$ , area and quantities associated to (angular) momentum and electric charge. The upshot is that these constrained saddles can possess nontrivial conical, helical, and holonomic singularities on  $\gamma$ .

A motivation for considering such constrained saddles is for the purpose of evaluating the gravitational partition function. The grand canonical partition function  $Z(\beta, \Omega, \Phi)$  is most often evaluated by a path integral in Euclidean signature, where smooth black holes are well-known saddles. Alternatively, one may reorganize the path integral as we have in section 4 so as to leave for last the integrals over the Bekenstein-Hawking entropy  $\mathcal{S}$ , (angular) momentum  $\mathcal{J}$ , and integrated electric flux  $\mathcal{Q}$  evaluated locally on a codimension-two surface  $\gamma$ . The aforementioned constrained saddles are then saddles for the initial integral over subcontours of fixed  $(\mathcal{S}, \mathcal{Q}, \mathcal{J})$  and can be constructed by modifying smooth black holes to make their bifurcation surfaces conically, helically, and holonomically singular. The resulting constrained saddle-point contribution to the grand canonical partition function takes the form given by eqs. (4.29) and (4.30). Although the evaluation of the gravitational partition function is often associated with Euclidean signature, due to the conformal mode, the Euclidean gravitational action is unbounded from below on the integration contour over real Euclidean geometries [1]. The path integral over this contour is therefore manifestly divergent and ill-defined.

Turning to Lorentz signature, where integrals are instead oscillatory and have a distributional meaning, the need to consider singular configurations in the path integral becomes more pronounced. In this context, the grand canonical partition function  $Z(\beta, \Omega, \Phi)$  is given by an integral transform (5.37) on the time period  $T$  of a Lorentzian path integral  $Z_L(T, \Omega, \Phi)$ . As previously emphasized by ref. [6], in order to receive contributions analogous to Euclidean black holes, it is necessary to allow at least conically singular surfaces  $\gamma$  in the Lorentzian configurations where the time circle can contract to a point. In section 5, we generalized ref. [6]’s Lorentzian construction to include also helical and holonomic singularities on  $\gamma$ . The resulting saddle-point evaluation of the Lorentzian path integral  $Z_L(T, \Omega, \Phi)$  indeed receives contributions, given in eqs. (5.58) and (5.59), from singular constrained saddles constructed from black holes. Performing the integral transform from  $T$  to  $\beta$ , one again recovers the expected black hole contributions to the thermal partition function  $Z(\beta, \Omega, \Phi)$ , given in (4.29) and (4.30).

## 6.2 Contributing saddles and the stability of black holes

What have we gained by including helical and holonomic singularities in our analysis? One result of our more inclusive analysis is a better understanding of which saddles are relevant for the gravitational thermal partition function. In particular, we will address below some puzzles left open by the study of purely conical singularities in ref. [6], regarding the thermodynamic stability of relevant black hole saddles, with respect to variations in (angular) momentum and charge.

A direct result of including more general types of singularities is a richer set of constrained saddles. In particular, we saw explicitly in our evaluation of the Lorentzian path integral  $Z_L(T, \Omega, \Phi)$  how helical and holonomic, as well as conical, singularities appear in constrained saddles where (angular) momentum  $\mathcal{J}$  and electric charge  $\mathcal{Q}$ , as well as area  $\mathcal{S}$ , are fixed to arbitrary values. The integrals over these quantities can therefore all be saved for last while the constrained saddles provide a saddle-point evaluation of the Lorentzian path integral  $Z_L(T, \Omega, \Phi; \mathcal{S}, \mathcal{J}, \mathcal{Q})$  over subcontours of fixed  $(\mathcal{S}, \mathcal{J}, \mathcal{Q})$  — see eq. (5.47).

(As we will see, the order of integration can play an important role when analyzing the thermodynamic stability of saddles relevant to the final thermal partition function.)

However, the mere existence of a saddle, *e.g.* a constrained saddle constructed from black holes in section 5.2.2, does not guarantee that it contributes with nonzero weight to a path integral, *e.g.*  $Z_L(T, \Omega, \Phi; \mathcal{S}, \mathcal{J}, \mathcal{Q})$ . Having chosen the integration contour to be over real Lorentzian configurations, one can in principle determine the weight with which a saddle contributes using Morse theory, as reviewed in ref. [6, 19]. Let us summarize some of the pertinent results in this regard.

In general, let us consider an integral  $\int_{\mathfrak{X}} dx e^{iI(x)}$  over a middle-(real-)dimensional contour  $\mathfrak{X}$  in a complex manifold  $X$ . The idea is then to deform  $\mathfrak{X} = \sum_p \mathfrak{n}_p \mathfrak{J}_p$  into some multiples of particular contours  $\mathfrak{J}_p$ , called Lefschetz thimbles, with coefficients  $\mathfrak{n}_p$ , while leaving the value of integral unchanged. For each isolated<sup>59</sup> critical point  $p$  of the action  $I$ , the corresponding Lefschetz thimble  $\mathfrak{J}_p$  is simply the contour of steepest descent for the Morse function  $\text{Re}(iI)$ ; meanwhile, the coefficient  $\mathfrak{n}_p$  is given by the intersection number of the original contour  $\mathfrak{X}$  with the contour  $\mathfrak{K}_p$  of steepest ascent for  $\text{Re}(iI)$ . In this way, we may decompose the integral

$$\int_{\mathfrak{X}} dx e^{iI(x)} = \sum_p \mathfrak{n}_p \int_{\mathfrak{J}_p} dx e^{iI(x)} \quad (6.1)$$

into a weighted sum over Lefschetz thimbles. If one so wishes, the integral over each Lefschetz thimble can then be perturbatively approximated as a Gaussian with corrections.

A simplifying observation [6] is that, if  $\text{Re}(iI)$  is constant on  $\mathfrak{X}$ , then  $\mathfrak{n}_p$  must take values  $\pm 1$  for saddles  $p$  lying on  $\mathfrak{X}$ . Indeed, if we decompose the subcontour integral  $Z_L(T, \Omega, \Phi; \mathcal{S}, \mathcal{J}, \mathcal{Q})$  into discrete sectors in which the number of lightcone components  $\mathcal{N}_\ell$  for each connected component  $\gamma_\ell$  of  $\gamma$  is fixed, then the imaginary part of the action (5.18) takes a constant value  $-\mathcal{S}$  in the sector with no lightcones for  $\gamma$ . Moreover, the (constrained) saddles constructed in section 5.2.2 do lie on the original contour of integration over Lorentzian configurations in the lightcone-less sector. The upshot then is that all such saddles do contribute with weight  $\mathfrak{n}_p = \pm 1$  to the subcontour integral  $Z_L(T, \Omega, \Phi; \mathcal{S}, \mathcal{J}, \mathcal{Q})$ .

As described around (5.37) and (5.59), to recover the grand canonical partition function  $Z(\beta, \Omega, \Phi)$ , we must perform the integral transform (5.37) from  $T$  to  $\beta$  and the final integrals over  $(\mathcal{S}, \mathcal{J}, \mathcal{Q})$ . The final result should then agree with the answer (4.30) deduced from the naive Euclidean analysis (provided the integral transform in  $T$  behaves in the expected manner, as we will elaborate in section 6.3.1). However, whereas the Euclidean path integral did not even have a good and natural choice of integration contour to speak of, we have now argued that the natural choice of Lorentzian contour can be deformed into appropriate Lefschetz thimbles so as to recover the expected black hole contribution (4.30) to the grand canonical partition function.

To make the connection to the more standard Euclidean analysis of purely smooth configurations, let us consider the leading semiclassical approximation, where we ignore

---

<sup>59</sup>Ref. [19] also considers cases with non-isolated critical points, *i.e.* critical manifolds, with generalized Lefschetz thimbles  $\mathfrak{J}_p$  where the label  $p$  now enumerates the middle-(real-)dimensional cycles of critical manifolds.

$Z_{\text{BH}}^{\text{QFT}}$  and take the saddle-point values for the  $(\mathcal{S}, \mathcal{J}, \mathcal{Q})$  integrals in eq. (4.30). Then, the saddle-point values for  $(\mathcal{S}, \mathcal{J}, \mathcal{Q})$  are simply the on-shell values for the Bekenstein-Hawking entropy, (angular) momentum, and charge for a black hole with the values of  $(\beta, \Omega, \Phi)$  prescribed by the grand canonical ensemble; in particular, the Euclidean counterparts of these black holes are smooth everywhere, including the bifurcation surface  $\gamma$ . In this sense, smooth Euclidean black holes are saddles for the thermal partition function, as one might have guessed by considering a naive path integral over Euclidean configurations. However, let us emphasize again that this naive path integral is plagued by the conformal factor problem, so it was therefore important for us to derive this result from a Lorentzian starting point.

From eq. (4.30), we can also see how the thermodynamic stability of a given on-shell black hole comes into play. In particular (again in the semiclassical limit), local maxima of the integrand in eq. (4.30), correspond to black holes minimizing the free energy

$$F(\beta, \Omega, \Phi; \mathcal{S}, \mathcal{J}, \mathcal{Q}) = E(\mathcal{S}, \mathcal{J}, \mathcal{Q}) - \Omega \mathcal{J} - \Phi \mathcal{Q} - \frac{1}{\beta} \mathcal{S}, \quad (6.2)$$

with respect to variations in  $(\mathcal{S}, \mathcal{J}, \mathcal{Q})$ , where  $E(\mathcal{S}, \mathcal{J}, \mathcal{Q})$  is the energy of an on-shell black hole with Bekenstein-Hawking entropy  $\mathcal{S}$ , (angular) momentum  $\mathcal{J}$ , and electric charge  $\mathcal{Q}$ . Equivalently,

$$F(\beta, \Omega, \Phi; E, \mathcal{J}, \mathcal{Q}) = E - \Omega \mathcal{J} - \Phi \mathcal{Q} - \frac{1}{\beta} \mathcal{S}(E, \mathcal{J}, \mathcal{Q}) \quad (6.3)$$

is minimized with respect to the more standard set of independent quantities  $(E, \mathcal{J}, \mathcal{Q})$ , while  $\mathcal{S}(E, \mathcal{J}, \mathcal{Q})$  is a function giving the on-shell Bekenstein-Hawking entropy of a black hole with prescribed energy  $E$ . Black hole solutions which are thermodynamically unstable in any of the directions in the space of  $(\mathcal{S}, \mathcal{J}, \mathcal{Q})$  or equivalently  $(E, \mathcal{J}, \mathcal{Q})$  will extremize but not locally maximize the integrand in eq. (4.30). The question of whether such unstable black holes contribute to the partition function subtly depends on definitions, as we will elaborate in section 6.3.2. Indeed, we will argue there that such contributions can sometimes be poorly defined (not just subleading) unless the integrals along the Lefschetz thimbles of thermodynamically stable black holes are specified precisely.

To appreciate what we have gained from allowing helical and holonomic singularities into our Lorentzian path integral, it is helpful to contrast the above with the limited stability condition found by ref. [6]. The story told by ref. [6], summarized in section 1.1, is similar to the above, except that only  $\mathcal{S}$  is fixed then integrated last:

$$Z(\beta, \Omega, \Phi) = \int d\mathcal{S} dT f_{\beta}(T) Z_{\text{L}}(T, \Omega, \Phi; \mathcal{S}). \quad (6.4)$$

Saddles for the Lorentzian fixed- $\mathcal{S}$  path integral  $Z_{\text{L}}(T, \Omega, \Phi; \mathcal{S})$  have purely conical singularities and can be constructed from Lorentzian black holes as in section 4.2.2. (Helical and holonomic singularities, even if they are allowed in the path integral  $Z_{\text{L}}(T, \Omega, \Phi; \mathcal{S})$ , do not appear in saddles for this path integral where  $\mathcal{J}$  and  $\mathcal{Q}$  are integrated over and not fixed.) Going through the same argument as presented above, one finds that the conically singular



saddles  $p$  all contribute with weight  $\mathbf{n}_p = \pm 1$  to  $Z_L(T, \Omega, \Phi; \mathcal{S})$ . Naively performing the integral transform from  $T$  to  $\beta$ , one seems to find that a sufficient condition for a black hole solution to correspond to a local maximum for the  $\mathcal{S}$  integrand in eq. (6.4) is for it to minimize

$$F(\beta, \Omega, \Phi; \mathcal{S}) = E(\Omega, \Phi; \mathcal{S}) - \Omega J(\Omega, \Phi; \mathcal{S}) - \Phi Q(\Omega, \Phi; \mathcal{S}) - \frac{1}{\beta} \mathcal{S} \quad (6.5)$$

with respect to  $\mathcal{S}$ , where  $E(\Omega, \Phi; \mathcal{S})$ ,  $J(\Omega, \Phi; \mathcal{S})$ , and  $Q(\Omega, \Phi; \mathcal{S})$  are functions giving the energy, angular momentum, and charge of an on-shell black hole with a prescribed (angular) velocity  $\Omega$ , electric potential  $\Phi$ , and Bekenstein-Hawking entropy  $\mathcal{S}$ . In other words, one seems to find only a stability condition in the  $\mathcal{S}$  direction, which can be equivalently rephrased again in terms of energy and corresponds to the positivity of specific heat  $C$  as defined in (1.15).

In contrast, by performing the integrals over  $(\mathcal{S}, \mathcal{J}, \mathcal{Q})$  after the integral transform in  $T$ , we have found a stronger set of conditions corresponding to a more complete notion of thermodynamic stability. Though this is a desirable result, one is led to wonder: how was it possible for us to obtain a stronger set of stability conditions by simply reorganizing the path integral?

### 6.3 Unstable saddles and the integral transform on Lorentzian time $T$

The emergence of the extra stability conditions we have found relative to ref. [6] clearly has something to do with the order of integration in  $\mathcal{J}$  and  $\mathcal{Q}$  versus the integral transform in  $T$ . To understand this subtlety, it will be instructive to retreat to a very simple toy example where we can fully dissect the calculation in section 6.3.1. By considering a slightly more complete example in section 6.3.2, we will also explain whether and in what sense an unstable saddle can contribute to the thermal partition function.

#### 6.3.1 A simple Gaussian toy example

Let us first study an example that is perhaps overly simple but nonetheless instructive for understanding how the integral transform (5.37) acts on contributions to the Lorentzian path integral  $Z_L(T, \Omega, \Phi)$  from the Lefschetz thimbles of various saddles. Here, we consider a toy analogue for these contributions from saddles which are “stable” (+) or “unstable” (−) — in the sense to be explained below — with respect to  $\mathcal{J}$  or  $\mathcal{Q}$ ,

$$z_L^\pm(T) = \int \frac{dx}{\sqrt{\hbar}} e^{-\frac{i}{\hbar} T (H_0 \pm \omega x^2)} = \sqrt{\frac{\pi}{\pm i T \omega}} e^{-\frac{i}{\hbar} T H_0}, \quad (6.6)$$

where  $H_0$  is a constant,  $\omega > 0$  is an energy scale introduced to make  $x$  dimensionless, and we have restored  $\hbar$ . For real  $T$ , the integration contour can be taken to be  $\mathbb{R}$ , which is then deformable to the Lefschetz thimble for the saddle at  $x = 0$  so the integral converges. In this analogy,  $x$  plays the role of  $\mathcal{S}$ ,  $\mathcal{J}$ , or  $\mathcal{Q}$ , which are integrated over in  $Z_L(T, \Omega, \Phi)$ .

However, it should be noted that  $z_L^\pm(T)$  is a purely oscillatory integral, while the Lorentzian gravitational action has an imaginary part given by  $-\mathcal{S}$  (in the no-lightcone sector). Relatedly,  $z_L^\pm(T)$  is a well-defined (branched) function of  $T$  unlike the gravitational

path integral  $Z_L(T, \Omega, \Phi)$  which must be interpreted as a distribution, as described below eq. (5.36). The simplicity of our example therefore allows  $z_L^\pm(T)$  to be continued to complex values of  $T$  by inspection. The integral expression (6.6) for  $z_L^\pm(T)$  continues to complex  $T$  as well, provided the integration contour rotates along with the Lefschetz thimble of  $x = 0$  to ensure convergence. By considering the defining integral (6.6) at even just real  $T$ , it is easy to see that the branch cut of the analytic continuation lies respectively in the upper (+) or lower (-) half  $T$ -plane.

The analytic continuation of  $z_L^\pm(T)$  to negative imaginary values of  $T$  in particular,

$$z^\pm(\beta) \equiv \int \frac{dx}{\sqrt{\hbar}} e^{-\frac{1}{\hbar}\beta(H_0 \pm \omega x^2)} = z_L^\pm(-i\beta) = \sqrt{\frac{\pi}{\pm\beta\omega}} e^{-\frac{1}{\hbar}\beta H_0}, \quad (6.7)$$

has the interpretation, in this toy example, as the corresponding contribution to the thermal partition function  $Z(\beta, \Omega, \Phi)$ . A few things are noteworthy here. Firstly, we see that the sign  $\pm$  multiplies the piece of the ‘‘Euclidean action’’  $\beta(H_0 \pm \omega x^2)$  or the ‘‘free energy’’  $H_0 \pm \omega x^2$  quadratic in the fluctuation away from the saddle  $x = 0$ . Thus, depending on the sign  $\pm$ , one would ordinarily refer to the saddle as stable (+) or unstable (-).<sup>60</sup> Secondly, in the unstable case,  $z^-(\beta)$  has a sign ambiguity due to the aforementioned branch cut. Using a more complete example in section 6.3.2, we will explain how to make sense of this sign-ambiguous contribution to the partition function in terms of Stokes phenomena.

Instead of analytically continuing by inspection, let us now instead apply the integral transform (5.37) to  $z_L^\pm(T)$ , using the integral kernel  $f_\beta(T)$  given in eq. (5.39). As we have emphasized in section 5.2, our prescription is always to perform *first* this  $T$  integral *then* the remaining integrals over  $(\mathcal{S}, \mathcal{J}, \mathcal{Q})$ . In this toy example, the correct prescription is therefore to evaluate

$$\int \frac{dx}{\sqrt{\hbar}} \int_{-\infty}^{\infty} dT f_\beta(T) e^{-\frac{i}{\hbar}T(H_0 \pm \omega x^2)} = \int \frac{dx}{\sqrt{\hbar}} f_\beta(T) e^{-\frac{i}{\hbar}T(H_0 \pm \omega x^2)} = z^\pm(\beta), \quad (6.8)$$

where we have applied the residue theorem in the first equality, taking advantage of the analyticity of  $e^{-\frac{i}{\hbar}T(H_0 \pm \omega x^2)}$  and the exponential suppression of  $f_\beta(T) e^{-\frac{i}{\hbar}T(H_0 \pm \omega x^2)}$  in the lower half  $T$  plane, provided the constant  $E_0$  in  $f_\beta(T)$  is chosen to be less than  $H_0$ .<sup>61</sup> As expressed in the second equality, this matches the analytic continuation (6.7).

However, ref. [6] implicitly takes the opposite ordering of the  $\mathcal{J}$  and  $\mathcal{Q}$  integrals versus the  $T$  integral transform. Let us see the consequences of this alternative ordering of the  $T$  and  $x$  integrals in our example.

Similar to the above, as long as  $E_0 < H_0$ ,  $f_\beta(T) z_L^\pm(T)$  is exponentially suppressed at large negative imaginary  $T$ . Moreover,  $z_L^+(T)$  is analytic in the lower half  $T$ -plane, so we

<sup>60</sup>This notion of stability comes from considering real perturbations of  $x$ . Of course, the saddle is always a maximum for the magnitude of the integrand along the Lefschetz thimble of saddle. For the ‘‘unstable’’ case, the Lefschetz thimble is along the imaginary  $x$  axis. We will see in the more complete toy example of section 6.3.2 how such thimbles can combine with those of other ‘‘stable’’ saddles to give an integration contour deformable to the real line.

<sup>61</sup>Recall again that we are integrating  $x$  along the Lefschetz thimble of the saddle  $x = 0$ , where the minimum value of  $H_0 \pm \omega x^2$  is  $H_0$ .

can again use the residue theorem to evaluate<sup>62</sup>

$$\int_{-\infty}^{\infty} dT f_{\beta}(T) z_{\text{L}}^{+}(T) = z_{\text{L}}^{+}(-i\beta) = z^{+}(\beta), \quad (6.9)$$

which agrees with the analytic continuation (6.7). For this stable case, the order of integration therefore does not matter in this simple example.

In the unstable case,  $z_{\text{L}}^{-}(T)$  possesses a branch cut in the lower half plane. Choosing this branch cut to be along negative imaginary  $T$  where the pole of  $f_{\beta}(T)$  also resides,

$$\int_{-\infty}^{\infty} dT f_{\beta}(T) z_{\text{L}}^{-}(T) = \frac{e^{-\frac{1}{\hbar}\beta E_0}}{\sqrt{\pi}} \text{PV} \int_0^{\infty} d\beta' \frac{e^{-\frac{1}{\hbar}\beta'(H_0-E_0)}}{\sqrt{\beta'\omega}(\beta-\beta')} \quad (6.10)$$

$$= \frac{2e^{-\frac{1}{\hbar}\beta E_0}}{\sqrt{\beta\omega}} F\left(\sqrt{\frac{\beta(H_0-E_0)}{\hbar}}\right) \quad (6.11)$$

can be expressed as a principal value (PV) integral along the branch cut. The result can be written, as in the second equality, in terms of the Dawson  $F$  function<sup>63</sup> and disagrees with the analytic continuation (6.7). The Dawson  $F$  function has an asymptotic<sup>64</sup> power law expansion at large argument,

$$F(y) = \frac{1}{2y} + \mathcal{O}\left(\frac{1}{y^3}\right), \quad (6.12)$$

so the prefactor in eq. (6.11) determines the exponential scaling in the semiclassical limit  $\hbar \rightarrow 0$ . Unexpectedly, this is set by the somewhat arbitrary choice of  $E_0$  rather than  $H_0$  as in eq. (6.7).

To summarize what we have learned from this example, we see that, for an unstable saddle, the order of the integral transform (5.37) in  $T$  versus the integration over  $x$  — the analogue of  $(\mathcal{S}, \mathcal{J}, \mathcal{Q})$  — does matter. In particular, our prescription of first performing the integral transform in  $T$  while saving the  $x$ -integral for last leads to the expected analytic continuation (6.7) from Lorentzian to Euclidean time. This contribution to the thermal partition function is weighted exponentially by minus the “classical Euclidean action”  $\beta H_0$  and has the expected “one-loop determinant”  $\sqrt{\frac{\pi}{\pm\beta\omega}}$ , though the ambiguous sign from the choice of branch in the unstable ( $\pm = -$ ) case requires a more complete example to explain in section 6.3.2. In contrast, the opposite prescription leads to a contribution to the thermal partition function which nonsensically depends on the parameter  $E_0$  introduced in the integral kernel  $f_{\beta}(T)$  in eq. (5.39). This parameter has no bearing on the physical system and so should drop out from any physical calculation. Altogether, we view this

<sup>62</sup>Equations (6.9) and (6.10) are the only equations in this paper where we take seriously the written order of performing the integral transform in  $T$  after other, either implicit or explicit, integrals in the integrand. Elsewhere, *e.g.* in eq. (5.37), our convention of performing the  $(\mathcal{S}, \mathcal{J}, \mathcal{Q})$  integrals last, as explained below that equation, always prevails.

<sup>63</sup>Specifically,  $F(y)$  is given by `DawsonF[y]` in Mathematica.

<sup>64</sup>There is a non-perturbative correction  $\sim e^{-y^2}$  to the expansion eq. (6.12) which becomes important when the argument has a large imaginary part.

toy example as illustrating what can go wrong if the integral transform in  $T$  is performed before other integrals, over naively “unstable” variables in the path integral.

In particular, this explains why the analysis of ref. [6] found only the positivity of the specific heat to be relevant for evaluating the significance of a black hole saddle to the thermal partition function. Instead, by performing the integrals over  $\mathcal{J}$  and  $\mathcal{Q}$ , as well as  $\mathcal{S}$ , after the integral transform in  $T$ , we ensure that the latter does not misbehave when acting on saddles which are unstable with respect to  $(\mathcal{S}, \mathcal{J}, \mathcal{Q})$ . Locally maximizing the integrand for the final integrals over  $(\mathcal{S}, \mathcal{J}, \mathcal{Q})$  then leads to a more complete thermodynamic stability condition as described in section 6.2.

Before moving on, let us mention that the analyticity of  $z_L^+(T)$  in the lower half  $T$ -plane in this example is not a general property shared by integrals over the Lefschetz thimbles of all stable saddles in more nontrivial examples. In particular, non-analyticity in  $T$  can occur if the Lefschetz thimble jumps as  $T$  varies across a Stokes ray, as we will see in section 6.3.2. Because these jumps occur at finite separation from the saddle, we expect the non-analyticity to appear only beyond the perturbative expansion around the stable saddle. Nonetheless, if (opposing our general prescription) we perform the  $T$  integral transform *after* the integral over the Lefschetz thimbles of these stable saddles, the non-analyticity in the lower half  $T$ -plane can lead to unexpectedly large pathologies, similar to what we saw above for unstable saddles.

In fact, as we will see in section 6.3.2 using an example with multiple saddles for a given integral, the non-analyticities of the contributions from unstable and stable saddles can cancel against each other. Let us suppose we are able to *exactly* evaluate the integrals over the Lefschetz thimbles of all relevant saddles. Then, analyticity in the lower half  $T$ -plane of the sum of exact contributions would imply that performing the  $T$  integral transform last still corresponds to taking the expected analytic continuation  $T \rightarrow -i\beta$ . However, if we keep only perturbative expansions around each saddle or if we were to study the contribution of each saddle individually, then this ordering of the integrals can become problematic, as in the example studied above.

### 6.3.2 A more complete toy example: do unstable saddles contribute?

The question of whether and how saddles that are unstable (in the sense described above) contribute to an integral can subtly depend on definitions. We will demonstrate this explicitly by studying a slightly more complete toy example<sup>65</sup> which includes both stable and unstable saddles. We will see that ambiguities in specifying the contribution from an unstable saddle stems from ambiguities in specifying the Lefschetz thimbles for the stable saddles. Consequently, when these ambiguities are present, unless the integrals along the latter thimbles are specified to non-perturbative accuracy, it can sometimes be meaningless to include contributions from the unstable saddles.

---

<sup>65</sup>Recently, while this paper was in preparation, ref. [20] appeared, which studied the same kind of toy example and others in its appendices.

The example we will consider starts with the following “Lorentzian” integral,

$$z_{\mathbb{L}}(T) = \int_{\mathfrak{X}} \frac{dx}{\sqrt{\hbar}} e^{iI(x)}, \quad I(x) = -\frac{1}{\hbar} T \omega \left( -\frac{x^2}{2} + \frac{x^4}{4} \right), \quad (6.13)$$

where  $\omega > 0$  is again a constant introduced for dimensional consistency and, for real  $T$ , the contour of integration is  $\mathfrak{X} = \mathbb{R}$  (very slightly rotated to ensure convergence). We view this integral as a toy analogue for  $Z_{\mathbb{L}}(T, \Omega, \Phi)$  where again  $x$  can represent any of  $(\mathcal{S}, \mathcal{J}, \mathcal{Q})$ .

Equation (6.13) is a slightly richer toy example compared to the Gaussian example of section 6.3.1, because we now have three saddle points, at  $x = -1, 0, 1$ . But near each saddle, the integrand of eq. (6.13) is still approximated by that of the Gaussian example (6.6) (for possibly differing  $\omega$ ), so we can again classify the saddles by their stability. In the language of section 6.3.1, the  $x = -1, 1$  saddles are stable while the  $x = 0$  saddle is unstable — again, this notion of stability will become more intuitive once we pass from  $T$  to thermal time  $\beta$  below in eq. (6.14).

The main question which we would like to understand with this toy example is whether the saddles  $x = -1, 0, 1$  contribute to the integral  $z_{\mathbb{L}}(T)$  and, more importantly, its “Euclidean” analogue (6.14) below which represents the thermal partition function. Let us therefore give a more precise definition for what counts as a contributing saddle. As briefly reviewed around eq. (6.1), the contour  $\mathfrak{X}$  chosen for an integral, *e.g.*  $\mathfrak{X} = \mathbb{R}$  for eq. (6.13), can be deformed into a linear combination  $\sum_p \mathfrak{n}_p \mathfrak{J}_p$  of Lefschetz thimbles. We shall say that a given saddle  $p$  contributes to the integral if the saddle’s corresponding Lefschetz thimble  $\mathfrak{J}_p$  appears in this linear combination with nontrivial coefficient  $\mathfrak{n}_p \neq 0$ .

In the “Lorentzian” case of real  $T$ , all three saddles contribute. This follows from the fact that, at real  $T$ , the integral (6.13) defining  $z_{\mathbb{L}}(T)$  is purely oscillatory on  $\mathfrak{X} = \mathbb{R}$ , so the same argument given in the paragraph following eq. (6.1) applies and says that  $\mathfrak{X}$  has intersection number  $\mathfrak{n}_p = \pm 1$  with the contours of steepest ascent  $\mathfrak{K}_p$  for saddles  $p \in \mathfrak{X}$ . For our relatively simple example, we can be even more explicit and illustrate all pertinent contours in fig. 10. The left- and right-most panels here are relevant for the case of real  $T$  currently under consideration. It is clear that the integration contour  $\mathfrak{X} = \mathbb{R}$  (green line) intersects each ascent contour  $\mathfrak{K}_p$  (red curve) once and can be deformed into a sum of all Lefschetz thimbles  $\mathfrak{J}_p$  (dark blue curves).<sup>66</sup>

The analogue of a thermal partition function in this simple example is

$$z(\beta) \equiv \int \frac{dx}{\sqrt{\hbar}} e^{-\frac{1}{\hbar} \beta \omega \left( -\frac{x^2}{2} + \frac{x^4}{4} \right)} = z_{\mathbb{L}}(-i\beta), \quad (6.14)$$

obtained by analytically continuing the integrand in the defining integral (6.13). As illustrated in fig. 10, we can continue to make the choice  $\mathfrak{X} = \mathbb{R}$  of integration contour everywhere in the lower half  $T$ -plane — in particular, the contour  $\mathfrak{X} = \mathbb{R}$  connects asymptotic regions in the  $x$ -plane where  $\text{Re}(iI(x)) \rightarrow -\infty$ . Because  $z_{\mathbb{L}}(T)$  is merely a (branched) function of  $T$ , we also have the option to analytically continue  $z_{\mathbb{L}}(T)$  to negative imaginary  $T$  after performing the  $x$ -integral like in section 6.3.1.

<sup>66</sup>The sign of  $\mathfrak{n}_p$  just corresponds to how one chooses to define the orientations of  $\mathfrak{J}_p$  and  $\mathfrak{K}_p$ .

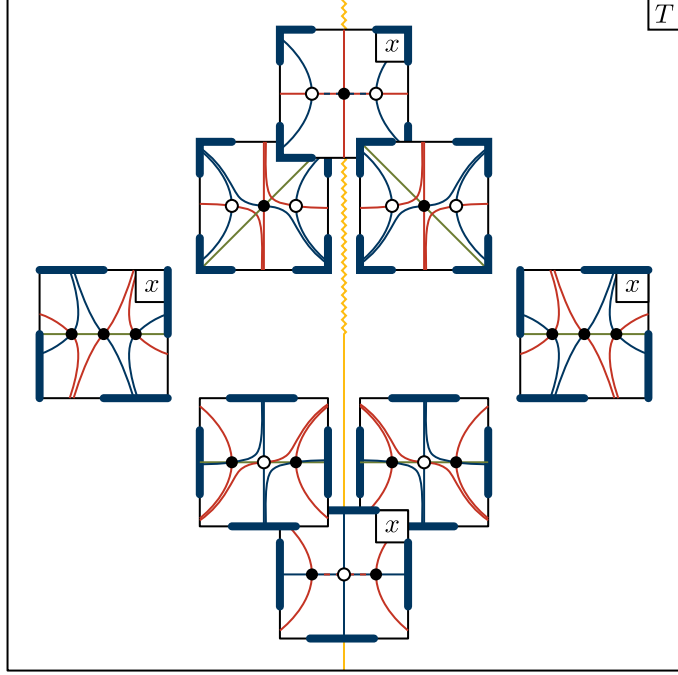


**Figure 10:** Pertinent contours for the integral  $z_L(T)$  given in eq. (6.13). This figure illustrates the complex  $x$  plane “fibred” over the complex  $T$  plane: negative and positive  $T$  correspond to the left- and right-most panels while imaginary  $T$  correspond to the top- and bottom-most panels; additional panels showing limits approaching the imaginary  $T$ -axis from the left and right are positioned accordingly. **For the  $x$ -plane in each panel:** Saddle points for the action  $I(x)$  are illustrated by dots, which are solid if  $\text{Re}(iI(x))$  is maximized among the three saddle points. Lefschetz thimbles (*i.e.* contours of steepest descent) and contours of steepest ascent for the Morse function  $\text{Re}(iI(x))$  are respectively illustrated by dark blue and red curves. All contours that give convergent integrals, *e.g.* the Lefschetz thimbles, must be in the relative homology of the asymptotic regions indicated by thick dark blue lines where  $\text{Re}(iI(x)) \rightarrow -\infty$ . The green line indicates the contour of integration  $\mathfrak{X}$  defining  $z_L(T)$ . **In the  $T$ -plane:** Stokes rays lie on the imaginary  $T$  axis, as highlighted in yellow. The function  $z_L(T)$ , with the aforementioned choice of integration contours, has a branch cut in the upper half  $T$ -plane, say along the positive imaginary axis as shown by a zigzag; otherwise,  $z_L(T)$  is analytic in  $T$ .

In reality though, the Lorentzian gravitational path integral  $Z_L(T, \Omega, \Phi)$  is not a function but a distribution in real  $T$  as described below eq. (5.36). The thermal partition function  $Z_L(T, \Omega, \Phi)$  is therefore obtained by an integral transform (5.37) rather than by a naive analytic continuation. However, granted we perform integrals in the correct order, we expect this integral transform to amount to an analytic continuation of the *integrand* before the  $(\mathcal{S}, \mathcal{J}, \mathcal{Q})$  integrals, *e.g.* taking eq. (5.59) to eq. (4.30). This is certainly true in both the simpler toy example of section 6.3.1 and the current toy example: applying the integral transform (5.37) before the  $x$ -integral, as per our prescription, simply has the effect of analytically continuing the  $x$ -integrand to  $T = -i\beta$ . It just so happens in these toy examples

that we can equivalently perform the analytic continuation after the  $x$  integral as well.<sup>67</sup>

Let us now work towards answering the question of whether the saddles  $x = -1, 0, 1$  contribute to  $z(\beta)$ . To this end, we consider again the Lefschetz thimbles  $\mathfrak{J}_p$  and steepest ascent contours  $\mathfrak{K}_p$  for each saddle point  $p$ . As illustrated in the bottom-most panel of fig. 10, the Lefschetz thimble of the  $x = 0$  saddle lies on the imaginary  $x$  axis, while those of the  $x = -1, 1$  saddles include the negative and positive real  $x$  axes respectively. In particular, the latter thimbles connect the  $x = -1, 1$  saddles to the  $x = 0$  saddle, but it then becomes somewhat ambiguous whether and in which direction one should extend these thimbles after that point. Correspondingly, the steepest ascent contour  $\mathfrak{K}_{x=0}$  for  $x = 0$  has an ambiguous intersection number with the original integration contour  $\mathfrak{X} = \mathbb{R}$ . This situation where multiple saddle points are connected by Lefschetz thimbles is known as a Stokes phenomenon<sup>68</sup> and the aforementioned ambiguities are closely tied to the question of whether and with what sign the “unstable” saddle  $x = 0$  contributes to  $z(\beta)$ .

To better appreciate this phenomenon, let us move slightly off the so-called Stokes ray — here, the negative imaginary  $T$  axis — and consider limits where we approach this ray from the left and right. This is illustrated in the two panels closely straddling but not directly on the negative imaginary  $T$  axis in fig. 10. Decomposing  $\mathfrak{X} = \mathbb{R}$  into the Lefschetz thimbles, going between the two panels, it is clear that the contribution to  $z(\beta)$  from the Lefschetz thimble of  $x = 0$  flips sign, as the direction of integration along the imaginary  $T$  axis reverses. Additionally, we see that pieces of the Lefschetz thimbles for the  $x = -1, 1$  saddles jump discontinuously from positive to negative imaginary  $T$  and vice versa. In total, the sign flip in the contribution from the  $x = 0$  saddle and the discontinuous jumps in the Lefschetz thimbles of the  $x = -1, 1$  saddles cancel to give a function  $z_L(T)$  that is analytic across the negative imaginary  $T$  axis, so the value of the thermal partition function  $z(\beta) = z_L(-i\beta)$  remains unambiguous.

We are now in a position to give an answer to the question of whether various saddles contribute to the thermal partition function. This answer is based purely on our simple toy example — we leave it for future work to generalize the qualitative lessons learned here to more realistic examples arising from the gravitational path integral. “Stable” saddles, in this example  $x = -1, 1$ , unambiguously contribute as their Lefschetz thimbles  $\mathfrak{J}_p$  are included with unambiguous coefficients in the decomposition  $\mathfrak{X} = \sum_p \mathbf{n}_p \mathfrak{J}_p$  of the contour of integration. There is nonetheless a question of whether one wants to extend thimbles after they run into an “unstable” saddle, in this example  $x = 0$ , when we have a Stokes phenomenon. If not, then we should not include the Lefschetz thimble of the unstable saddle. If we choose to extend the Lefschetz thimbles of stable saddles after they reach unstable saddles, then, as in this example, there might be an ambiguity in which direction they should be extended. However, these ambiguities are to be exactly cancelled by the equally ambiguous contribution from the Lefschetz thimble of the unstable saddle.

<sup>67</sup>In the current example, due to the analyticity of  $z_L(T)$  in the lower half  $T$ -plane, it is possible also to perform the  $T$  integral transform after the  $x$  integral, as mentioned at the end of section 6.3.1. But again, this can be dangerous if the  $x$  integral is evaluated approximately using saddle-point methods.

<sup>68</sup>We refer the reader to [19] for an accessible review of Morse theory including a discussion of Stokes phenomena.

In particular, in situations where we only have perturbative knowledge of the integrals along the Lefschetz thimbles of the stable saddles, it might seem pointless to include any contributions from the Lefschetz thimbles of the unstable saddle. After all, it is not immediately obvious how the perturbative expansion of the integral along the Lefschetz thimble of a stable saddle can know about the choice of extension, if any, of this Lefschetz thimble at finite separation from the saddle. Even if we wanted to include the non-perturbatively small correction from the unstable saddle, would we even know what sign to assign to it?

However, let us again emphasize that further study is required to generalize the analysis carried out here for a very simple toy example, in particular involving a *one-dimensional* integral. For example, ref. [20] advocates in certain situations for the inclusion of saddles with an even number of unstable variables. In particular, on a Stokes ray, ref. [20] suggests taking an average from both sides of the ray. With this prescription, it might be possible to define an unambiguous nonzero coefficient  $\mathfrak{n}_p$  for a saddle  $p$  with an even number of unstable variables. Moreover, ref. [20] provides examples where the contributions from unstable saddles, unambiguously so defined, can provide sizable corrections to the (potentially asymptotic, optimally truncated) perturbative expansions around stable saddles. We will leave further study of these ideas for future work.

#### 6.4 Equivalent boundary conditions, inequivalent singularities, and black hole sums

On the topic of saddles, another interesting feature worth discussing is the sum over constrained saddles constructed from black holes — see eqs. (4.29) and (5.58). Around eq. (4.31), we already explained how this sum gives rise to a discrete spectrum for angular momentum and charge. Let us review how these sums came about from identifying equivalent boundary conditions and distinguishing inequivalent “internal” structures of helical and holonomic singularities. Below, we will also relate one of the integer sums in eq. (4.29) to the sum over an integer-parameter subset of the  $SL(2, \mathbb{Z})$  black holes in  $AdS_3$  [12].

The Euclidean and Lorentzian path integrals studied in sections 4 and 5.2 were in part specified by supplying grand canonical boundary conditions at the spacetime boundary  $\partial\mathcal{M} = Y_{\text{space}} \times S_{\text{time}}^1$ , parameterized by an inverse temperature  $\beta$  in the Euclidean case or a Lorentzian time period  $T$ , a(n angular) velocity  $\Omega$ , and an electric potential  $\Phi$ .<sup>69</sup> In particular, we noted that it is natural to identify different values of  $\Omega$  and  $\Phi$  as equivalent if they related by discrete increments which are finite for the case of rotation or a compact Maxwell gauge group. This discrete identification of  $\Omega$ , given in eqs. (4.8) and (5.41), arose from the observation that a full rotation or a double rotation ought to act trivially — if a dual boundary theory exists, then the distinction corresponds to whether the dual theory has fermions that are anti-periodically identified under the rotation. Similarly, a full rotation around the Maxwell gauge group should be tantamount to the identity, motivating the identification of  $\Phi$  given in eqs. (4.9) and (5.42).

One might wonder whether there are further identifications that should be made between naively distinct boundary conditions. While we have been vague about the precise

---

<sup>69</sup>Recall that the  $S_{\text{time}}^1$  is the orbit of the co-rotating Killing vector given in eq. (4.3) or eq. (5.40), and is not metric-orthogonal to  $Y_{\text{space}}$  when  $\Omega \neq 0$ .



spacetime asymptotics at  $\partial\mathcal{M}$  we are considering, with an eye towards AdS/CFT, one setting we are particularly interested in is when the cosmological constant is negative and the spacetime is asymptotically locally AdS. In this case, it is natural to identify boundary conditions related by all modular transformations for the conformal boundary (preserving spin structure, if present). For the case of  $D = 3$  bulk spacetime dimensions, a (Euclidean<sup>70</sup>) boundary torus  $\partial\mathcal{M} = S^1_{\text{space}} \times S^1_{\text{time}}$  can be specified in the usual way by identifying a complex plane under shifts by 1 and by a modular parameter  $\tau$  in the upper half plane — specifically, the line segments from 0 to 1 and  $\tau$  respectively correspond to the  $S^1_{\text{space}}$  and  $S^1_{\text{time}}$  cycles. The modular transformations are then given by

$$\tau \mapsto \frac{a\tau + b}{c\tau + d}, \quad \begin{pmatrix} a & b \\ c & d \end{pmatrix} \in \text{PSL}(2, \mathbb{Z}), \quad (6.16)$$

Our identification (4.8) on  $\Omega$  is generated by<sup>71</sup>

$$\mathcal{T} = \begin{pmatrix} 1 & 1 \\ 0 & 1 \end{pmatrix} \in \text{PSL}(2, \mathbb{Z}) \quad (6.17)$$

if states come back to themselves after one full rotation, or  $\mathcal{T}^2$  if two rotations are required.

In sections 4.2.2 and 5.2.2, we saw how the identifications in  $\Omega$  and  $\Phi$  naturally give rise to a discrete set of constrained saddles, labelled by two integers  $m, n \in \mathbb{Z}$ , at fixed  $(\beta \text{ or } T, \Omega, \Phi; \mathcal{S}, \mathcal{J}, \mathcal{Q})$ . These constrained saddles are actually diffeomorphic and gauge equivalent to each other *if* we cut out the singular surface  $\gamma$ . However, as described in section 2.2.1, the helical and holonomic singularities in these constrained saddles are distinguished by the way in which a small neighbourhood  $\mathcal{N}_\epsilon$  of  $\gamma$  is smoothly filled in by the regulated versions of these configurations. For example, the constrained saddles labelled by different  $m$  have different combinations of the boundary cycles which are contractible in the (regulated<sup>72</sup>) bulk. Specifically, if we choose the  $m = 0$  constrained saddle to be one in which  $S^1_{\text{time}}$  is contractible, then more general  $m$  will have contractible cycles  $m S^1_{\text{space}} + S^1_{\text{time}}$  or  $2m S^1_{\text{space}} + S^1_{\text{time}}$  respectively if boundaries  $\partial\mathcal{M}$  related by  $\mathcal{T}$  or  $\mathcal{T}^2$  are deemed equivalent. Thus, the internal structures of these helical singularities are physically inequivalent and such distinct configurations should be summed over in the path integral. Similar comments can be made about constrained saddles with different  $n$  and different contractible cycles in the Maxwell principal fibre bundle.

<sup>70</sup>In relation to the parameters  $\beta$  and  $\Omega$  specifying Euclidean boundary conditions as described in section 4.1,

$$\tau = i\beta \left( \frac{1}{2\pi} - \frac{\Omega}{\text{Period}(\varphi)} \right) \quad (6.15)$$

where we recall that  $\Omega$  is imaginary in order for the boundary to be Euclidean.

<sup>71</sup>This is the usual “ $T$ ” element of  $\text{PSL}(2, \mathbb{Z})$  and  $\mathcal{T}$  in eq. (6.19) below is the usual “ $S$ ”; we use script symbols, because  $T$  already refers to a Lorentzian time period in this paper.

<sup>72</sup>The notion of contractibility might seem ambiguous in configurations where the helical singularity can prevent cycles from contracting to zero proper size. To precisely define contractibility, we therefore refer to regulated versions of such configurations where the helical singularity has been smoothed out over a small neighbourhood  $\mathcal{N}_\epsilon$  — see section 2.2.

Let us now connect this discussion back to previous work [12] which considered sums over *smooth*  $\mathrm{SL}(2, \mathbb{Z})$  black holes. As explained in section 6.2, smooth Euclidean black holes, in an appropriate sense, appear as saddles for the final  $(\mathcal{S}, \mathcal{J}, \mathcal{Q})$  integrals in the thermal partition function. Specifically, for a given Lorentzian or Euclidean constrained saddle labelled by  $m$  and  $n$ , the saddle-point values of  $(\mathcal{S}, \mathcal{J}, \mathcal{Q})$  (which can depend on  $m$  and  $n$ ) are precisely those for which the helical and holonomic singularities, as well as the Euclidean conical singularity, vanish. However, as we tune  $(\mathcal{S}, \mathcal{J}, \mathcal{Q})$  to their saddle-point values, the topology of each constrained saddle does not change; in particular, the smooth Euclidean saddles with different  $m$  must continue to have different boundary cycles  $m S_{\text{space}}^1 + S_{\text{time}}^1$  or  $2m S_{\text{space}}^1 + S_{\text{time}}^1$  that are contractible.

We can now identify these smooth Euclidean saddles as an integer-parameter subset of the  $\mathrm{SL}(2, \mathbb{Z})$  black holes in  $\mathrm{AdS}_3$  [12]. Let us recall that these latter geometries  $\mathcal{M}_{c,d}$  are labelled by two coprime integers  $c \geq 0$  and  $d$ . In particular,  $\mathcal{M}_{0,1}(\tau)$  is the thermal but otherwise empty  $\mathrm{AdS}_3$  saddle, described in section 4.2.1, with a contractible  $S_{\text{space}}^1$ . The other  $\mathcal{M}_{c,d}(\tau)$  can be constructed from  $\mathcal{M}_{0,1}$  using eq. (6.16),

$$\mathcal{M}_{c,d}(\tau) = \mathcal{M}_{0,1} \left( \frac{a\tau + b}{c\tau + d} \right). \quad (6.18)$$

(The RHS depends only on  $(c, d)$ , because we require  $ad - bc = 1$  in eq. (6.16) and because  $\mathcal{M}_{0,1}(\tau) = \mathcal{M}_{0,1}(\mathcal{T}(\tau))$ .) A notable example is the BTZ black hole

$$\mathcal{M}_{1,0}(\tau) = \mathcal{M}_{0,1}(\mathcal{S}(\tau)), \quad \mathcal{S} = \begin{pmatrix} 0 & -1 \\ 1 & 0 \end{pmatrix} \in \mathrm{PSL}(2, \mathbb{Z}) \quad (6.19)$$

where the time circle  $S_{\text{time}}^1$  is contractible. More generally, the contractible cycle in  $\mathcal{M}_{c,d}(\tau)$  is given by  $c S_{\text{time}}^1 + d S_{\text{space}}^1$ . We therefore expect our Euclidean saddles labelled by  $m$  to correspond to the geometries

$$\mathcal{M}_{1,m}(\tau) = \mathcal{M}_{0,1}(\mathcal{S} \circ \mathcal{T}^m(\tau)) \quad (6.20)$$

or  $\mathcal{M}_{1,2m}(\tau)$  respectively if boundaries  $\partial \mathcal{M}$  related by  $\mathcal{T}$  or  $\mathcal{T}^2$  are deemed equivalent.

Let us remark that our sum over inequivalent helical singularities bears close resemblance to the sum over different “KK instantons” (which we call holonomic singularities) in  $D = 2$  dimensions in ref. [11]. However, whereas our helical singularities are fundamentally singular, the (single insertions of) KK instantons are the dimensional reductions of the smooth bifurcation surfaces in  $\mathrm{SL}(2, \mathbb{Z})$  black holes. As described above, the sum over a subset of  $\mathrm{SL}(2, \mathbb{Z})$  black holes (and thus over a subset of single KK instanton insertions) corresponds to taking the on-shell values of  $(\mathcal{S}, \mathcal{J}, \mathcal{Q})$  in our sum over otherwise singular constrained saddles.

The above considerations naturally lead to some further open questions. Firstly, how might the other  $\mathrm{SL}(2, \mathbb{Z})$  black holes arise as saddles for the thermal partition function, starting from singular constrained saddles of a fixed- $(\mathcal{S}, \mathcal{J}, \mathcal{Q})$  path integral? Relatedly, one might also ask whether it is possible to recover the other  $\mathrm{SL}(2, \mathbb{Z})$  black holes from a purely Lorentzian starting point. Finally, once we understand whether and how each of

these  $\text{SL}(2, \mathbb{Z})$  black holes arise from a Lorentzian path integral, we can turn to the question of whether the Lefschetz thimble of each saddle really contributes to the path integral as described in sections 6.2 and 6.3. We will leave these questions largely for future study.

However, let us sketch in fig. 11 an example which inspires some hope that our construction of singular constrained saddles might also apply to these more general geometries. For simplicity, we have assumed in the preceding discussion that the constructions of constrained saddles in sections 4.2.2 and 5.2.2 start with a standard black hole, specifically with a contractible  $S_{\text{time}}^1$  if in Euclidean signature. However, one can consider other possibilities. In fig. 11, we instead start with a Lorentzian CRT-twisted black hole [13] which is a quotient of the standard BTZ black hole. The resulting constrained saddle in fig. 11c is a Lorentzian geometry in which the boundary cycle  $2S_{\text{time}}^1 - S_{\text{space}}$  is contractible in the bulk. Indeed, as refs. [21, 22] point out, the Euclidean counterpart of the CRT-twisted black hole is a Euclidean  $\text{SL}(2, \mathbb{Z})$  black hole  $\mathcal{M}_{2,-1}$ , which has a contractible  $2S_{\text{time}}^1 - S_{\text{space}}$  cycle. Running through the same analysis as in section 4.2.2 and discussed above, we might then expect to generate another integer-parameter subset of  $\text{SL}(2, \mathbb{Z})$  black holes, perhaps  $\mathcal{M}_{2,2m-1}$  or  $\mathcal{M}_{2,4m-1}$ , as saddles of the  $(\mathcal{S}, \mathcal{J}, \mathcal{Q})$  integrals.

## 6.5 Other open problems and future directions

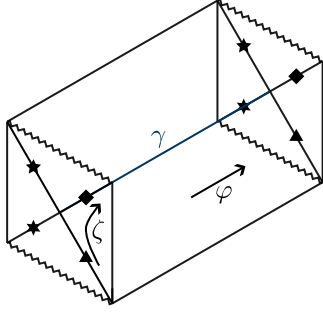
Let us conclude with a discussion of some additional open problems and possible avenues for future work.

### 6.5.1 Subtleties of our new singularities and their action

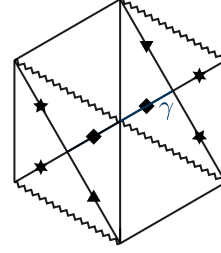
We started this paper by specifying in section 2.1 what we meant by conical, helical, and holonomic singularities on a codimension-two surface  $\gamma$  in a Euclidean spacetime. In particular, we described the strengths of these singularities in terms of three respective parameters  $(\kappa, v^i, \mu)$ . As summarized in section 2.1.3, we placed various restrictions on how we allow these singularity strengths to vary around and along  $\gamma$ . While this removed some subtleties related to the cutoff surface  $\partial\mathcal{N}_\varepsilon$  appearing in the action of singular configurations, these ad hoc restrictions were not really based on physical motivations. This became a poignant issue, for example, in the Lorentzian discussion of section 5.1.2, where we realized that a helical shift  $v^i$  which persists for all boost times  $\tau$  around  $\gamma$  will generically give rise to singularities on the lightcone emanating  $\gamma$ .

Should we allow these lightcone singularities? Relatedly, should we allow the singularity parameters  $(\kappa, v^i, \mu)$  to vary with respect to  $\tau$  and/or along the surface  $\gamma$ ? We leave these questions for future work. To answer these questions, one might attempt an analysis analogous to the appendices of ref. [14] and try to determine the most general form of  $(\kappa, v^i, \mu)$  and the near- $\gamma$  expansion of the metric and Maxwell field which would admit a solution to the Einstein-Maxwell equations away from  $\gamma$ .

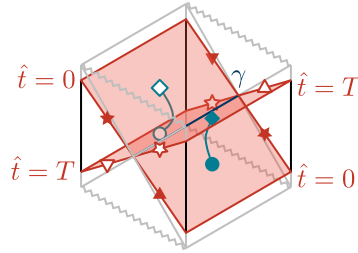
In section 3, we wrote down an action (3.1) for configurations with conical, helical, and holonomic singularities, motivated by the study in section 2.3 of curvatures in regulated configurations. In these regulated configurations, the singularity on  $\gamma$  is smoothed out over an  $\varepsilon$ -neighbourhood  $\mathcal{N}_\varepsilon$  of  $\gamma$ . In the limit where  $\varepsilon \rightarrow 0$ , contact terms in the Ricci



(a) A BTZ black hole. Points indicated by like shapes are identified along the spatial circle direction running between the front and back faces (where the Penrose diagram is drawn). Time translation, *i.e.* boosts around the bifurcation surface  $\gamma$ , are generated by the *non-rotating* Killing vector  $\zeta = \partial_{\hat{t}}$ . Rotation along the spatial circle is generated by the Killing vector  $\varphi$ . (These Killing vectors were originally defined in section 5.2.1 on the spacetime boundary  $\partial\mathcal{M}$ , but have obvious bulk extensions.) For simplicity let us take this BTZ black hole to be non-rotating,  $\Omega = 0$ .



(b) A quotient of the BTZ black hole gives the CRT-twisted black hole [13]. The halved depth of this figure relative to (a) is intentional. Notice that the front and back faces are identified after a twist around the bifurcation surface  $\gamma$ . Despite appearances, there is only one connected asymptotic region.



(c) A constrained saddle with a conical singularity on the bifurcation surface  $\gamma$  resulting from fixing area, *i.e.* the Bekenstein-Hawking entropy  $\mathcal{S}$ . Points marked by like shapes, respectively filled and empty, were already identified in the CRT-twisted black hole (b). We now also identify the  $\hat{t} = 0$  and  $\hat{t} = T$  red surfaces, such that all like shapes are identified, irrespective of filling. The spacetime of the constrained saddle lies in between these time slices and satisfies boundary conditions with  $T\Omega = \text{Period}(\varphi)/2$ . Away from  $\gamma$ , this configuration is diffeomorphic to the one shown in fig. 9. However, note the following differences, which we expect to become sharp when the singularity on  $\gamma$  is regulated — see section 2.2. Firstly,  $\gamma$  here contains half as many points as in fig. 9. Secondly, the contractible cycles shown in teal here and in fig. 9 differ. In particular, the teal cycle here is a bulk orbit of *non-rotating* time translation  $\zeta$  and is homologous to the boundary cycle  $2S_{\text{time}}^1 - S_{\text{space}}$ , where  $S_{\text{time}}^1$  is the orbit of  $\xi = \zeta + \Omega\varphi$  *rotating* with angular velocity  $\Omega$ . Thirdly, the hyperbolic opening angle around  $\gamma$  here is double that of fig. 9 and there is no helical singularity on  $\gamma$  here. More generically, one can also fix an *off-shell* value of the angular momentum  $\mathcal{J}$  evaluated on  $\gamma$  here, which will lead to a helical singularity but still with a strength differing from the construction in fig. 9. In fact, as before, we expect to have an integer-parameter family of constrained saddles with inequivalent helical singularities on  $\gamma$ .

**Figure 11:** A BTZ black hole, a CRT-twisted black hole [13], and a constrained saddle constructed from the latter.

curvature and Maxwell field strength are equated to an area term on  $\gamma$  and terms on the cutoff surface  $\partial\mathcal{N}_\varepsilon$ , as displayed in the action eq. (3.1).

This derivation, however, was somewhat ad hoc because we intentionally dropped terms which, in the  $\varepsilon \rightarrow 0$  limit, amount to ill-defined squared  $\delta$ -functions on  $\gamma$  with coefficients quadratic in the singularity strengths  $v^i$  and  $\mu^i$ . As sketched below eq. (2.29), this situation is quite analogous to having conical singularities in higher curvature theories [14, 16] — indeed, the Maxwell action is, in a sense, a curvature-squared term. For states of fixed geometric entropy in higher curvature theories, ref. [14] showed that the appropriate action for the conical singularities  $\gamma$  is given by the geometric entropy  $\sigma$  of  $\gamma$  times the singularity strength. Roughly speaking, this corresponds to isolating contributions to the action, coming from a neighbourhood  $\mathcal{N}_\varepsilon$  of  $\gamma$  in a regulated configuration, which are *linear* in the singularity strength [16]. Our derivation of the action (3.1) is essentially a naive re-enactment of this procedure for helical and holonomic singularities. Of course, ref. [14] justified their proposal for the action of fixed geometric entropy states, by showing that it leads to a good fixed- $\sigma$  variational principle with a careful derivation of the near- $\gamma$  asymptotics of (constrained) solutions. In section 3.3, we similarly studied the variation of the action at fixed area, (angular) momentum, and charge on  $\gamma$ ; however, as already mentioned, it still remains to show that the near- $\gamma$  asymptotics of Einstein-Maxwell constrained solutions indeed take the form we have assumed.

Another subtlety of the action (3.1) worth further investigation concerns the cutoff surface  $\partial\mathcal{N}_\varepsilon$  on which some of its terms live. As explained in section 3.1.1, the profile of the cutoff surface  $\partial\mathcal{N}_\varepsilon$  cannot be chosen arbitrarily without changing the value of the action, unless some restrictions are made on how the singularity parameters  $(\kappa, v^i, \mu)$  vary around and along  $\gamma$ . In particular, the cutoff surface  $\partial\mathcal{N}_\varepsilon$  prescribed by our derivation of the action is one which lies at constant proper separation (of order  $\varepsilon$ ) from  $\gamma$ . As described in section 5.1.2, this becomes particularly concerning when the action is continued to Lorentzian signature, because such a cutoff surface  $\partial\mathcal{N}_\varepsilon$  can now run affinely far away along any lightcones that  $\gamma$  might possess. Is this a bug or a feature? In section 5.1.2, we suggested that perhaps this might be a feature of the action which accounts for possible lightcone singularities. However, this claim clearly requires more careful justification.

Given the ad hoc nature of our derivation and the peculiarities of our action, one might wonder if there is a more elegant language with which to quantify helical singularities and their action. In earlier work where helical singularities arose from the backreaction of spinning particle worldlines, it was natural to describe these singularities in terms of torsion [9]. Just as the localized stress energy of a particle worldline (or brane world-volume in  $D > 3$  spacetime dimensions) gives rise to a distributional curvature recognized as a conical singularity, the localized spin density of a spinning particle imprints a distributional torsion through Einstein-Cartan equations of motion. Just as curvature quantifies rotational holonomy, *e.g.* conical deficit or excess, torsion similarly quantifies a translational holonomy [23], *e.g.* the helical shift  $v^i$  around a helical singularity [9]. Optimistically, one may therefore expect that helical singularities and their action can be described equally cleanly in Einstein-Cartan theory as conical singularities are in Einstein-Hilbert theory. Even having obtained such a description, however, the question still remains as to what it

might teach us about torsion-free gravitational theories.

### 6.5.2 Higher dimensions, angular momentum, and nonconstant modes on $\gamma$

We expect that the majority of the formalism developed in this paper applies to spacetimes of any dimension  $D \geq 3$ . At certain points in this paper, we have focused on  $D = 3$  for simplicity, so it may be worthwhile now to review some of the challenges that might arise in  $D > 3$  — these include divergences in the action and difficulty defining angular momentum  $\mathcal{J}$  on a codimension-two surface  $\gamma$ . Discussion of the latter will then invite the consideration of quantities other than  $(\mathcal{S}, \mathcal{J}, \mathcal{Q})$  on  $\gamma$ , somewhat reminiscent of non-constant edge modes.

Let start with the action. One new feature that appears in higher dimensions  $D > 3$  is a term (2.34) in the Einstein-Hilbert action  $\int_{\mathcal{M} \setminus \mathcal{N}_\varepsilon} R$  outside an  $\varepsilon$ -neighbourhood  $\mathcal{N}_\varepsilon$  of a helically singular surface  $\gamma$ . In  $D = 3$ , this term vanishes because the quadratic scalar (2.35) built from  $\mathcal{L}_v h_{ij}$  is identically zero, for any metric  $h_{ij}$  on  $\gamma$  and helical shift  $v^i$ . This is no longer true generically in  $D > 3$  and the contribution (2.34) to the Einstein-Hilbert action in fact diverges as  $\varepsilon \rightarrow 0$ . How should we treat this divergence? Should a counterterm be introduced to cancel it, like in the treatment of conical singularities in higher curvature theories [14]? Or, is this divergence indicating that we should restrict to configurations where  $\mathcal{L}_v h_{ij}$  satisfies eq. (2.35)? We leave these general questions for future work, but let us note that, at least for the highly symmetric constrained saddles built from black holes for the purpose of evaluating the thermal partition function, we expect  $\mathcal{L}_v h_{ij} = 0$  and this divergence to be absent.

Another simplification of choosing  $D = 3$  arose in defining a notion of angular momentum  $\mathcal{J}$  evaluated on  $\gamma$ . A distinguished role was played by black holes in the evaluation of the thermal partition function, so, for black holes, we would like  $\mathcal{J}$  (evaluated on the bifurcation surface  $\gamma$ ) to agree with the angular momentum of the black hole. On the other hand, to construct constrained saddles when fixing  $\mathcal{J}$ , we needed  $\mathcal{J}$  to be defined locally on  $\gamma$ , perhaps most naturally, as an integral of the Brown-York momentum density  $(p_{\text{BY}})_i$  — see eq. (3.26). In  $D = 3$ , the angular momentum of a black hole is given by one number and there is a natural constant vector  $\chi^i$  on the one-dimensional surface  $\gamma$  with which to define  $\mathcal{J} \propto \int_\gamma \chi^i (p_{\text{BY}})_i$ .

More generally, the angular momenta of black holes are valued in the  $[(D - 1)/2]$ -dimensional Cartan subalgebra of  $\mathfrak{so}(D - 1)$ . Additionally, in  $D \geq 4$ , there might not be a natural set of vector fields  $\chi_{(I)}^i$ , where  $I = 1, \dots, [(D - 1)/2]$ , which take the place of  $\chi^i$  to define  $\mathcal{J}_{(I)}$ . In highly symmetric configurations, such as rotating black holes or constrained saddles constructed from them, the Killing vectors on  $\gamma$  are natural candidates for  $\chi_{(I)}^i$ . Indeed, taking a Kaluza-Klein reduction, this symmetry is the reason why an analogous problem does not arise in the definition of charges  $\mathcal{Q}_{(I)}$  in the Yang-Mills generalization of our Maxwell analysis. The challenge, however, is to define  $\mathcal{J}_{(I)}$  in more general configurations appearing in the path integral, generically in the absence of such symmetry.

Rather than trying to isolate a handful of vector fields  $\chi_{(I)}^i$ , one might instead take the opposite, democratic approach of considering the infinite set of all vector fields  $\chi^i$  on  $\gamma$  — that is, in the path integral, fixing then later integrating over  $\mathcal{J}[\chi^i] \propto \int_\gamma \chi^i (p_{\text{BY}})_i$  for all vector fields  $\chi^i$ . Equivalently, one can view this as fixing then integrating over the local

momentum density  $(p_{BY})_i$  at every point on  $\gamma$ . Of course, such a calculation would require careful treatment of diffeomorphisms to ensure that gauge-equivalent momentum densities over  $\gamma$  are not over-counted. One might also wonder whether similar generalizations are applicable to the area, *i.e.* Bekenstein-Hawking entropy  $\mathcal{S}$ , and charge  $\mathcal{Q}$ , as measured by Gauss’s law on  $\gamma$ . In particular, instead of  $\mathcal{S}$  and  $\mathcal{Q}$ , one might instead fix then later integrate over the volume form  ${}^{(D-2)}\epsilon$  and the electric flux  $*F$  at every point on  $\gamma$ .

It is interesting to note the close resemblance of such calculations to the treatment of edge modes [24, 25].<sup>73</sup> For simplicity, let us review this for Maxwell theory in a non-dynamical spacetime. We will consider states on a Cauchy slice  $\Sigma = R \cup L$ , where the two pieces  $R$  and  $L$  are separated by an entangling surface  $\gamma$ . Here, Gauss’s law requires that the pullbacks of  $*F$  to  $\gamma$  from  $R$  and  $L$  must agree. Consequently, the physical Hilbert space on  $\Sigma$  is an “entangling product” [26] given, roughly speaking, by the kernel of this constraint in the product  $\mathcal{H}_R \otimes \mathcal{H}_L$  of the  $R$  and  $L$  Hilbert spaces. A physical state, viewed as a special state in  $\mathcal{H}_R \otimes \mathcal{H}_L$ , must then reduce to a density matrix on, say,  $R$  which commutes with the pullback of  $*F$  to  $\gamma$  from  $R$ . To isolate a given block of the density matrix for a given configuration of  $*F$  on  $\gamma$ , one then considers a path integral where  $*F$  is fixed to said configuration. In the end, the full density matrix or partition function is recovered by integrating over all configurations of  $*F$  on  $\gamma$  [24, 25]. In this paper, by fixing and then later integrating over the total electric flux  $\int_\gamma *F$ , we have effectively focused on the constant edge mode<sup>74</sup> on  $\gamma$ ; the other edge modes are associated to configurations of  $*F$  which integrate to zero over  $\gamma$ .

### 6.5.3 Unstable variables

As described in sections 6.2 and 6.3, to evaluate the thermal partition function as an integral transform of a Lorentzian path integral, particularly when using approximate saddle point methods, it is important to hold certain possibly “unstable” variables fixed until they are integrated at the end. In this paper, we have primarily focused on the quantities  $(\mathcal{S}, \mathcal{J}, \mathcal{Q})$  defined on the generically singular codimension-two surface  $\gamma$ . In principle, however, we should save the integrals over all possibly unstable variables for last. Might there be other such variables in the path integral beyond  $(\mathcal{S}, \mathcal{J}, \mathcal{Q})$ , perhaps the nonconstant modes described in section 6.5.2? Relatedly, what new types of singularities would appear in the corresponding constrained saddles and what additional stability conditions might arise from considering these other quantities?

For example, in certain parameter ranges, a black string (asymptotically flat Schwarzschild times a spatial circle) has two Euclidean negative modes [31]: one inherited from the instability of asymptotically flat Schwarzschild, and the other from the Gregory-Laflamme instability [32]. The former is symmetric under the isometries of the bifurcation surface and, in the formalism of ref. [6] and this paper, can be attributed to an instability under variations of  $\mathcal{S}$ . Indeed, asymptotically flat Schwarzschild and the black string have negative specific heat. The latter Gregory-Laflamme instability, however, involves a mode that

<sup>73</sup>For some more recent treatments of edge modes, see [26–30].

<sup>74</sup>This constant edge mode is disallowed in contexts where  $\Sigma$  has no boundary for electric field lines to escape to. Asymptotically AdS black holes, however, have such a boundary.

oscillates in the circle factor. To describe this latter type of instability in our formalism, one might then expect to have to consider the kinds of variables described in section 6.5.2 built from nonconstant modes on  $\gamma$ . An interesting question is whether there are examples of saddles which are stable under variations of  $(\mathcal{S}, \mathcal{J}, \mathcal{Q})$ , but are unstable under variations of these other variables.

We will leave further study of the above questions for future work. However, let us comment briefly that we do not expect the gravitational conformal mode to be among the list of unstable variables that must be integrated at the end, despite the conformal factor problem in Euclidean signature. (Indeed, if we are forced to perform a manifestly divergent integral over the conformal mode after the integral transform (5.37) from Lorentzian time  $T$  to Euclidean time  $\beta$ , then that would defeat the purpose of starting in Lorentz signature to avoid the conformal factor problem.) The reason is that the conformal mode is eliminated by constraints [2–4]. In the canonical form of the gravitational action, lapse and shift appear as Lagrange multipliers for the constraints. In a Lorentzian path integral, integrating over all<sup>75</sup> real<sup>76</sup> values of lapse and shift results in  $\delta$ -functionals imposing the constraints.<sup>77</sup> Thus, we expect the conformal mode to be eliminated in the Lorentzian path integral.

## Acknowledgments

I am very grateful to Donald Marolf for his guidance on this project and the time he spent reviewing the draft of this lengthy paper. I would like to thank José Padua-Argüelles for relevant discussions about torsion. I am further grateful for interesting conversations with Adam Ball, David Grabovsky, Jesse Held, and Maciej Kolanowski. I am supported by a Fundamental Physics Fellowship through the University of California, Santa Barbara.

## References

- [1] G.W. Gibbons, S.W. Hawking and M.J. Perry, *Path Integrals and the Indefiniteness of the Gravitational Action*, *Nucl. Phys. B* **138** (1978) 141.
- [2] K. Schleich, *Conformal Rotation in Perturbative Gravity*, *Phys. Rev. D* **36** (1987) 2342.

---

<sup>75</sup>In some older work on “third quantization”, *e.g.* ref. [33], the constant lapse mode is only integrated over positive reals, leading to gravitational wavefunctions which are Green’s functions, as opposed to solutions, for the Wheeler-de Witt constraint. However, ref. [34] instead advocates for integrating lapse over the full real line in the gravitational path integral. This leads to a group averaged inner product which projects down to the physical Hilbert space satisfying the Wheeler-de Witt constraint.

<sup>76</sup>In contrast, rotated integration contours must be used in Euclidean signature to achieve the same effect. Recently, for example, ref. [35] has highlighted how the rotated contour for the Euclidean lapse constant mode is needed to impose the Wheeler-de Witt constraint and explain an unexpected factor of  $i$  appearing in the gravitational path integral on a sphere (with a particle observer). The integral over real Lorentzian lapse and shift, on the other hand, seems far more natural.

<sup>77</sup>Ref. [7] makes similar comments in the context of a Lorentzian simplicial path integral. Instead of a canonical path integral, one may also consider a manifestly covariant path integral over the  $D$ -dimensional metric (as we implicitly have in this paper), *e.g.* obtained by integrating out the conjugate momenta of the  $(D - 1)$ -metric. In this language, a more appropriate set of words might be that the path integral over the conformal mode is cancelled by a Faddeev-Popov determinant or Jacobian arising from dividing out diffeomorphisms. (See eq. (3.20a) in [4] or the discussion around eqs. (2.28)-(2.33) in [3].)



- [3] P.O. Mazur and E. Mottola, *The Gravitational Measure, Solution of the Conformal Factor Problem and Stability of the Ground State of Quantum Gravity*, *Nucl. Phys. B* **341** (1990) 187.
- [4] J.B. Hartle and K. Schleich, *The Conformal Rotation in Linearised Gravity*, 2004.06635.
- [5] G.W. Gibbons and S.W. Hawking, *Action Integrals and Partition Functions in Quantum Gravity*, *Phys. Rev. D* **15** (1977) 2752.
- [6] D. Marolf, *Gravitational thermodynamics without the conformal factor problem: partition functions and Euclidean saddles from Lorentzian path integrals*, *JHEP* **07** (2022) 108 [2203.07421].
- [7] B. Dittrich, T. Jacobson and J. Padua-Argüelles, *de Sitter horizon entropy from a simplicial Lorentzian path integral*, *Phys. Rev. D* **110** (2024) 046006 [2403.02119].
- [8] S. Colin-Ellerin, X. Dong, D. Marolf, M. Rangamani and Z. Wang, *Real-time gravitational replicas: Formalism and a variational principle*, *JHEP* **05** (2021) 117 [2012.00828].
- [9] K.P. Tod, *Conical singularities and torsion*, *Classical and Quantum Gravity* **11** (1994) 1331.
- [10] W.Z. Chua and T. Hartman, *Black hole wavefunctions and microcanonical states*, *JHEP* **06** (2024) 054 [2309.05041].
- [11] H. Maxfield and G.J. Turiaci, *The path integral of 3D gravity near extremality; or, JT gravity with defects as a matrix integral*, *JHEP* **01** (2021) 118 [2006.11317].
- [12] A. Maloney and E. Witten, *Quantum Gravity Partition Functions in Three Dimensions*, *JHEP* **02** (2010) 029 [0712.0155].
- [13] D. Harlow and T. Numasawa, *Gauging spacetime inversions in quantum gravity*, 2311.09978.
- [14] X. Dong and D. Marolf, *One-loop universality of holographic codes*, *JHEP* **03** (2020) 191 [1910.06329].
- [15] A. Lewkowycz and J. Maldacena, *Generalized gravitational entropy*, *JHEP* **08** (2013) 090 [1304.4926].
- [16] X. Dong, *Holographic Entanglement Entropy for General Higher Derivative Gravity*, *JHEP* **01** (2014) 044 [1310.5713].
- [17] D. Marolf and S.F. Ross, *Boundary Conditions and New Dualities: Vector Fields in AdS/CFT*, *JHEP* **11** (2006) 085 [hep-th/0606113].
- [18] Y. Neiman, *The imaginary part of the gravity action and black hole entropy*, *JHEP* **04** (2013) 071 [1301.7041].
- [19] E. Witten, *Analytic Continuation Of Chern-Simons Theory*, *AMS/IP Stud. Adv. Math.* **50** (2011) 347 [1001.2933].
- [20] J.H. Lee and D. Stanford, *Bulk thimbles dual to trace relations*, 2412.20769.
- [21] Y. Chen and G.J. Turiaci, *Spin-statistics for black hole microstates*, *JHEP* **04** (2024) 135 [2309.03478].
- [22] D. Grabovsky and M. Kolanowski, *Spin-Refined Partition Functions and CRT Black Holes*, 2406.07609.
- [23] R.J. Petti, *On the local geometry of rotating matter*, *General Relativity and Gravitation* **18** (1986) 441.

- [24] W. Donnelly and A.C. Wall, *Geometric entropy and edge modes of the electromagnetic field*, *Phys. Rev. D* **94** (2016) 104053 [[1506.05792](#)].
- [25] W. Donnelly and A.C. Wall, *Entanglement entropy of electromagnetic edge modes*, *Phys. Rev. Lett.* **114** (2015) 111603 [[1412.1895](#)].
- [26] W. Donnelly and L. Freidel, *Local subsystems in gauge theory and gravity*, *JHEP* **09** (2016) 102 [[1601.04744](#)].
- [27] A. Blommaert, T.G. Mertens and H. Verschelde, *Edge dynamics from the path integral — Maxwell and Yang-Mills*, *JHEP* **11** (2018) 080 [[1804.07585](#)].
- [28] H.Z. Chen, R.C. Myers and A.-M. Raclariu, *Entanglement, soft modes, and celestial holography*, *Phys. Rev. D* **109** (2024) L121702 [[2308.12341](#)].
- [29] A. Ball, Y.T.A. Law and G. Wong, *Dynamical edge modes and entanglement in Maxwell theory*, *JHEP* **09** (2024) 032 [[2403.14542](#)].
- [30] H.Z. Chen, R. Myers and A.-M. Raclariu, *Entanglement, Soft Modes, and Celestial CFT*, [2403.13913](#).
- [31] M. Headrick, S. Kitchen and T. Wiseman, *A New approach to static numerical relativity, and its application to Kaluza-Klein black holes*, *Class. Quant. Grav.* **27** (2010) 035002 [[0905.1822](#)].
- [32] R. Gregory and R. Laflamme, *Evidence for stability of extremal black p-branes*, *Phys. Rev. D* **51** (1995) 305 [[hep-th/9410050](#)].
- [33] S.B. Giddings and A. Strominger, *Baby Universes, Third Quantization and the Cosmological Constant*, *Nucl. Phys. B* **321** (1989) 481.
- [34] E. Casali, D. Marolf, H. Maxfield and M. Rangamani, *Baby universes and worldline field theories*, *Class. Quant. Grav.* **39** (2022) 134004 [[2101.12221](#)].
- [35] J. Maldacena, *Real observers solving imaginary problems*, [2412.14014](#).